JUNE 2020 Ph.D. in Electrical and Electronics Engineering MAHMOUD ABUHUSSAIN

REPUBLIC OF TURKEY

GAZIANTEP UNIVERSITY

GRADUATE SCHOOL OF NATURAL & APPLIED SCIENCES

DESIGN OF X-BANDPASS WAVEGUIDE CHEBYSHEV FILTER BASED ON CSRR METAMATERIAL FOR TELECOMMUNICATION SYSTEMS

Ph.D. THESIS

IN

ELECTRICAL AND ELECTRONICS ENGINEERING

BY

MAHMOUD ABUHUSSAIN

JUNE 2020

DESIGN OF X-BANDPASS WAVEGUIDE CHEBYSHEV FILTER BASED ON CSRR METAMATERIAL FOR TELECOMMUNICATION SYSTEMS

Ph.D. Thesis
in
Electrical and Electronics Engineering
Gaziantep University

Supervisor

Prof. Dr. Uğur Cem HASAR

by

Mahmoud ABUHUSSAIN

June 2020

I hereby declare that all information in this document has been obtained and presented in accordance with academic rules and ethical conduct. I also declare that, as required by these rules and conduct, I have fully cited and referenced all material and results that are not original to this work.

Mahmoud ABUHUSSAIN

ABSTRACT

DESIGN OF X-BANDPASS WAVEGUIDE CHEBYSHEV FILTER BASED ON CSRR METAMATERIAL FOR TELECOMMUNICATION SYSTEMS

ABUHUSSAIN, Mahmoud
Ph.D. in Electrical and Electronics Engineering
Supervisor: Prof. Dr. Uğur Cem HASAR
June 2020
118 pages

A fifth-order waveguide bandpass filter is designed by two different methods, the first method used the conventional technology which rectangular waveguide cavities and direct *H-plane* junction. The other method used metamaterial (MM) complementary split-ring resonators (CSRR) technology, both methods are implemented with Chebyshev response. The waveguide bandpass filter is designed at *X-band* with 10 GHz center frequency and operates at [9.15 GHz – 10.44 GHz] bandwidth. By using the CSRR upper and lower sections that are placed on the same transverse plane and are not on the same parallel line, CSRR sections are shifted from each other. A simple model of lumped elements RLC is introduced and calculated as well for both technologies. Hereafter, by selecting proper physical parameters and optimizing the overall CSRR geometrical dimensions by taking into consideration the coupling effect between resonators; a shortened length of the overall filter and a wider bandwidth over the conventional one are obtained. As a result, the MM bandpass waveguide filter is compared with the conventional bandpass waveguide filter, in addition to other studies that have used the metamaterial technique. The MM bandpass filter reduces the overall physical length by 31% and enhances the bandwidth of up to 37.5%. An Electromagnetic (EM) simulator CST is utilized to design the filter by employing both parameters sweep and optimization techniques to achieve the required filter response. The simulation results show that the response of MM filter meets the requirements in terms of return loss, compactness and bandwidth.

Key Words: Chebyshev Filter, Metamaterial, Waveguide, Bandpass, Simulation

ÖZET

TELEKOMÜNİKASYON SİSTEMLERİ İÇİN METAMALZEME X-BAND GEÇİREN FİLTRE CSRR TASARIMI

ABUHUSSAIN, Mahmoud
Doktora Tezi, Elektrik ve Elektronik Mühendisliği
Danışman: Prof. Dr. Uğur Cem HASAR
Haziran 2020
118 Sayfa

Beşinci dereceden bir dalga kılavuzu bant geçiren filtre, iki farklı yöntemle tasarlanmıştır; ilk yöntem olarak, dikdörtgen dalga kılavuzu boşlukları ve doğrudan H-düzlem birleşimini sağlayan klasik teknoloji kullanılmıştır. Bir diğer yöntem icin metamalzeme tamamlayıcı bölünmüş halka rezonatörleri CSRR teknolojisi kullanılmıştır, her iki yöntem icin de Chebyshev yanıtı uygulanmıştır. [9.15 GHz - 10.44 GHz] aralığında çalısan dalga kılavuzu bant geçiren filtre 10 GHz merkez frekanslı X-bandında tasarlanmıştır. Aynı enine düzleme yerleştirilen fakat aynı paralel çizgi üzerinde olmayan CSRR, üst ve alt bölümleri kullanılarak CSRR bölümleri birbirinden kaydırılır. RLC her iki teknoloji için de topaklanmış elemanların basit bir modeli olarak tanıtılır ve hesaplanır. Daha sonra, uygun fiziksel parametreleri seçerek ve rezonatörler arasındaki kuplaj etkisini dikkate alarak ve aynı zamanda genel CSRR geometrik boyutlarını optimize ederek; genel filtrenin kısaltılmış uzunluğu ve geleneksel filtreden daha geniş bir bant genişliği elde edilir. Sonuç olarak, MM bant filtre geçiren, metamalzeme tekniğini kullanan diğer çalışmalara ek olarak geleneksel bant geçiren dalga kılavuzu filtresi ile karşılaştırılır. MM bant geçiren filtre, toplam fiziksel uzunluğu %31 azaltır ve bant genişliğini %37,5' e kadar artırır. Bir elektromanyetik simülasyon yazılımı olan CST, hem parametre tarama hem de optimizasyon tekniklerini kullanarak gerekli yanıtı elde etmek ve filtreyi tasarlamak için kullanılır. Simülasyon sonuçları, metamalzeme filtresinin yanıtının geri dönüş kaybı ve bant genişliği açısından gereksinimleri karşıladığını göstermektedir.

Anahtar kelimeler: Chebyshev Filtresi, Metamalzeme, Dalga kılavuzu, Bant Geçiren, Simülasyon.

“Dedicated to my sister Suhaila “

ACKNOWLEDGEMENTS

First, I am grateful to the Almighty God for establishing me to complete this thesis. There are several people without whom this thesis might not have been written, and to whom I am greatly indebted.

I am deeply indebted to my supervisor **Prof. Dr. Ugur Cem Hasar** whose stimulating, motivation, and valuable ideas helped me to complete this work, and who expertly guided me through my graduate education and who shared the excitement of a year of discovery. I also thank the University of Gaziantep for its helping and supporting.

To my parents, Mousa and Mazuza, I thank you for your encouragement and inspiration to me throughout my life, thank you both for giving me strength to reach for the stars and chase my dreams. An incredibly special thank you for providing and for nurturing me through the months of authoring this thesis.

Special thanks to my grateful wife, Nour, for her moral support and always standing by me in my challenging times during this work. Also, I never forget my sons, Omar and Asem, and my daughter, Tala, they supported me a lot in this work and blessed me with a life of joy in the hours when I was tired. I also indebted to my family, brothers and sisters, whose values to me only grows with age and deserve my wholehearted thanks as well.

To all my friends, thank you for your understanding and encouragement in my many, many moments of crisis. I also place on record, my sense of gratitude to one and all who, directly or indirectly, have lent their helping hand in this thesis.

TABLE OF CONTENTS

Page

LIST OF TABLES

Page

LIST OF FIGURES

Page

LIST OF SYMBOLS

$\boldsymbol{\varepsilon}$	Epsilon – Electrical Permittivity
$\boldsymbol{\mu}$	Mu – Magnetic Permeability
$\boldsymbol{\pi}$	Pi
$\boldsymbol{\beta}$	Beta- Phase Shift
$\boldsymbol{\sigma}$	Sigma – Conductivity
$\boldsymbol{\omega}$	Omega – Angular Frequency
$\boldsymbol{\gamma}$	Zeta – Complex Propagation Constant
$\boldsymbol{f_0}$	Center Frequency
$\boldsymbol{N}$	Filter Order
$\boldsymbol{S_{11}}$	Return Loss
$\boldsymbol{S_{21}}$	Insertion Loss
$\mathbf{WR-90}$	Waveguide X-Band Cross Section $a > b$
$\boldsymbol{\Omega}$	Ohm
$\boldsymbol{\eta}$	Eta – Intrinsic Impedance
$\boldsymbol{z_w}$	Wave Impedance
$\boldsymbol{\lambda}$	Lambda – Free Space Wavelength
$\boldsymbol{\lambda_g}$	Lambda g – Guided Wavelength

LIST OF ABBREVIATIONS

MMs	Metamaterials
WG	Waveguide
BPF	Bandpass Filter
IL	Insertion Loss
SRR	Split Ring Resonator
CSRR	Complementary Split Ring Resonator
ADS	Advanced Design System
CST	Computer Simulation Technology
UWB	Ultra-Wide Band
FGW	Full air-Gapped Waveguide
SIW	Substrate Integrated Waveguide
FBW	Fractional Bandwidth
Q	Quality Factor
q_e	External Quality Factor
IEEE	International Electrical and Electronics Engineers
LNA	Low Noise Amplifier
EBG	Electromagnetic Bandgap
LH	Left-Handed
PBG	Photonic Bandgap
RHM	Right-Handed Material
DPS	Double-Positive
ENG	Epsilon Negative
DNG	Double Negative
MNG	Mu-Negative
NRI	Negative Refractive Index
SNG	Single Negative

FSS	Frequency Selective Surface
LTCC	Low Temperature Co-Fired Ceramic
MIMO	Multi Inputs Multi Outputs
TEM	Transverse Electromagnetic
TE	Transvers Electric
TM	Transvers Magnetic
RADAR	Radio Detection and Ranging

CHAPTER 1

INTRODUCTION

Microwaves, in general, are a term used to describe the Electromagnetic (EM) waves with frequencies at range 300 MHz - 300 GHz, and they are types of electromagnetic radiations along the frequency spectrum. Microwaves correspond to the wavelengths in free space between 1 m and 1 mm. The free space medium is characterized by constitutive parameters such as electrical medium parameter or permittivity $\varepsilon_0 = 8.85 \times 10^{-12}\ F/m$, magnetic medium parameter or permeability $\mu_0 = 4\pi \times 10^{-7}\ H/m$ and the conductivity of the medium $\sigma \approx 0$ [1]. In addition, the EM waves with frequencies ranges more than 30 GHz and up to 300 GHz are usually called millimeter waves due to their wavelengths which are in the millimeter range between $1\ mm - 10\ mm$. According to the International Radio Consultative Committee (CCIR), the frequency ranges are designed as regards bands as shown in Figure 1.1 and Table 1.1 [1, 2].

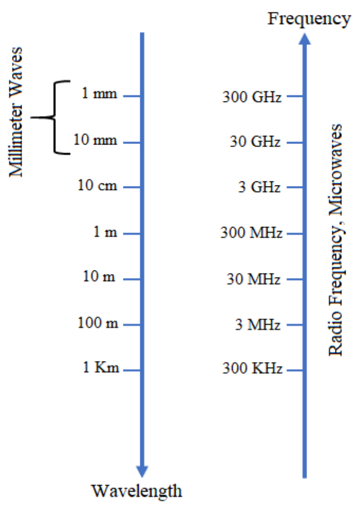

Figure 1.1 RF/microwave spectrum.

Table 1.1 The frequency ranges and designation bands.

Band Designation (GHz)	Frequency Range
140-220	*G*-band
110-170	*D*-band
75-110	*W*-band
60-90	*E*-band
50-70	*V*-band
40-60	*U*-band
33-50	*Q*-band
26.5-40	*Ka*-band
18-26.5	*K*-band
12.4-18	*Ku*-band
8-12.4	***X*-band**
4-8	*C*-band
2-4	*S*-band
1-2	*L*-band
0.3-3	*UHF*-band
0.03-0.3	*VHF*-band

The microwave spectrum increases of interest to communication engineers and systems designers due to a good bandwidth (BW) available for carrying communications channels at this frequency range. Such wider bandwidth is valuable in supporting wireless communication applications such as high-speed data transferring and video transmission particularly for satellite communication [1-3].

Generally, the lumped circuit element theory may not be proper at high radio frequency (RF) and microwave/millimeter frequencies.

Microwave elements or fundamentals regularly act as distributed elements, which the phase of the voltage (V) or current (I) changes crucially over the physical extent of the device since the device's physical dimensions are on the order of the electrical wavelength [1].

1.1 X- Band Overview

X-band is a segment of the radio allocation region of the electromagnetic spectrum, and designation within the range of microwave frequency between 8 GHz and 12 GHz specified by the institute of electrical and electronics engineering (IEEE). X-band is permitted worldwide for high capacity point to point communication link, and for wireless systems. X-band is available which offers full-duplex connectivity at high data rates and higher cost-effective radio architectures [4].

1.2 X-Band Applications

X-band technology is well-suited for a variety of applications as follows [5-8]

- RAdio Detection And Ranging (RADAR) transceiver circuits in satellite communication systems.
- Wireless communication networks in a terrestrial system.
- Low Noise Amplifier besides filter or antenna applications.
- Radiolocation applications.
- Wireless computer networks.
- Medical accelerators in high energy.

1.3 Overview of Microwave Filter and Applications

Microwave filters are fundamental components and vital devices for any radio link which are two-port network used commonly to suppress (attenuate) the unwanted bands in telecommunication systems or to transmit signals in specified frequency bands [9]. Microwave filters generally are aligned with low noise amplifiers (LNA) or bring into line with antennas [10] as shown in Figure 1.2. Microwave filters with decreasing size, flatting insertion loss, high passband selectivity, and wider bandwidth are highly desirable for wireless and satellite communication systems.

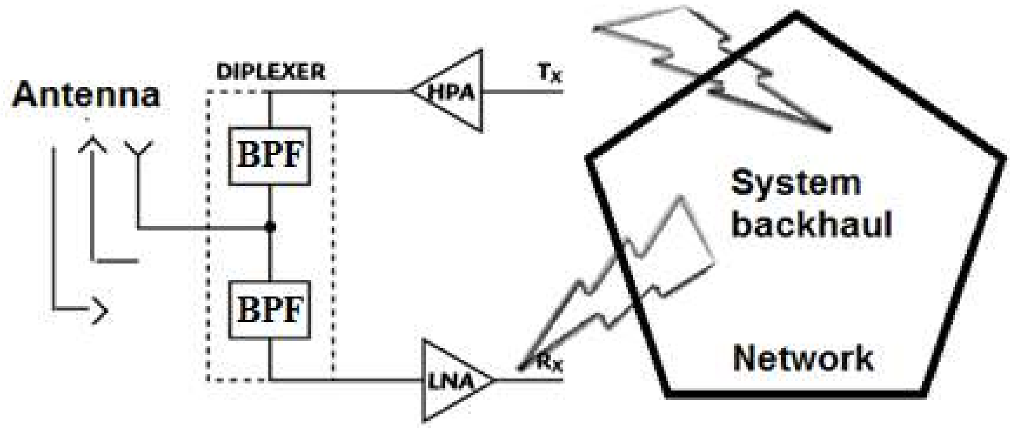

Figure 1.2 Communication network which contains microwave filters with low noise amplifier (LNA) with antenna system.

Currently, most designed filters at microwave and millimeter-wave frequencies are implemented in the waveguide as shown in Figure 1.3. Rectangular waveguide resonators $a > b$ where a and b denote the physical dimensions have been a sustainable key used to design robust, high power circuit and low loss at microwave and millimeter-wave bands [11].

Electrically, microwave filters are devices with sharply tuned resonating circuits to transmit or attenuate signals as desired. Microwave filters may be classified in terms of frequency band to high-pass, low-pass, band-pass, and band-stop. For instance, in communication systems, the band-pass filters in the transmitter path (BPF-TX) stop the transmitter noise and artificially increase the receiver noise figure, while the bandpass filters in the receiver path (BPF-RX) stop the transmitter signal overloading the receiver [12].

The working principles of microwave filters that operate at high frequencies are remarkably similar to those of lumped elements in series or parallel form (RLC) operating at low frequencies in circuit theory [1].

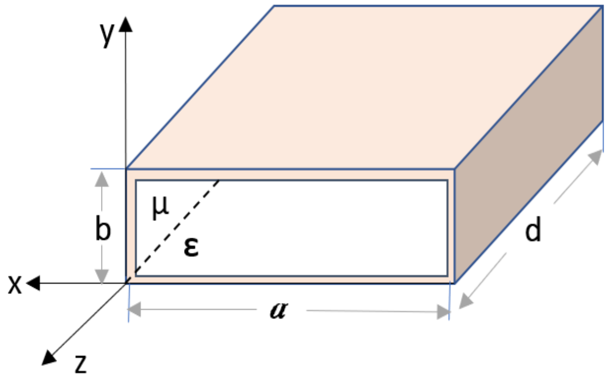

(a)

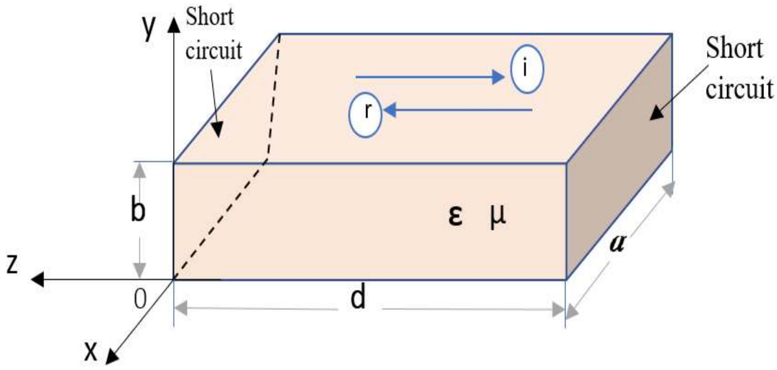

(b)

Figure 1.3 (a) Rectangular waveguide with physical dimensions $a > b$; (b) Rectangular waveguide cavity with length d, shorted both ends and perfect electric conductor for all sides.

1.4 Fundamentals of Rectangular Waveguide

Waveguides, in general, are hollow tubes from metal or any dielectric material which are used for transmitting signals typically 1 GHz and above. They are available in many shapes with respect to its cross-section such as rectangular, circular, and elliptical waveguides. Generally, rectangular waveguides are used in communication systems such as filters, combiners, diplexers, etc. A rectangular waveguide as shown in Figure 1.3 (a) can only support two modes, transverse electric mode (TE) which means no electric filed in the direction of propagation i.e., $E_z = 0$, as shown in Figure

1.4 (a), and transverse magnetic mode (TM) as shown in Figure 1.4 (b), which means no magnetic field in the direction of propagation i.e., $H_z = 0$.

The electromagnetic wave is constructed from two coupled waves, electric wave $\bar{E}$ and magnetic wave $\bar{H}$, and they should satisfy the wave equation given as [12]

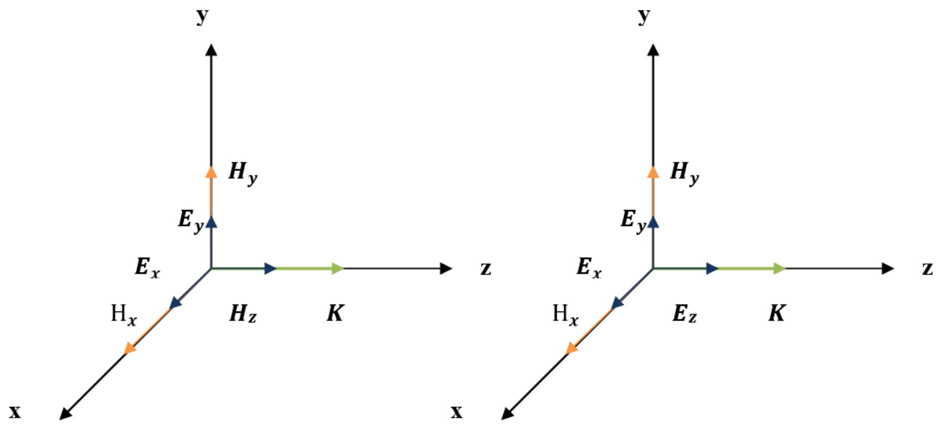

(a) (b)

Figure 1.4 Components of EM fields in a rectangular waveguide
(a) TE mode, E_z=0 (b) TM mode, $H_z = 0$.

$$\left(\frac{\partial^2}{\partial^2 x} + \frac{\partial^2}{\partial^2 y} + k_c^2\right) H_z(x, y, z) = 0 \tag{1.1}$$

where $k_c = \sqrt{k^2 - \beta^2}$ is the cutoff wavenumber and β is the propagation constant. To solve the wave equation that is given in (1.1), separation by variables method could be used, then H_z is given as [13]

$$H_z(x, y, z) = A_{mn} \cos\frac{m\pi x}{a} \sin\frac{n\pi y}{b} e^{-j\beta z} \tag{1.2}$$

where A_{mn} is an arbitrary amplitude constant, m and n are integer numbers $0,1,2 \cdots$

The transverse field components of TE_{mn} mode is given as

$$E_x(x, y, z) = \frac{j\omega\mu n\pi}{k_c^2 b} A_{mn} \cos\frac{m\pi x}{a} \sin\frac{n\pi y}{b} e^{-j\beta z} \tag{1.3}$$

$$E_y(x, y, z) = -\frac{j\omega\mu m\pi}{k_c^2 a} A_{mn} \sin\frac{m\pi x}{a} \cos\frac{n\pi y}{b} e^{-j\beta z} \tag{1.4}$$

$$H_x(x, y, z) = \frac{j\beta m\pi}{k_c^2 a} A_{mn} \sin\frac{m\pi x}{a} \cos\frac{n\pi y}{b} e^{-j\beta z} \tag{1.5}$$

$$H_Y(x, y, z) = \frac{j\beta n\pi}{k_c^2 b} A_{mn} \sin\frac{m\pi x}{a} \cos\frac{n\pi y}{b} e^{-j\beta z} \tag{1.6}$$

From equations (1.3) – (1.6), if $m = 0$, the E_x component will be existing, and others will be vanished, in other words, the E_y, H_x, and H_y components are zeros. If $n = 0$, the E_x component will be vanished and equal zero, and others will be existing, in other words, the E_y, H_x, and H_y components are non-zeros. In addition, it is noticed that from the same equations (1.3) – (1.6) the dominant modes are TE_{10} or TE_{01} for transverse electric and TM_{11} for transverse magnetic modes.

From previous equations (1.1) to (1.6), the propagation constant of EM wave can be determined as

$$\beta = \sqrt{k^2 - \left(\frac{m\pi}{a}\right)^2 - \left(\frac{n\pi}{b}\right)^2} \tag{1.7}$$

and $\quad k = \omega\sqrt{\varepsilon\mu}$

The waveguide will not be in the propagation mode at all if $\omega^2\mu\varepsilon < \left(\frac{m\pi}{a}\right)^2 + \left(\frac{n\pi}{b}\right)^2$ or $\beta = 0, \gamma = \alpha$, all field components will decay exponentially away from the source of excitation. However, when β is real the wave inside waveguide will be propagated along z direction. Then, the condition for real β is given by $k > k_c = \sqrt{\left(\frac{m\pi}{a}\right)^2 + \left(\frac{n\pi}{b}\right)^2}$, each combination of m and n has a cutoff frequency which is given as [1]

$$fc_{mn} = \frac{k_c}{2\pi\sqrt{\mu\varepsilon}} = \frac{1}{2\pi\sqrt{\mu\varepsilon}}\sqrt{\left(\frac{m\pi}{a}\right)^2 + \left(\frac{n\pi}{b}\right)^2} \tag{1.8}$$

The physical dimensions of the waveguide define the field patterns or modes that could exist inside the waveguide.

Cutoff frequencies as shown from equation (1.8) change as the medium inside the waveguide change as well, meaning that different modes depending on the values of permittivity and permeability of a medium. In addition, cutoff frequency determines the order in which different patterns or modes in the waveguide. The dominant mode (the lowest mode) TE_{10} will be used in filter design. For the dominant mode operation, the electric field components are given as [1, 13]

$$E_x^+ = 0,$$

$$E_y^+ = -\frac{A_{10}}{\epsilon}\frac{\pi}{a}\sin\left(\frac{\pi}{a}x\right)e^{-j\beta_z z}, \tag{1.9}$$

$$E_z^+ = 0,$$

The magnetic components for the dominant mode TE_{10} are given as [1,13]

$$H_x^+ = A_{10}\frac{\beta_z}{\omega\mu\epsilon}\frac{\pi}{a}\sin\left(\frac{\pi}{a}x\right)e^{-j\beta_z z}, \tag{1.10}$$

$$H_y^+ = 0,$$

$$H_z^+ = -j\frac{A_{10}}{\omega\mu\epsilon}\left(\frac{\pi}{a}\right)^2\cos\left(\frac{\pi}{a}x\right)e^{-j\beta_z z}, \tag{1.11}$$

Microwave resonators are constructed by enclosing (short-circuiting) both ends of waveguide structures by metallic walls as shown in Figure 1.3(a).

For instance, Figure 1.3 (b) shows the geometry of a rectangular waveguide resonator $a > b$, with length d and shorted at both ends $z = 0$, and $z = d$. Here, it is assumed that the waveguide is extending along the z-axis, and propagation will be in the same direction of waveguide extension.

Electromagnetic energy as the Poynting vector principle (in the electric and magnetic waves) states, is stored within the box enclosure as shown in Figure 1.4, and this energy reaches its maximum value at the perfect coupling between electric and magnetic fields inside the box. In addition, the dissipation power will be in the metallic walls and/or within the filling dielectric material $\varepsilon = \varepsilon_0\varepsilon_r$, where ε_r is a medium's relative permittivity [13].

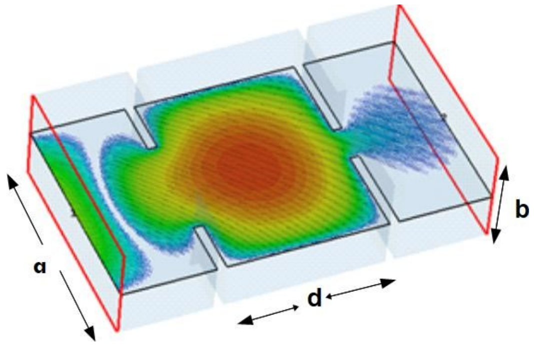

Figure 1.5 Electromagnetic energy stored in the rectangular waveguide resonator $a > b$ with length d.

By applying the Poynting vector between electric and magnetic vectors in a waveguide cavity, power will be purely imaginary, and time-averaged power density (real part) will be zero [13].

$$\bar{P} = \bar{E} \times \bar{H} \tag{1.12}$$

This means that there is no real power in/out the cavity that will be transferred. However, the imaginary part means that there is stored energy in electromagnetic fields inside the cavity [1] as shown in Figure 1.5.

1.5 Overview of Metamaterial Technology

Naturally, all materials such as diamond, glass or aluminum, etc. have positive constitutive parameters (positive electrical permittivity constant ε and/or positive magnetic permeability constant μ) as well as positive refractive index n according to the formula $n^2 = \varepsilon_r\mu_r = \mp\sqrt{|\varepsilon_r\mu_r|}$. Metamaterials (MMs) are artificially engineered or fabricated materials exhibiting features that are not available in natural materials. The term "Metamaterial" has been used for the first time within the scientific community working on complex medium in order to refer to artificial material made or composed by some natural materials whose irregular properties cannot be found in any of the constituents [14]. Researchers have been devoted much time and significant efforts to MMs topic in recent twenty years because of their capability of controlling the wave propagation of EM energy in ways never realized prior [15].

The MMs field has generated plenty of attention since the experimental demonstration of negative refractive index n, such an anomalous response came out the engineering capability of MMs. They can obtain almost any optical response at any given frequency by structuring the geometrics [16]. There are plenty of examples where MMs have posed promising solutions in conforming to free-space radiation. In 1968, Veselago presented theortically left-handed MMs as periodically structured fabricated materials designed to obtain instantaneously negative values of permittivity ε and permeability μ over the frequency band [17].

Generally, split ring resonators (SRRs) are used periodically or in array to have negative values of effective μ [18]. Whilst to obtain or produce negative values of effective ε over a specified bandwidth, the thin wire arrays are used [19]. Due to the properties of artificial materials and based on their constitutive parameters, MMs alternatively called with negative index materials (NIM), backward wave (BW) materials, double negative (DNG) materials or left-handed (LH) materials [16-22].

The essential resonance frequencies of metamaterial (MM) structures are extremely sensitive to changes in the inductive L and capacitive C effects due to their electromagnetic behaviors that may be demonstrated and modeled by LC resonant circuits [20] (lumped element circuit). In chapter 3, metamaterial technology and its applications in various fields will be discussed and shown in more detail.

1.6 Thesis Motivation

Wireless communication system needs have through the past decades increased expeditiously, which has fulfilled in the totally covered frequency spectrum particularly for the range that most of today's technologies can deal with [23]. The term "wideband" in communication system comes up with a message bandwidth once considerably exceeds the coherence bandwidth of the uplink or downlink channel. In addition, the wideband bandwidth has been forced to use for any communication link due to an immense of transferred data rate between channels. To achieve high data rate and wideband bandwidth, microwave filter is a vital component in the communication system as well and is considered as one of limitation components in the system design [1-10].

Microwave filters have been designed with distinct purposes of selecting, transmitting, or rejecting signals over specified band. Despite the various forms of microwave filters available in the literature, they all have the same common point of performance and they consist of periodic structures. A vast number of scientific papers and studies are published on filter design and on how to obtain low insertion loss, high quality factor, high selectivity, simplicity, and wideband bandwidth characteristic.

The main goal of this thesis is the analysis and designs a microwave waveguide filter based on metamaterial technology for X-band applications. Due to the limitations of microwave filter designs used the conventional procedures particularly in physical size and control the bandwidth or selectivity, a modern technology of metamaterial will be applied to overcome these limitations such as wideband bandwidth and compactness of microwave filter.

The microwave filter will be used as a front-end in the microwave transceiver of a point-to-point in telecommunication system applications, which offers high selectivity, wider bandwidth, and good insertion loss over the conventional filters as well as miniaturizing physical size. It is specified to work at the frequency channel bands [9.15 GHz and 10.44 GHz] and 10 GHz center frequency.

The waveguide bandpass filter will be designed using two methods and then the comparison will take place between them: the first method uses waveguide H-plane junction between waveguide resonators and will be mentioned as the conventional method, and the second method takes the advantage of the metamaterial technology such as complementary SRRs (CSRRs) and will be referred to the proposed method. The performance of all design techniques will be evaluated in terms of compactness and return loss with bandwidth as well.

1.7 Thesis Overview

The objective of this thesis is to synthesize, design and analyze a waveguide bandpass filter based on metamaterial and is specified to work at the Chebyshev frequency response for X-band [9.15 GHz and 10.44 GHz] with 10 GHz center frequency. The waveguide bandpass filter is designed for two ports network and the aim is to obtain good insertion loss, high selectivity, and wider bandwidth to transmit gigabit rate signals.

Chapter 2 explains several types of microwave filters and their applications. It presents the derivation of the coupling matrix for the filter network and transformation methodology.

Chapter 3 presents the background of metamaterial technology and its applications in microwave filter designs.

Chapter 4 presents the design procedure of microwave filters for the X-band system and the relationship between the coupling coefficients and the physical structure of coupled resonators to find a proper physical dimension of the filter. Then, it shows the whole structure of the filter and its response resulting from Computer Simulation Technology (CST) based on the Finite Integral Technique (FIT). Finally, a comparison between two conventional and proposed waveguide bandpass filter designs are shown and discussed.

Chapter 5 provides a summary and conclusions drawn from this thesis and future work.

CHAPTER 2

MICROWAVE FILTERS AND APPLICATIONS

2.1 Introduction

Microwave filters are vital components in a vast variety of electronic systems including satellite communications, mobile radio, and radar systems. Filters are used to select or reject signals at different frequencies in the system. Even though the physical realization of microwave filters may differ, the lumped circuit network theory is common to all microwave filter designs operates at low or high frequencies [24]. Naturally, microwave filters are distributed networks that are usually amount to periodic structures to manifest stopband and passband characteristics in different frequency bands. Interestingly, in a design method of microwave filter, it would be able to determine the physical dimensions of a whole structure as considered to the desired characteristics.

To present, research on microwave filters have extended more than seventy years, and the number of contributions devoted to the design methods of microwave filters is much considerable in several ways and technologies. Historically, reviews on the microwave filter topics and distinctive designs procedures can be found in [25-50].

2.2 Coupled Resonators and Filters

Commonly, coupled resonators circuit prototypes are mostly used in the design of microwave filters. Despite the diversity of their physical structures or designs, the prototype theory of low pass filter can be applied to any type of coupled resonators to design microwave filters [51]. Coupled resonators have been applied to the design of many filter circuits with varied frequency band, such as coaxial cavity filters [52, 53] which could be employed for base transceiver station applications as illustrated in Figure 2.1. Waveguide filters [54, 55] are used for Ka and X-band applications as shown in Figure 2.2, dielectric resonator filters [56] are employed for 5G networks as shown in Figure 2.3, ceramic combine filters [57] are very attractive for frequency applications between UHF and C-band, as illustrated in Figure 2.4.Microstrip filters [58-61] usually are desirable choices for wireless communication and mobile systems as illustrated in Figure 2.5.

Superconducting filters [62] are used for ultra-wide band (UWB) applications to obtain a good performance as shown in Figure 2.6, micro-machined filters [63] are used in sensing and material characterizations for terahertz frequencies as shown in Figure 2.7, and metamaterial filters [64-67] are used for variety of communication applications because of their ability to control bandwidth and selectivity as shown in Figure 2.8. Designing method of microwave filters is based on the theory of coupling coefficients of the inter-coupled resonators along with the external couplings of the resonators [2]. Therefore, the relationship between the coupling coefficients and the physical structures of the filter needs to be well-established. Formulations for extracting the coupling coefficients of any resonating filter are given in next section for different cases.

Figure 2.1 Prototype five-pole coaxial cavity filter for base transceivers [52].

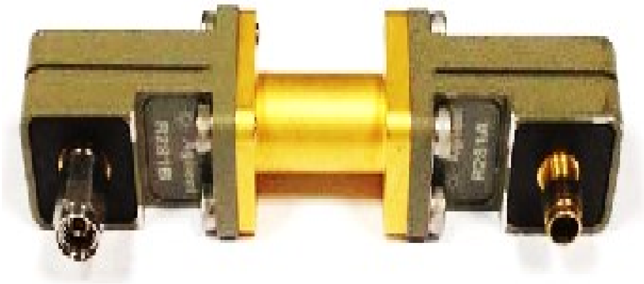

Figure 2.2 A full air-gapped waveguide (FGW), rectangular waveguide, and iris rectangular waveguide bandpass filter [54].

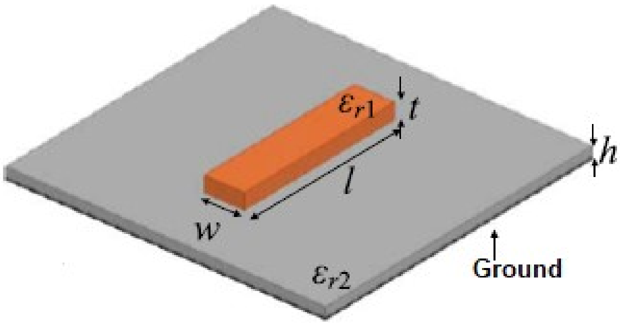

Figure 2.3 Construction of a ceramic coaxial resonator [56] which w , l are slab width and length respectively, $\varepsilon_{r1}, \varepsilon_{r2}$ are relative permittivity of slab and substrate respectively.

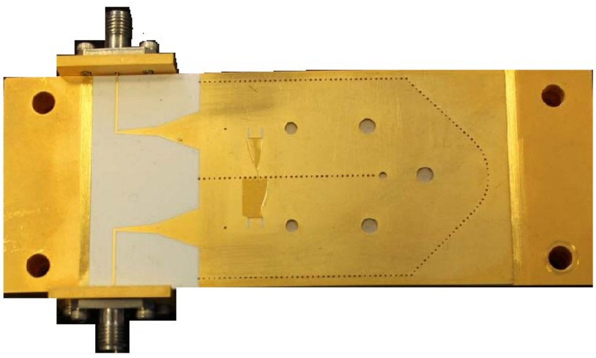

Figure 2.4 Substrate integrated waveguide (SIW) filter with high-K ceramic [57].

Figure 2.5 Microstrip microwave filter [59].

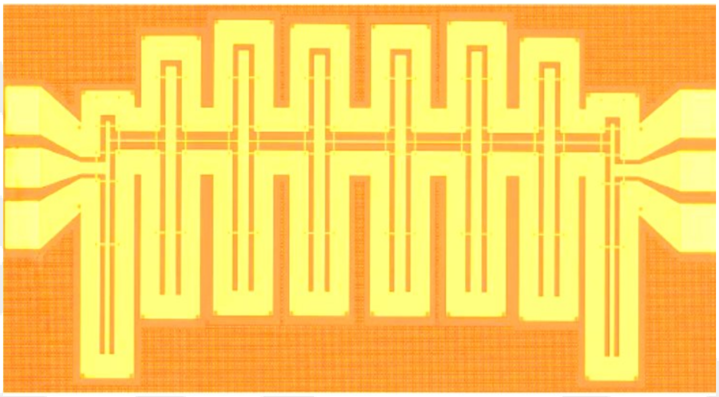

Figure 2.6 Superconducting microstrip filters [62].

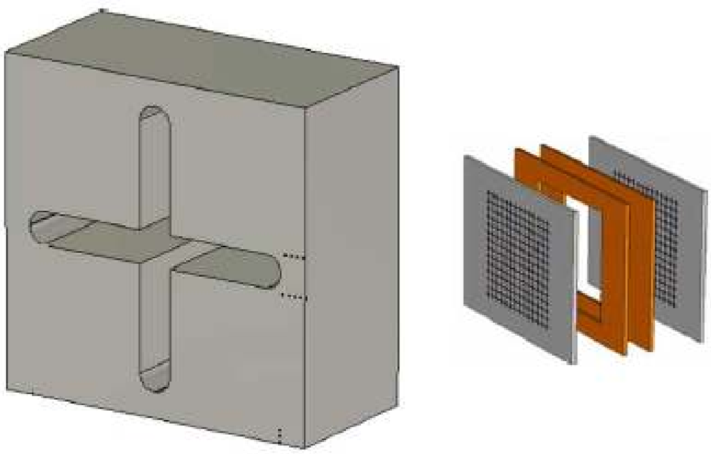

Figure 2.7 Micro-machined thick mesh filter [63].

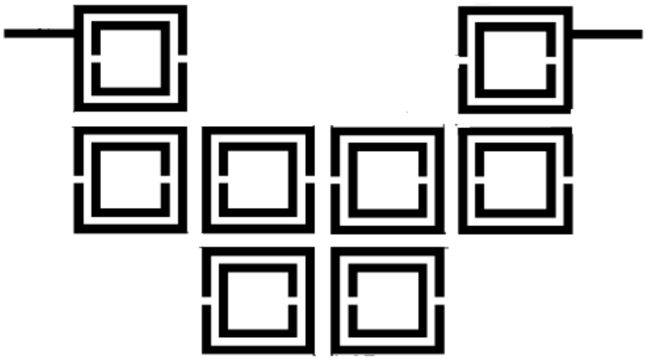

Figure 2.8 Superconducting filter based on split ring resonator structure [67].

2.3 Coupling Matrix Representation for Coupled Resonators

In general, the coupling effect between adjacent or crossed any microwave resonators as shown in Figure 2.9 can be either electric, magnetic or mixed electric-magnetic coupling as illustrated in Figure 2.10. It is considered important to design microwave filters for different topologies [2].

In the case of magnetic coupling between resonators and to extract coupling from the circuit, by using Kirchhoff's voltage law, the loop equations have been obtained mathematically from the equivalent lumped element circuit model as shown in Figure 2.11 (a). Representing the coupling between resonators is analyzed by the impedance matrix form.

For the electric coupled resonators, using Kirchhoff's current law, node equations are obtained from the equivalent lumped element circuit model in Figure 2.11 (b), and it represented an admittance matrix form. The mathematical derivations show that the normalized admittance matrix has an identical form to the normalized impedance matrix [1, 2].

2.3.1 Magnetically Coupled Resonators

Figure 2.11 (a) shows an equivalent lumped circuit of n-coupled resonators, however, L , C, and R denote to the inductance, capacitance, and resistance of the lumped circuit, respectively. Using Kirchhoff's voltage law, the equations have been derived as follows [2]

$$\begin{aligned}
&\left(R_1 + j\omega L_1 + \frac{1}{j\omega C_1}\right) i_1 - j\omega L_{12} i_2 \cdots - j\omega L_{1n} i_n = e_s \\
&-j\omega L_{12} i_1 + \left(j\omega L_2 + \tfrac{1}{j\omega C_2}\right) i_2 \cdots\ j\omega L_{2n} i_n = 0 \\
&\vdots \\
&-j\omega L_{n1} i_1 - j\omega L_{n2} i_2 + \cdots + j\omega L_{(n-1)2} i_{(n-1)} + \left(R_n + j\omega L_n + \tfrac{1}{j\omega C_n}\right) i_n = 0
\end{aligned} \tag{2.1}$$

where $L_{ij} = L_{ji}$ denotes to the mutual inductance between coupled resonators I and j, which can be represented in the matrix form.

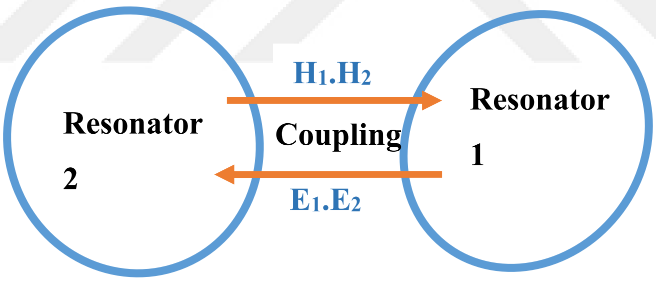

Figure 2.9 General coupled RF/microwave cavities where cavities1 and 2 may be different in physical structure and work at different frequency bands.

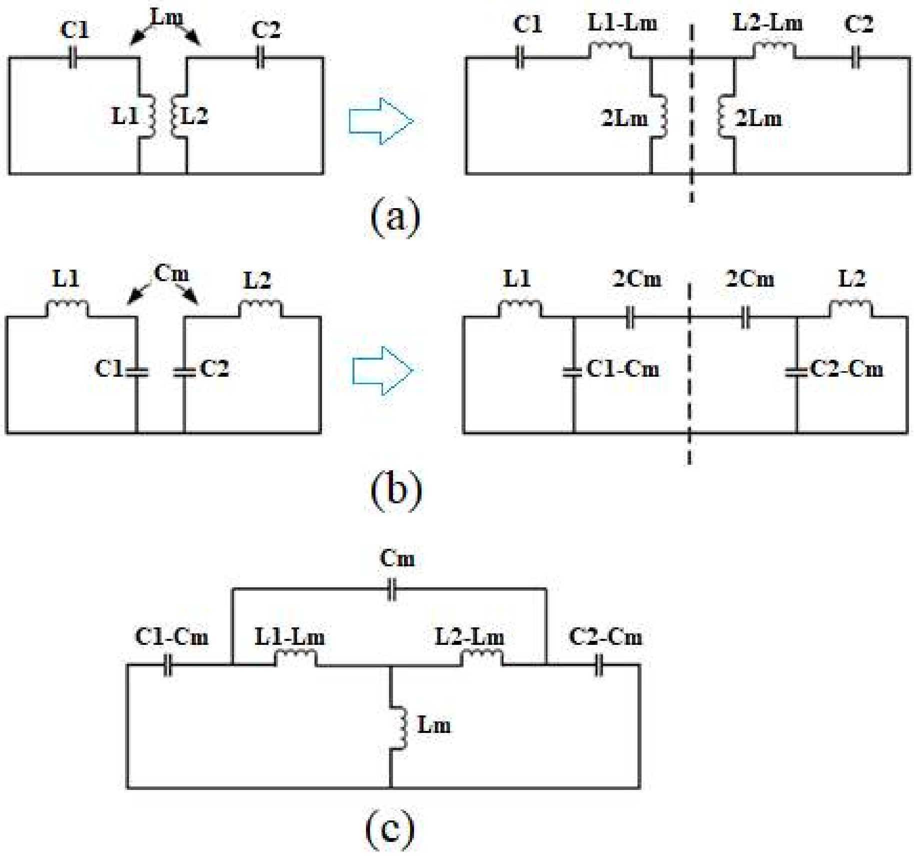

Figure 2.10 Inter-coupling between RF/microwave coupled resonators lumped elements circuit. (a) Coupled resonators circuit with electric coupling. (b) Coupled resonators circuit with magnetic coupling. (c) Coupled resonators circuit with mixed electric and magnetic coupling.

$$\begin{bmatrix} R_1 + j\omega L_1 + \frac{1}{j\omega C_1} & -j\omega L_{12} & \cdots & -j\omega L_{1n} \\ -j\omega L_{21} & j\omega L_2 + \frac{1}{j\omega C_2} & \cdots & -j\omega L_{2n} \\ & \vdots & & \\ -j\omega L_{n1} & -j\omega L_{n2} & \cdots & R_n + j\omega L_n + \frac{1}{j\omega C_n} \end{bmatrix} \begin{bmatrix} i_1 \\ i_2 \\ \vdots \\ i_n \end{bmatrix} = \begin{bmatrix} e_s \\ 0 \\ \vdots \\ 0 \end{bmatrix} \quad (2.2)$$

Equation (2.2) can be written in the form

$$[Z].[i] = [e]$$

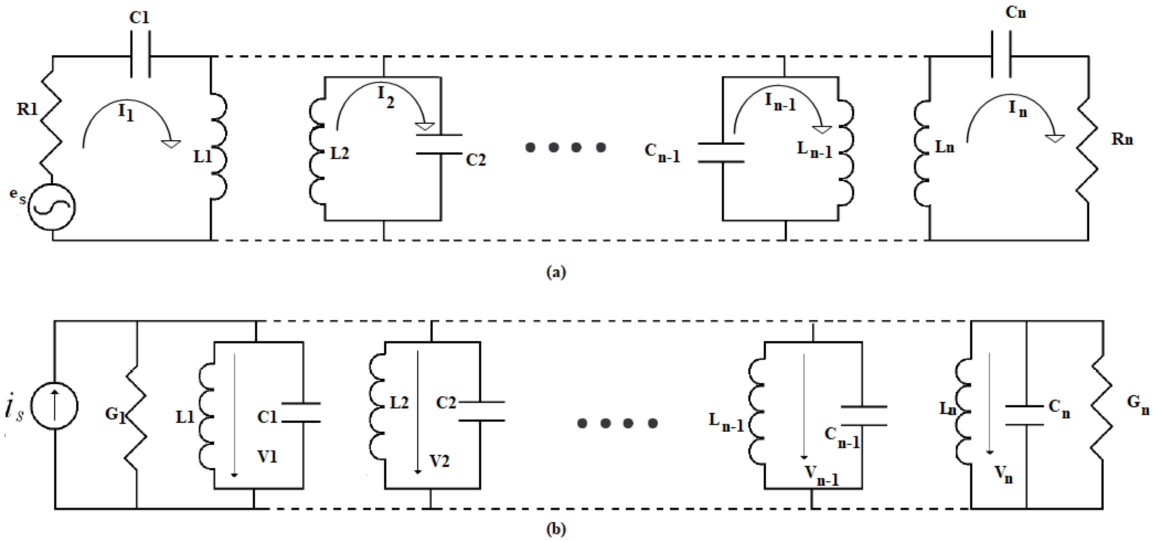

Figure 2.11 (a) Equivalent circuit model of magnetically resonator filters, (b) Equivalent circuit model of electrically resonator filters.

where $[Z]$ $n \times n$ impedance matrix of the coupled circuit, and for simplicity, we can first suppose a synchronously tuned filter; which means, all the coupled resonators in the system have the same resonant frequency $\omega_0 = 1/\sqrt{LC}$, where $L = L_1 = L_2 = \cdots L_n$ and $C = C_1 = C_2 = \cdots C_n$.

The impedance matrix $[Z]$ may be expressed in another form by $[Z] = \omega_0 L.FBW.\overline{[Z]}$, where $FBW = \Delta\omega/\omega_0 = \omega_2 - \omega_1/\omega_0$ is the fractional bandwidth of the filter circuit and $\overline{[Z]}$ is the normalized impedance matrix of a circuit, and given by [2]

$$\overline{[Z]} = \begin{bmatrix} \frac{R_1}{\omega_0 L.FBW} + P & -\frac{j\omega L_{12}}{\omega_0 L}\frac{1}{FBW} & \cdots & -\frac{j\omega L_{1n}}{\omega_0 L}\frac{1}{FBW} \\ -\frac{j\omega L_{21}}{\omega_0 L}\frac{1}{FBW} & P & \cdots & -\frac{j\omega L_{2n}}{\omega_0 L}\frac{1}{FBW} \\ & \vdots & & \\ -\frac{j\omega L_{n1}}{\omega_0 L}\frac{1}{FBW} & -\frac{j\omega L_{n2}}{\omega_0 L}\frac{1}{FBW} & \cdots & \frac{R_n}{\omega_0 L.FBW} + P \end{bmatrix} \tag{2.3}$$

where $P = \frac{j}{FBW}\left(\frac{\omega}{\omega_0} - \frac{\omega_0}{\omega}\right)$ is the complex low-pass frequency parameter. It should be noticed that for series external circuit.

$$\frac{R_i}{\omega_0 L} = \frac{1}{Q_{ei}} \qquad i = 1,2,3, \ldots n \tag{2.4}$$

where Q_{e1} is the input external quality factor and Q_{en} is the output external quality factor of resonators of the circuit. Defining the coupling coefficients K as

$$K_{ij} = L_{ij}/L \tag{2.5}$$

By simplifying the equation (2.3) and assuming $\omega/\omega_0 \approx 1$, we obtained the equation as follows [2]

$$\overline{[Z]} = \begin{bmatrix} \frac{1}{q_{e1}} + P & -jk_{12} & \cdots & -jk_{1n} \\ -jk_{21} & P & \cdots & -jk_{2n} \\ & \vdots & & \\ -jk_{n1} & -jk_{n2} & \cdots & \frac{1}{q_{en}} + P \end{bmatrix} \tag{2.6}$$

where q_{ei} is the scaled external quality factor ($q_{ei} = Q_{ei}.FBW$) and k_{ij} is the normalized coupling coefficient ($K_{ij} = k_{ij}.FBW$).

A network representation of the circuit of Figure 2.11(a) is shown in Figure 2.12, where V_1, V_2 and I_1, I_2 are the voltages and currents variables at the filter ports in the circuit, and the wave variables are denoted by a_1, b_1, a_2, b_2 entering wave at port1, reflected wave at port 1, entering wave at port 2 and reflected wave at port 2 respectively.

By observing the circuit of Figure 2.10 (a) and the network of Figure 2.11, it can be identified that $I_1 = i_1$, $I_2 = -i_n$ and $V_1 = e_s - i_i.R_1$ [46]. The input and reflected waves can be expressed as

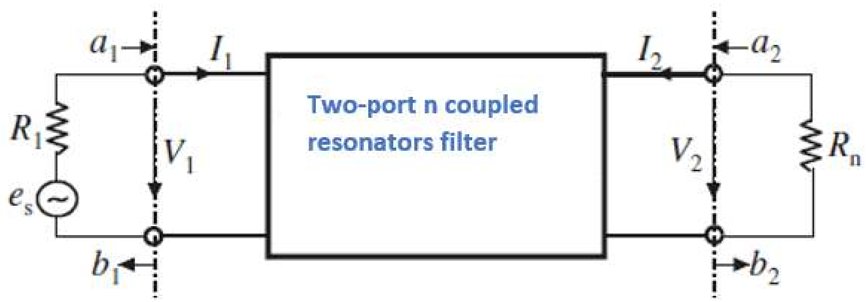

Figure 2.12 Equivalent circuits of n-coupled resonators filter for magnetic coupling.

$$\left.\begin{array}{ll} a_1 = \frac{e_s}{2\sqrt{R_1}} & b_1 = \frac{e_s - 2i_1R_1}{2\sqrt{R_1}} \\ a_2 = 0 & b_2 = i_n\sqrt{R_n} \end{array}\right\} \tag{2.7}$$

and, hence,

$$\left.\begin{array}{l} S_{11} = \left.\frac{b_1}{a_1}\right|_{a_2=0} = 1 - \frac{2R_1i_1}{e_s} \\ S_{21} = \left.\frac{b_2}{a_1}\right|_{a_2=0} = \frac{2\sqrt{R_1R_n}i_n}{e_s} \end{array}\right\} \tag{2.8}$$

Here S_{11} and S_{21} are reflection and transmission scattering parameters, respectively.

By solving equation (2.1) for i_1 and i_n, we obtained

$$\left.\begin{array}{l} i_i = \frac{e_s}{\omega_0 L.FBW}\overline{[Z]}_{11}^{-1} \\ i_n = \frac{e_s}{\omega_0 L.FBW}\overline{[Z]}_{n1}^{-1} \end{array}\right\} \tag{2.9}$$

and after substitution of equations (2.9) into equations (2.8), equation (2.10) is obtained

$$\left.\begin{array}{l} S_{11} = 1 - \frac{2R_1}{\omega_0 L.FBW}\overline{[Z]}_{11}^{-1} \\ S_{21} = \frac{2\sqrt{R_1R_n}}{\omega_0 L.FBW}\overline{[Z]}_{n1}^{-1} \end{array}\right\} \tag{2.10}$$

In terms of the scaled external quality factors $q_{ei} = \omega_0 L.FBW/R_i$, the S-parameters will read as

$$\left.\begin{array}{l} S_{11} = 1 - \frac{2}{q_{e1}}\overline{[Z]}_{11}^{-1} \\ S_{21} = \frac{2}{\sqrt{q_{e1}q_{en}}}\overline{[Z]}_{n1}^{-1} \end{array}\right\} \tag{2.11}$$

where S_{11} is the reflection coefficient of the two-port network, and S_{21} is the transmission coefficient of the two-port network.

In the case that the coupled-resonator circuit of Figure 2.10 (a) is asynchronously tuned, and each resonator may be different in the resonant frequency that is given by $\omega_{0i} = 1/\sqrt{L_iC_i}$, the coupling coefficient of an asynchronously filter is derived as [2]

$$K_{ij} = \frac{L_{ij}}{\sqrt{L_i L_j}} \quad \text{for } i \neq j. \tag{2.12}$$

It can be shown that equation (2.6) becomes for asynchronous tuned filter

$$\overline{[z]} = \begin{bmatrix} \frac{1}{q_{e1}} + P - jk_{11} & -jk_{12} & \cdots & -jk_{1n} \\ -jk_{21} & P - jk_{21} & \cdots & -jk_{2n} \\ & \vdots & & \\ -jk_{n1} & -jk_{n2} & \cdots & \frac{1}{q_{en}} + P - jk_{nn} \end{bmatrix} \tag{2.13}$$

Notice that, the normalized impedance matrix of equation (2.13) is nearly similar to equation (2.6), however, it has the entries k_{ii} for asynchronous tuning.

2.3.2 Electrically Coupled Resonators

Up to now, we have discussed and derived magnetically coupled resonators of the filter circuit. The coupling coefficients presented and shown in the above section are all based on the mutual inductance and, hence, the identified couplings are magnetic couplings.

The formulation of the coupling coefficients for a two-port n-coupled resonators filter with electric couplings will be explained in this section as well in the same manner that we showed in the previous section. Consider the n-coupled resonators circuit shown in Figure 2.11 (b), where v_i denotes to the node voltage, G represents to the conductance of circuit and i_s is the source current of the two-port network [1, 2]. According the current law in a circuit system, which states that the algebraic summation of all currents where leave a node in a network is zero. With a driving or external current of i_s, the node equations for the circuit of Figure 2.11 (b) are [1] as

$$\left(G_1 + j\omega C_1 + \frac{1}{j\omega L_1}\right) v_1 - j\omega C_{12} v_2 \cdots - j\omega C_{1n} v_n = i_s$$

$$-j\omega C_{12} i_1 + \left(j\omega C_2 + \frac{1}{j\omega L_2}\right) v_2 \cdots - j\omega C_{2n} v_n = 0 \tag{2.14}$$

$$\vdots$$

$$-j\omega C_{n1} v_1 - j\omega C_{n2} v_n + \ldots + j\omega C_{(n-1)2} v_{(n-1)} + \left(G_n + j\omega C_n + \frac{1}{j\omega L_n}\right) v_n = 0$$

where $C_{ij} = C_{ji}$ denotes the mutual capacitance between coupled resonators a and b. The matrix form representation of the previous equations is shown as below

$$\begin{bmatrix} G_1 + j\omega C_1 + \frac{1}{j\omega L_1} & -j\omega C_{12} & \cdots & -j\omega C_{1n} \\ -j\omega C_{21} & j\omega C_2 + \frac{1}{j\omega L_2} & \cdots & -j\omega C_{2n} \\ & \vdots & & \\ -j\omega C_{n1} & -j\omega C_{n2} & \cdots & G_n + j\omega C_n + \frac{1}{j\omega L_n} \end{bmatrix} \begin{bmatrix} v_1 \\ v_2 \\ \vdots \\ v_n \end{bmatrix} = \begin{bmatrix} i_s \\ 0 \\ \vdots \\ 0 \end{bmatrix} \qquad (2.15)$$

or $[Y].[v] = [i]$, where $[Y]$ is an $n \times n$ admittance matrix.

Similarly, the admittance matrix in equation (2.15) could be expressed by

$$[Y] = \omega_0 C.FBW.\overline{[Y]} \qquad (2.16)$$

where $\omega_0 = 1/\sqrt{LC}$ is the resonant frequency of the filter circuit, FBW is the fractional bandwidth and $\overline{[Y]}$ is the normalized admittance matrix of the filter circuit. In the case of synchronously tuned filter, or all the resonators/cavities have the same resonant frequency, $\overline{[Y]}$ is given by [2]

$$\overline{[Y]} = \begin{bmatrix} \frac{G_1}{\omega_0 C.FBW} + P & -\frac{j\omega C_{12}}{\omega_0 C}\frac{1}{FBW} & \cdots & -\frac{j\omega C_{1n}}{\omega_0 C}\frac{1}{FBW} \\ -\frac{j\omega l_{21}}{\omega_0 L}\frac{1}{FBW} & P & \cdots & -\frac{j\omega C_{2n}}{\omega_0 C}\frac{1}{FBW} \\ & \vdots & & \\ -\frac{j\omega C_{n1}}{\omega_0 C}\frac{1}{FBW} & -\frac{j\omega C_{n2}}{\omega_0 C}\frac{1}{FBW} & \cdots & \frac{G_n}{\omega_0 C.FBW} + P \end{bmatrix} \qquad (2.17)$$

where P is the complex low-pass frequency parameter.

Notice that,

$$\frac{G_i}{\omega_0 C} = \frac{1}{Q_{ei}} \quad i = 1,2,3 \cdots n \qquad (2.18)$$

which Q_{e1} is the input external quality factor and Q_{en} is the external quality factors of the coupled resonators. Defining the coupling coefficients as [2]

$$K_{ij} = \frac{C_{ij}}{C} \tag{2.19}$$

and by assuming the factor $\omega/\omega_0 \approx 1$ for the narrow band estimation. A simpler expression of equation (2.17) is derived

$$\overline{[Y]} = \begin{bmatrix} \frac{1}{q_{e1}} + P & -jk_{12} & \cdots & -jk_{1n} \\ -jk_{21} & P & \cdots & -jk_{2n} \\ & \vdots & & \\ -jk_{n1} & -jk_{n2} & \cdots & \frac{1}{q_{en}} + P \end{bmatrix} \tag{2.20}$$

where $q_{ei} = Q_{ei}.FBW$ is the scaled external quality factor and $K_{ij} = k_{ij}.FBW$ is the normalized coupling coefficient of the coupled-resonator circuit.

Similarly, if the coupled resonators circuit of Figure 2.10 (b) is asynchronously tuned circuit which the resonant frequency of all resonators is not the same, then the equations (2.19) and (2.20) become as follows

$$\overline{[Y]} = \begin{bmatrix} \frac{1}{q_{e1}} + P - jk_{11} & -jk_{12} & \cdots & -jk_{1n} \\ -jk_{21} & P - jk_{22} & \cdots & -jk_{2n} \\ & \vdots & & \\ -jk_{n1} & -jk_{n2} & \cdots & \frac{1}{q_{en}} + P - jk_{nn} \end{bmatrix} \tag{2.21}$$

$$K_{ij} = \frac{C_{ij}}{\sqrt{C_i C_j}} \text{ for } i \neq j$$

To obtain and derive the two-port *S*-parameters of the coupled-resonator filter network, the circuit of Figure 2.11 (b) is represented by a two-port network as in Figure 2.13, which all the variables at the filter ports are the same as those in Figure 2.12. In this case, $V_1 = v_1$, $V_2 = -v_n$, and $I_1 = i_s - v_1 G_1$

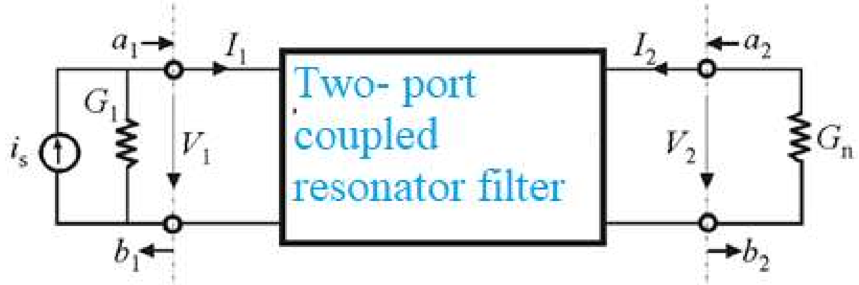

Figure 2.13 Equivalent circuit model of n-coupled resonators tuned filter for electric coupling.

$$\left.\begin{aligned} a_1 &= \frac{i_s}{2\sqrt{G_1}} \\ b_1 &= \frac{-i_s + 2v_1 G_1}{2\sqrt{G_1}} \\ a_2 &= 0 \\ b_2 &= v_n\sqrt{G_n} \end{aligned}\right\} \tag{2.22}$$

$$\left.\begin{aligned} S_{11} &= \frac{b_1}{a_1}\bigg|_{a_2=0} = -1 + \frac{2G_1 v_1}{i_s} \\ S_{21} &= \frac{b_2}{a_1}\bigg|_{a_2=0} = \frac{2\sqrt{G_1 G_n}\, v_n}{i_s} \end{aligned}\right\} \tag{2.23}$$

Finding the unknown node voltages v_1 and v_n from equation (2.15)

$$v_1 = \frac{i_s}{\omega_0 C.FBW}\,[\overline{Y}]_{11}^{-1}$$

$$v_n = \frac{i_s}{\omega_0 C.FBW}\,[\overline{Y}]_{n1}^{-1} \tag{2.24}$$

Substituting the equation (2.24) into the equation (2.23), we obtain

$$S_{11} = -1 + \frac{2G_1}{\omega_0 C.FBW}\,[\overline{Y}]_{11}^{-1}$$

$$S_{21} = \frac{2\sqrt{G_1 G_n}}{\omega_0 C.FBW}\,[\overline{Y}]_{n1}^{-1} \tag{2.25}$$

This can be simplified as [1]

$$S_{11} = -1 + \frac{2}{q_{e1}} \overline{[Y]}_{11}^{-1}$$

$$S_{21} = \frac{2}{\sqrt{q_{e1} q_{en}}} \overline{[Y]}_{n1}^{-1} \tag{2.26}$$

2.3.3 General Coupling Matrix

In the prior derivation, we notice that the formulations of the normalized impedance matrix $\overline{[Z]}$ is identical to that of the normalized admittance matrix $\overline{[Y]}$ of the coupled-resonator circuit. This is especially important because it implies the unified formulation for an n-coupled resonators tuned filter regardless of whether the coupling is electric or magnetic or electric-magnetic (mixed). Accordingly, equations (2.11) and (2.27) can be represented into a general equation [2] as

$$S_{21} = \frac{2}{\sqrt{q_{e1} \cdot q_{en}}} [A]_{n1}^{-1} \tag{2.27}$$

$$S_{11} = \pm\left(1 - \frac{2}{q_{e1}} [A]_{11}^{-1}\right) \tag{2.28}$$

$$[A] = [q] + p\,[U] - j[k] \tag{2.29}$$

$$[A] = \begin{bmatrix} \frac{1}{q_{e1}} & \cdots & 0 & \cdots & 0 \\ \vdots & \ddots & \vdots & \vdots & \vdots \\ 0 & \cdots & 0 & \cdots & 0 \\ \vdots & \vdots & \vdots & \ddots & \vdots \\ 0 & \cdots & 0 & \cdots & \frac{1}{q_{en}} \end{bmatrix} + p \begin{bmatrix} 1 & \cdots & 0 & 0 \\ \vdots & \ddots & \vdots & \vdots \\ 0 & \cdots & 1 & 0 \\ 0 & \cdots & 0 & 1 \end{bmatrix} - j \begin{bmatrix} k_{11} & \cdots & k_{1(n-1)} & k_{1n} \\ \vdots & \ddots & \vdots & \vdots \\ k_{(n-1)1} & \cdots & k_{(n-1)(n-1)} & k_{(n-1)n} \\ k_{n1} & \cdots & k_{n(n-1)} & k_{nn} \end{bmatrix} \tag{2.30}$$

where $[U]$ is the $n \times n$ unit or identity matrix, p is the complex low-pass frequency parameter, $[q]$ is an $n \times n$ matrix with all entries zero, except for $q_{11} = 1/q_{e1}$ and $q_{nn} = 1/q_{en}$, and $[k]$ is so-called the general coupling matrix of coupled circuit, which is $n \times n$ reciprocal matrix (that is, $k_{ij} = k_{ji}$).

Note that, it is allowed to get non zero diagonal variables k_{ii} for an asynchronously tuned filter [2].

2.3.4 Theory of Coupling

A general methodology to design any coupled-resonators filter circuit (see Figure 2.9) relies on the coupling coefficients of internal coupled resonators and the external Q_e factors of the input and output resonators in the tuned filter circuit. The external quality factor Q_e is characterized by the external coupling between a microwave resonator and the external circuit which is generally the ports of the filter circuit, which is shown as Q_{ea} and Q_{eb} in Figure 2.14.

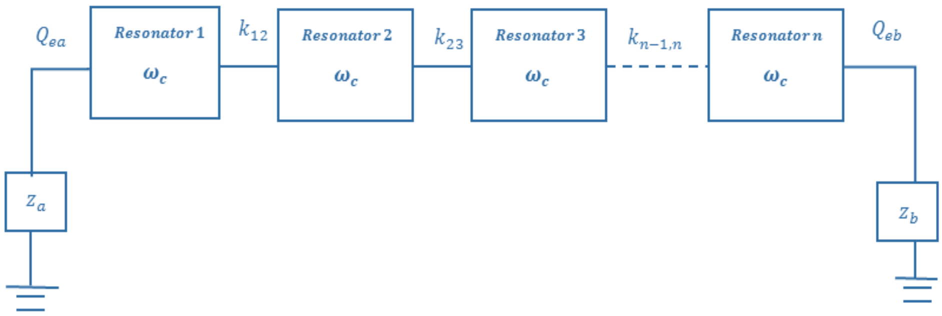

Figure 2.14 The scheme of a microwave filter structure.

2.3.5 Coupling Coefficient

The coupling coefficient K_{ij} of two coupled microwave cavities or resonators may be defined on the basis of the ratio of coupled energy of resonators to stored energy in the coupled resonators circuit. It can be derived mathematically [1, 2] as

$$K_{12} = \frac{\int\int\int \varepsilon \vec{E}_1 \bullet \vec{E}_2 dv}{\sqrt{\int\int\int \varepsilon |\vec{E}_1|^2 dv \times \int\int\int \varepsilon |\vec{E}_2|^2 dv}} + \frac{\int\int\int \mu \vec{H}_1 \bullet \vec{H}_2 dv}{\sqrt{\int\int\int \mu |\vec{H}_1|^2 dv \times \int\int\int \mu |\vec{H}_2|^2 dv}} \tag{2.31}$$

where $\vec{E}$ and $\vec{H}$ represent the electric field and magnetic field vectors between coupled resonators, respectively; The interaction of the coupled resonator is mathematically defined by the dot operation of their space vectors fields which allows the coupling between resonators to get either negative or positive sign. A positive sign implies that the coupling boosts the stored energy of uncoupled resonators, whereas a negative sign indicates a reduction of energy.

Therefore, the coupling whether is magnetic or electric coupling could either has the same effect if they agree with the signs or have the opposite effect if they are contrary with signs [2]. The magnitude of the coupling coefficient of coupled resonators defines the separation d between two resonance peaks as illustrated in Figure 2.15. The stronger coupling means wider separation d between the two resonance peaks of $|S_{21}|$, and deeper the trough in the middle [2].

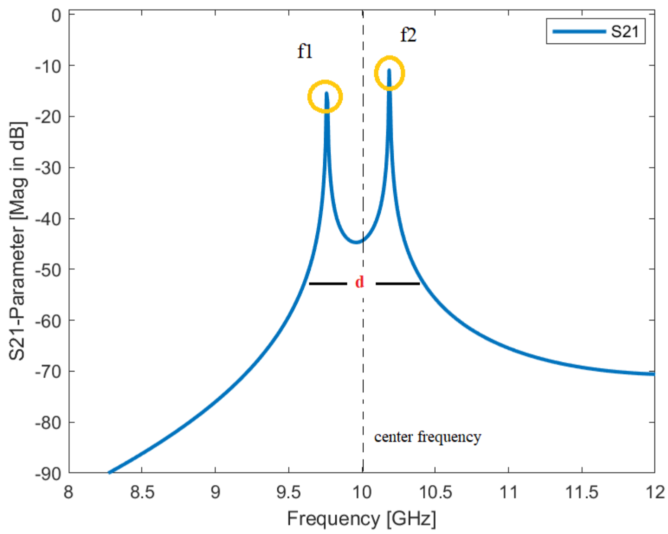

Figure 2.15 Resonant response of the coupled-resonators structure.

The coupling coefficient can be defined with respect to both frequencies f_1 and f_2

$$K = \pm\frac{f_2^2 - f_1^2}{f_2^2 + f_1^2} \tag{2.32}$$

where f_1 is the lower frequency and f_2 is the higher frequency of coupled resonators.

2.4 Quality Factor (Q)

The selectivity of a filter is determined by its quality factor Q and its useful measure of sharpness as well as energy loss of the resonator circuit. The microwave filter's sharpness or stopband property depends on the source of load resistance and the quality factor of capacitor and inductor as well. The quality factor can be derived [1, 2] as

$$Q = \omega \frac{\text{average energy stored}}{\text{average energy loss/second}}$$

As it can be observed from the definition of the quality factor, low loss implies a higher quality factor, Q of microwave filter.

The external quality factor Q_e can be obtained in terms of resonance frequency f_0 and bandwidth Δf of the resonant circuit at $-3dB$, which is stated below [1, 2]

$$Q_e = \frac{f_0}{\Delta f_{-3dB}} \tag{2.33}$$

where the difference frequency at $-3dB$ is

$$\Delta f = f_2 - f_1$$

A high Q factor effect on the steep roll-off of the tuned filter and narrow bandwidth as shown in Figure 2.16 [39].

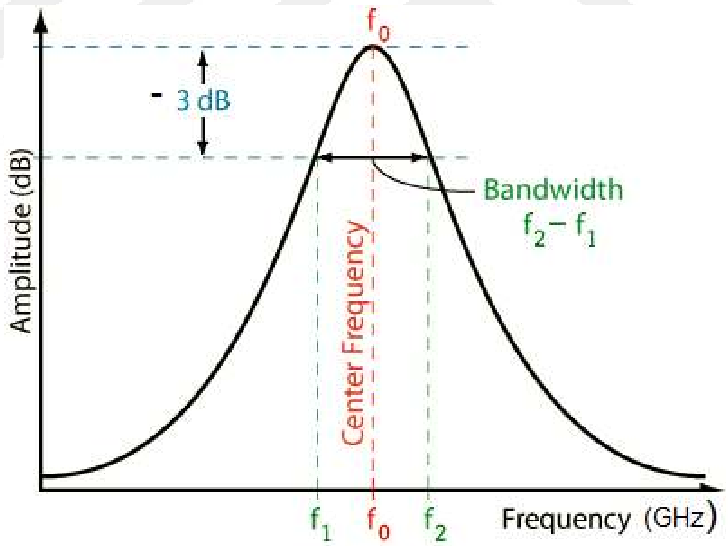

Figure 2.16 The quality factor of the microwave resonant circuit.

2.5 Microwave Filter Design Procedure

In various applications of microwave circuits, a single resonant circuit may not be enough to provide enticing attenuation for a circuit. One possible solution is to couple two or more resonant circuits to each other using either capacitor, inductor, or active devices.

This section introduces the basic concepts of microwave filter design methodology. The procedure of designing a low-pass prototype filter using passive elements such as inductors or capacitors to meet the required specifications will be shown later.

By given a prototype low pass filter, all other filter configurations, including high-pass filter (HPF), a bandpass filter (BPF) and a band-stop filter (BSF) can be readily designed and implemented as well [1].

2.5.1 Chebyshev Response

The Chebyshev filter response has an equal ripple in the passband and a maximally flat stopband as shown in Figure 2.17. The transfer function of the Chebyshev filter response is defined by the amplitude squared of the insertion loss parameter S_{21} as [2]

$$|S_{21}(j\Omega)|^2 = \frac{1}{1+\varepsilon^2 T_n^2(\Omega)} \tag{2.34}$$

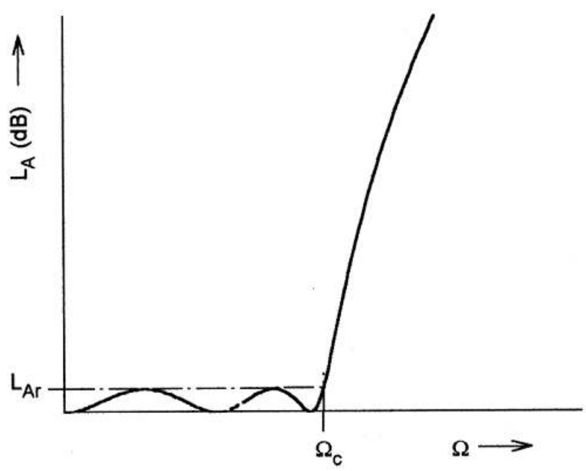

Figure 2.17 Chebyshev lowpass filter response [1].

where ε is the ripple constant and given by

$$\varepsilon = \sqrt{10^{\frac{L_{Ar}}{10}} - 1} \tag{2.35}$$

Here, L_{Ar} is the passband ripple in dB [46, 47] and $T_n(\Omega)$ is the first kind Chebyshev function of order n, defined by

$$T_n(\Omega) = \begin{cases} \cos(n\cos^{-1}\Omega) & |\Omega| \leq 1 \\ \cosh(n\cosh^{-1}\Omega) & |\Omega| \geq 1 \end{cases} \tag{2.36}$$

The Chebyshev filter has the following general rational transfer function [2]

$$S_{21}(P) = \frac{\prod_{i=1}^{n}[\eta^2+\sin^2(i\pi/n)]^{1/2}}{\prod_{i=1}^{n}[p+p_i)]} \tag{2.37}$$

where

$$p_i = j\cos\left[\sin^{-1}j\eta + \frac{(2i-1)\pi}{2n}\right] \tag{2.38a}$$

$$\eta = \sinh\left(\frac{1}{h}\sinh^{-1}\frac{1}{\varepsilon}\right) \tag{2.38b}$$

From the Chebyshev filter's transfer function response, all the transmission zeros are located at infinity left-hand. Therefore, the Chebyshev filters are considered as all-pole filters. The poles of the Chebyshev filter are located on an ellipse in the left half-plane with a major axis of size $\sqrt{1+\eta^2}$ on the $j\Omega$-axis and minor axis of size η on the σ-axis [2]. For an 5^{th} order Chebyshev filter, as we will design our filter later, the pole distribution is shown in Figure 2.18.

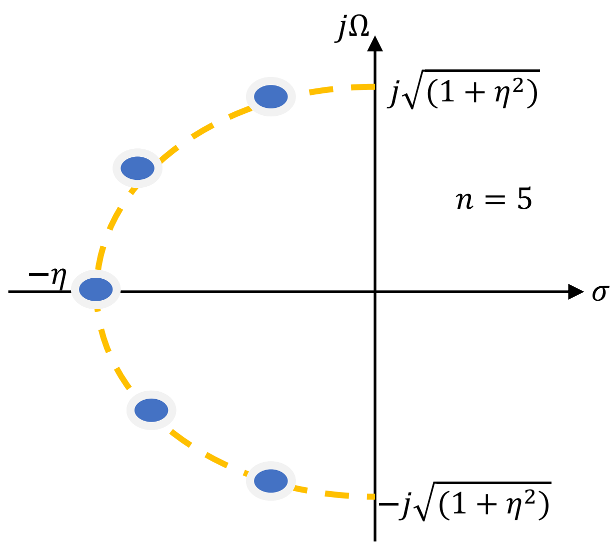

Figure 2.18 Poles distribution of Chebyshev response.

In general, the lowpass prototype filter has the elements values which are normalized to make the source resistance equal to unity $g_0 = 1$, and the angular cutoff frequency $\Omega_c = 1$ (rad/sec). Commonly, the N -pole lowpass prototype filters for Butterworth, Chebyshev, and Gaussian responses have two possible forms or are called dual circuits that give the same response.

The forms are dual from each other, low pass prototype if the first element is inductor from left, and high pass prototype filter if the first element is capacitor from left, both are shown in Figure 2.19. And g_i for $i = 1, \ldots . n$ represents a series inductor or shunt (parallel) capacitor, where n is the order of the microwave filter (number of resonators that construct the whole filter) and represents the number of reactive elements in the prototype structure.

g_0 is known as the source resistance or inductance and is unity, whereas g_{n+1} is defined as the load resistance or the load conductance [2,69].

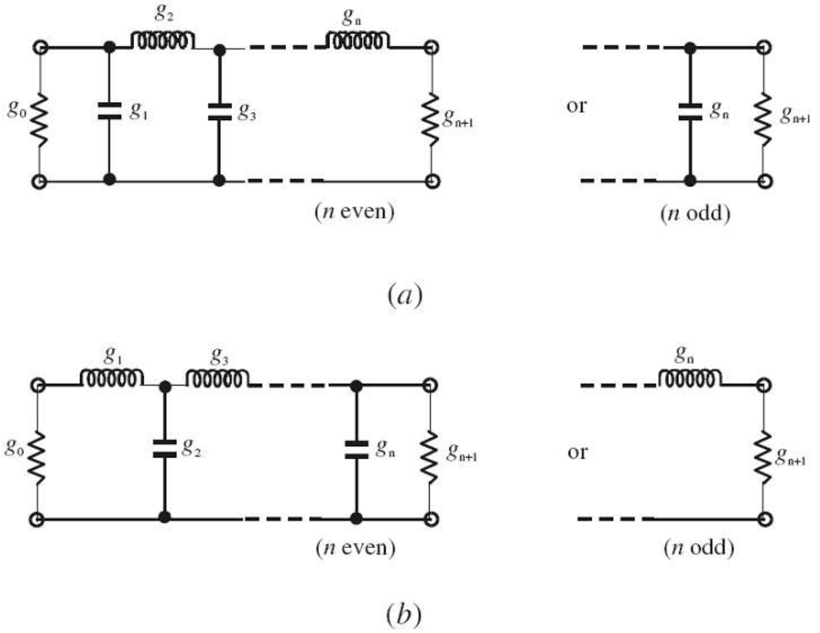

Figure 2.19 N-pole low-pass prototype microwave tuned filter with (a) ladder structure of high pass filter and (b) its dual low pass filter.

2.5.2 Chebyshev Lowpass Prototype

The element values for Chebyshev lowpass prototype filters shown in Figure 2.19 may be obtained for a given passband ripple L_{Ar} and the angular cutoff frequency of $\Omega_c = 1$ (rad/sec) using the following equations [2]

$$g_0 = 1 \tag{2.39}$$

$$g_1 = \frac{2}{\gamma}\sin\left(\frac{\pi}{2N}\right) \tag{2.40}$$

$$g_i = \frac{1}{g_{i-1}}\frac{4\,sin\left[\frac{(2i-1)\pi}{2N}\right].sin\left[\frac{(2i-3)\pi}{2N}\right]}{\gamma^2+sin^2\left[\frac{(i-1)\pi}{N}\right]} \tag{2.41}$$

where $g_i = 1,2,3,\ldots\ldots,N$

$$g_{N+1} = \begin{cases} 1 & N-odd \\ \coth^2\left(\frac{\beta}{4}\right) & N-even \end{cases} \tag{2.42}$$

where

$$\beta = \ln\left[\coth\left(\frac{L_{Ar}}{17.37}\right)\right] \tag{2.43}$$

$$\gamma = \sinh\left(\frac{\beta}{2N}\right) \tag{2.44}$$

The element values for Chebyshev lowpass prototype filter for passband ripple $L_{Ar} = 0.04321$ are given in Table 2.1 for various filter orders $n = 1,\ldots,9$, and $g_0 = 1$ and $\Omega_c = 1$, and other passband ripple tables for $L_{Ar} = 0.1dB$, and for ripple $L_{Ar} = 0.01dB$ can be found in [2], the first kind of Chebyshev polynomials are derived by the recursive relation as [68]

$$T_0(x) = 1$$
$$T_1(x) = x$$
$$T_{n+1} = 2xT_n(x) - T_{n-1}(x)$$

As we are going to design a fifth-order bandpass filter $N = 5$, so the Chebyshev polynomial will be as

$$T_5(x) = 16x^5 - 20x^3 + 5x$$

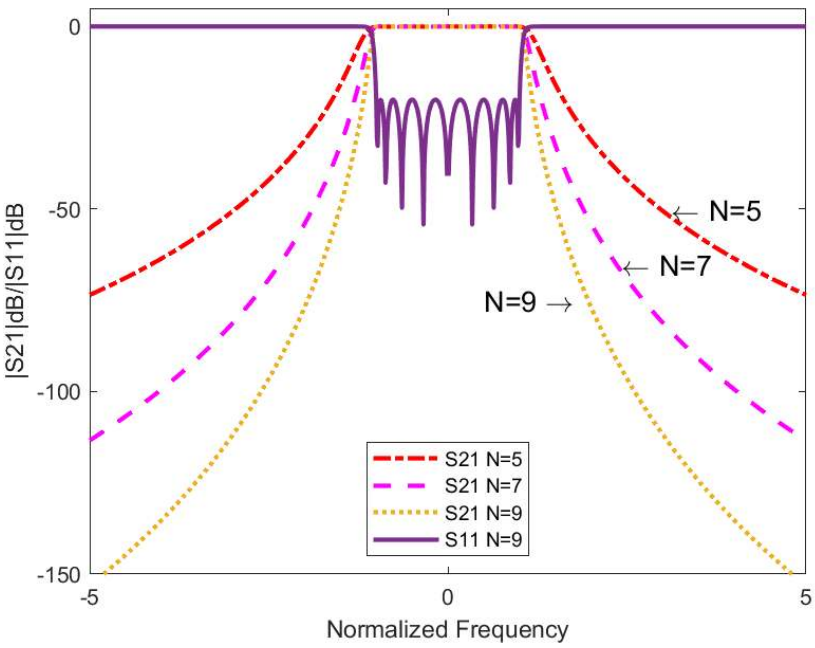

Figure 2.20 Variations of the Chebyshev frequency response in terms of the bandwidth and the sharpness for distinct numbers of resonators $N = 5{,}7$ and 9.

The order n of microwave filter is determined according to the desired specifications; such as the minimum stopband attenuation L_{As} at $\Omega = \Omega_s$ for $\Omega_s > 1$ and passband rippleL_{Ar}. The order of Chebyshev lowpass prototype response is calculated by [1,2] and must be an integer

$$n \geq \frac{\cosh^{-1}\sqrt{\frac{10^{0.1L_{As-1}}}{10^{0.1L_{Ar-1}}}}}{\cosh^{-1}\Omega_s} \tag{2.45}$$

In Chapter 4, the design of the microwave filter will be shown clearly.

The Chebyshev filter response exhibits the equal ripple in passband and maximally flat in stopband [1, 2]. The change of the Chebyshev response as well as change the bandwidth and sharpness (selectivity) of a filter may be implemented based on the number of its resonators, order N.

This means that an increase in microwave filter order N will give more sharpness (selectivity of filter will be better) and enhance the bandwidth (will be wider at the resonant frequency).

In the meanwhile, design of bandpass filter will be more complicated due to the increasing number of filter's resonators and takes more time to get physical dimensions through electromagnetic simulator. Figure 2.20 shows the distinct sharpness of a filter with a Chebyshev response at different orders.

Table 2.1 g_i elements values for Chebyshev lowpass prototype filter for $L_{Ar} = 0.04321\ dB$ [2].

n	g_1	g_2	g_3	g_4	g_5	g_6	g_7	g_8	g_9	g_{10}
1	0.2	1.0								
2	0.6648	0.5445	1.221							
3	0.8516	1.1032	0.8516	1.0						
4	0.9314	1.2920	1.5775	0.7628	1.2210					
5	0.9714	1.3721	1.8014	1.3721	0.9714	1.0				
6	0.9940	1.4131	1.8933	1.5506	1.7253	0.8141	1.2210			
7	1.008	1.4368	1.9398	1.6220	1.9398	1.4368	1.008	1.0		
8	1.0171	1.4518	1.9667	1.6574	2.0237	1.6107	1.7726	0.8330	1.2210	
9	1.0235	1.4619	1.9837	1.6778	2.0649	1.6778	1.9837	1.4619	1.0235	1.0

The sharpness of a filter with a Chebyshev response gets better with an increase in a filter order N, as expected as shown in Figure 2.20. The amplitude-squared transfer function as equation 2.34 describes this type of response, and is given in [1,2].

2.5.3 Bandpass Transformation

According to the International Electrical and Electronics Engineers (IEEE) standard for microwave filter definitions, the bandpass filter is a frequency selective network which has a low attenuation frequency range called the pass-band, that goes between a lower and upper stop-band, both of which have higher attenuation as compared to the pass-band [70].

To transform a lowpass prototype filter circuit which includes passive elements to a bandpass response with passband edge angular frequencies of ω_1 and ω_2, the following transformation formula is used [2]

$$\Omega = \frac{\Omega_c}{\mathrm{FBW}}\left(\frac{\omega}{\omega_0} - \frac{\omega_0}{\omega}\right) \tag{2.46}$$

with

$$FBW = \frac{\omega_2 - \omega_1}{\omega_0} \quad \text{and } \omega_0 = \sqrt{\omega_1 \omega_2} \tag{2.47}$$

where FBW is the fractional bandwidth and ω_0 is the center angular frequency. For inductive elements in the prototype network, the reactance is [1, 2]

$$\Omega_g \rightarrow \omega \frac{\Omega_c g}{FBW\omega_0} - \frac{1}{\omega}\frac{\Omega_c \omega_0 g}{FBW} = \omega L - \frac{1}{\omega C} \tag{2.48}$$

So, the inductive elements g in the lowpass prototype network are transformed into a series LC resonator in the bandpass filter. The elements of the series resonator taking into consideration the impedance scaling [2]

$$\left.\begin{aligned} L_s &= \left(\frac{\Omega_c}{FBW\omega_0}\right)\gamma_0 g \\ C_s &= \left(\frac{FBW}{\omega_0 \Omega_c}\right)\frac{1}{\gamma_0 g} \end{aligned}\right\} \tag{2.49}$$

correspondingly, for capacitive element g in the lowpass prototype network, the admittance is shown as

$$\Omega_g \rightarrow \omega \frac{\Omega_c g}{FBW\omega_0} - \frac{1}{\omega}\frac{\Omega_c \omega_0 g}{FBW} = \omega C - \frac{1}{\omega L} \tag{2.50}$$

So, the capacitive elements g in the lowpass prototype network are transformed into a parallel LC resonator in the BPF filter. The elements of the parallel resonator taking into consideration the impedance scaling [2]

$$\left.\begin{aligned} L_p &= \left(\frac{FBW}{\omega_0 \Omega_c}\right)\frac{\gamma_0}{g} \\ C_p &= \left(\frac{\Omega_c}{FBW\omega_0}\right)\frac{g}{\gamma_0} \end{aligned}\right\} \tag{2.51}$$

Note that the center angular frequency $\omega_0 = \frac{1}{\sqrt{LC}}$, and hence for the series resonator $\omega_0 L_s = \frac{1}{\omega_0 C_s}$, and for parallel resonator $\omega_0 L_p = \frac{1}{\omega_0 C_p}$ [2].

$$\gamma_0 = \begin{cases} Z_0/g_0 & g_0 \text{ being the resistance} \\ g_0/Y_0 & g_0 \text{ being the conductance} \end{cases}$$

The lowpass prototype network to bandpass element transformation is shown in Figure 2.21 [1-2, 68].

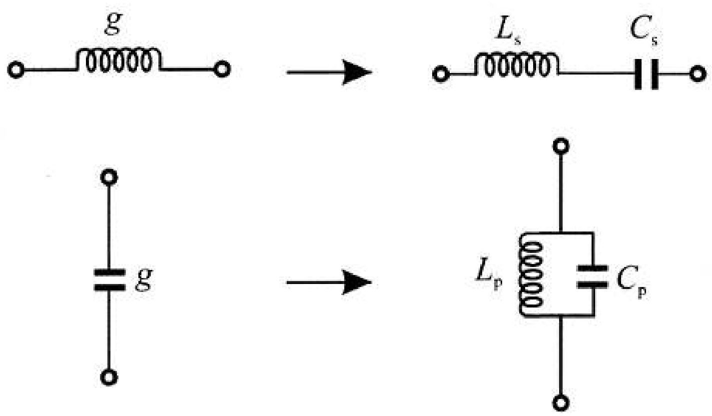

Figure 2.21 Transformation of elements from lowpass prototype to bandpass.

The transformation of the lowpass prototype network of the circuit shown in Figure 2.19 to the bandpass network is shown in Figure 2.22 [2], and the transformation of bandpass filter either shunt combinations is shown in Figure 2.23 (a) or series combinations as shown in Figure 2.23 (b).

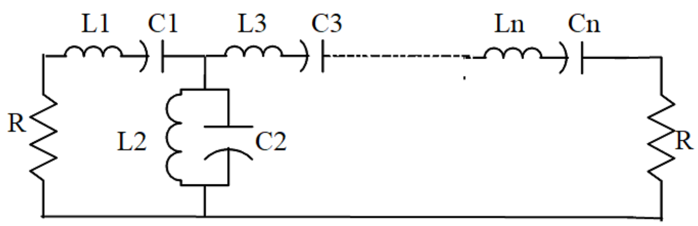

Figure 2.22 Lumped element Bandpass filter.

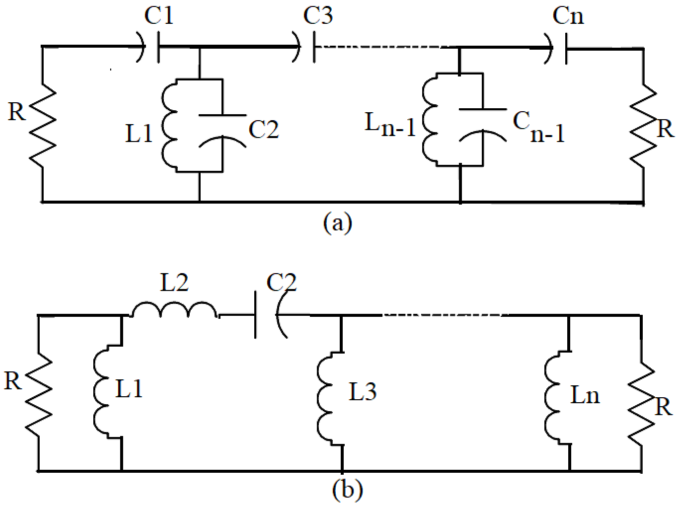

Figure 2.23 Bandpass filter circuits (a) capacitive coupling between resonators (b) inductive Coupling between resonators.

2.5.4 Prototype *k* and *q* values

Define k and q as prototype values, where k represents the coupling between two coupled resonators, and q represents the external coupling. The q prototype values can be derived from prototype g vales as follows [37]

$$q_1 = g_0 g_1 \tag{2.52}$$

$$q_n = \begin{cases} g_n g_{n+1} & \text{for } n \text{ odd} \\ g_n / g_{n+1} & \text{for } n \text{ even} \end{cases} \tag{2.53}$$

where q_1 is the input coupling coefficient and q_n is the output coupling coefficient. The prototype value is derived from prototype g values as follows

$$K_{ij} = k_{ij} \frac{BW}{f_0} \tag{2.54}$$

$$\left. \begin{aligned} Q_1 &= q_1 \frac{f_0}{BW} \\ Q_n &= q_n \frac{f_0}{BW} \end{aligned} \right\} \tag{2.55}$$

The external quality factor, and the external coupling coefficient are related together as to

$$K_e = \frac{1}{Q_e} \tag{2.56}$$

$$Q_{ea} = \frac{g_0 g_1}{FBW} \tag{2.57}$$

$$Q_{eb} = \frac{g_n g_{n+1}}{FBW} \tag{2.58}$$

where Q_e and K_e are the external quality factor and the external coupling coefficient, respectively. The coupling between resonators is given as

$$Kc_k = \frac{FBW}{\sqrt{g_k g_{k+1}}} \tag{2.59}$$

$$FBW = \frac{B.W}{f_0}. \tag{2.60}$$

2.6 Summary

In this chapter, the coupled resonators circuits with two port networks have been presented and discussed in detail. The obtaining of the coupling matrix representation of magnetic, electric and mixed coupled cavities/resonators circuits has been presented as well. The distinct types of microwave filters networks despite the physical structure or configurations have been shown. In addition, the transformation method of low pass prototype filter to bandpass practical filter response has been discussed and derived. In the next chapter, metamaterial technology and its application to synthesize microwave filters will be discussed.

CHAPTER 3

OVERVIEW OF METAMATERIALS AND APPLICATIONS

3.1 Introduction

Submillimeter and millimeter wave components are employed in various applications of electromagnetic filed such as satellite applications, communications, and spectroscopy devices. The bulk of research devoted and presented the number of studies and publications of metamaterials (MMs) with new uncommon constitutive parameters. In this thesis, a waveguide Chebyshev filter based on metamaterial (MM) structure for X-band is proposed and designed. This component can be used as a front-end in the RADAR transceiver circuits or Low Noise Amplifier (LNA) aligned with the antenna in the backhaul application that offers high data rate wireless connectivity. The proposed waveguide filter is stated to work at the X-band frequency [9.15 GHz to 10.44 GHz] centered at 10 GHz resonant frequency. The proposed filter is designed based on the innovative technology of MMs. Hence, in this chapter, an overview covering MMs technology and filter structures based on applications will be briefly discussed.

3.2 Theory of Metamaterial

In general, MMs possess crucial electromagnetic properties that are not available among natural materials [21, 71] and noticeably Negative Index Materials (NIM). They are artificial electromagnetic materials and usually fabricated using various materials or by making a modality of a single material to get a new pattern and obtain required features [11, 16-18, 22, 72-78]. Theoretically, Veselago who investigated and realized the idea of materials whose simultaneous constitutive parameters (electrical permittivity and magnetic permeability) and refractive index could be negative once applied Maxwell's equations for electromagnetism [17].

However, at Veselago's time, there were no materials that have both negative constitutive parameters at the same time until Pendry and Smith et al. have come and made a negative material experimentally [18, 78].

Most popular structures of the MMs are the photonic crystals or electromagnetic bandgap materials (EBG), left-handed (LH) macroscopic parameters, negative permittivity ε , and negative permeability μ and plasmonic materials [22, 71]. The physical materials could be classified into four portions based on the sign of ε and μ of material as shown in Figure 3.1.

Photonic Crystals structures or Photonic bandgap materials (PBG)-structures are distributed periodically and usually synthetic from the dielectric materials [72]. The photonic crystal or PBG controls the propagation of electromagnetic waves and exhibits as a filter which allows to transmit certain band of frequency and block another band of electromagnetic wave [73]. Based on the permittivity and permeability of material and as mentioned above, physically, electromagnetic materials can be categorized into four quadrants. The first quadrant, both parameters are positive, or the electromagnetic wave is propagating forwardly $\varepsilon, \mu > 0$ in a right-handed material (RHM) or double-positive (DPS) material and most common natural dielectric materials (isotropic materials such as water and glass) fall under this quadrant [78].

At certain bands of frequency, electric Plasmas material exhibits the behavior in second quadrant $\varepsilon < 0, \mu > 0$ or Epsilon Negative (ENG) such as gold and silver in the visible frequency domains and support evanescent waves, and sometimes this quadrant is also identified as electrical MM structures [78]. Mu-Negative (MNG) $\varepsilon > 0, \mu < 0$ or magnetic MM structure which whose material falls under the fourth quadrant. Furthermore, if one of the constitutive parameters epsilon or mu is negative then the refractive index becomes an imaginary value this means be attenuation. Materials exhibit and fall under third quadrant Left-Handed Materials (LHM) $\varepsilon < 0, \mu < 0$ or Double Negative (DNG) materials and propagating waves travel backwardly (backward media); which is a combination of epsilon negative and mu negative materials and once the place with each other periodically as a unit cells leads to both negative refractive index.

Artificial or engineered materials have been constructed which have also DPS, MNG and ENG properties. Currently, the third quadrant is considered the common demonstration of artificial materials [71], all quadrants are classified in Figure 3.1 in details.

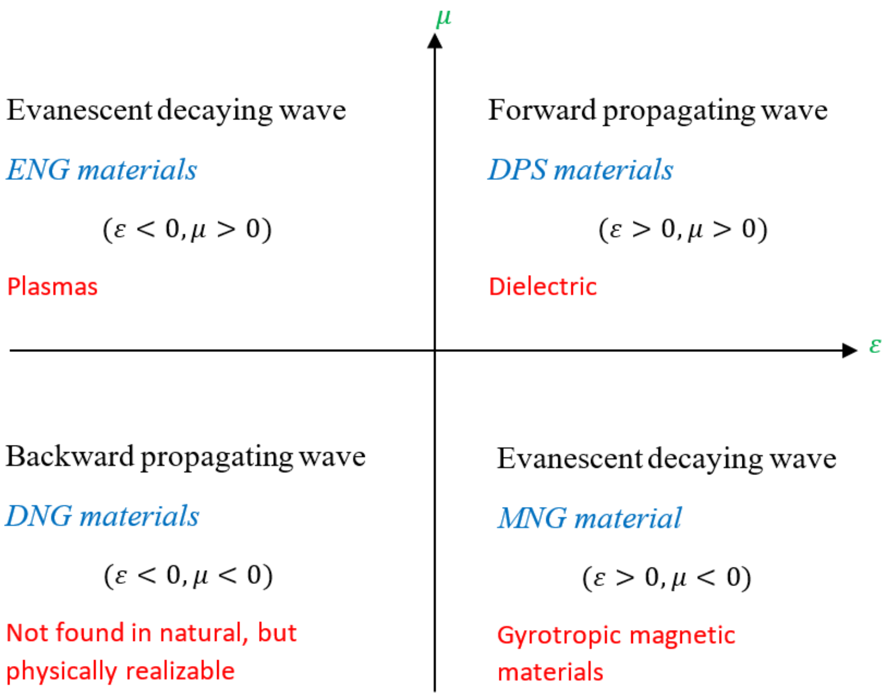

Figure 3.1 Classification of material based on the constitutive parameters [71].

Eventually, double negative materials have been realized from metallic patterns such as arrays of thin metallic wires and aligned with open metallic loops or rings which are called Split Ring Resonators (SRRs) [78]. SRRs and Complementary SRRs (CSRRs) provided negative μ, and negative ε, respectively, and later negative constitutive materials were realized by loading the transmission lines with capacitors and inductors as discussed in [18, 76-78].

3.3 Electromagnetism and Metamaterials

Due to the time-varying motion of electric charges in a material and generating magnetic field $\vec{H}$ as coupled with electric filed $\vec{E}$, the interaction between the magnetic field and electric field, physically, is known as electromagnetic filed [1].

The electromagnetic wave is propagating in a medium and is manipulated by the constitutive parameters (permeability μ, permittivity ε, and conductivity σ) of medium and these parameters determine the response and reaction of physical material once exposed to electromagnet filed, usually external time-varying wave. It is well known most materials are dispersive and lossy materials which mean constitutive parameters are complex and they depend on frequency. An isotropic plane wave propagation means conductivity will be zero. The complex propagation constant γ, and the intrinsic impedance η and the refractive index are given in [1].

$$\gamma = \alpha + j\beta = j\omega\sqrt{\mu\varepsilon} \tag{3.1}$$

$$\eta = \sqrt{\frac{\mu}{\varepsilon}}$$

$$n = \sqrt{\varepsilon_r \mu_r} \tag{3.2a}$$

where ω is the angular frequency, α is attenuation constant, and β is the phase shift or wave number. From equation 3.1, if the permittivity and permeability of medium are real constants and have the same sign, then the propagation constant will be purely imaginary. Meaning that the electromagnetic wave is in propagating mode and intrinsic impedance will be real as well. However, if one of the constitutive parameters is negative, then the propagation constant will be real and intrinsic impedance will be imaginary, i.e. either capacitive or inductive.

The tricky case is when permittivity and permeability are negative, the sign of phase shift β may be either negative or positive if equation 3.1 is substituted due to the square root.

$$\vec{k} = \beta\hat{k} \tag{3.3}$$

$$\vec{k} \times \vec{H} = -\omega\varepsilon\vec{E} \tag{3.3a}$$

$$\rightarrow \ \hat{k} \times \hat{H} = -\frac{\varepsilon}{|\varepsilon|}\hat{E} \tag{3.3b}$$

$$\rightarrow \ \hat{k} = \frac{\varepsilon}{|\varepsilon|}\hat{E} \times \hat{H} \tag{3.3c}$$

where $\hat{k}$ propagation vector and the hat above the vector represents the unit vector $\frac{\vec{a}}{|a|}$ parallel to the vector, and $\vec{a}$ any vector. $\vec{E}$, $\vec{H}$ are the electric field intensity and magnetic field intensity, respectively [1].

In a like manner,

$$\vec{k} \times \vec{E} = \omega\mu\vec{H} \tag{3.4a}$$

$$\rightarrow \ \hat{k} \times \hat{E} = \frac{\mu}{|\mu|}\hat{H} \tag{3.4b}$$

$$\rightarrow \ \hat{k} = \frac{\mu}{|\mu|}\hat{E} \times \hat{H} \tag{3.4c}$$

Once applying the Poynting power vector which represents the instantaneous power density vector or the energy flow vector associated with the electromagnetic waves at a given point [1]

$$\hat{S} = \hat{E} \times \hat{H} \tag{3.5}$$

By comparing the previous equations (3.3), (3.4) and (3.5) it could be noticed that if both permittivity and permeability parameters are positive quantities then the Poynting power vector $\hat{S}$ and propagation vector $\hat{k}$ are parallel with perpendicular wave propagation. However, if both constitutive parameters are negative then the Poynting power vector $\hat{S}$ and propagation vector $\hat{k}$ are antiparallel, meaning that vector $\hat{k}$ points towards the source or two vectors are in opposite direction.

If only one of the constitutive parameters is negative, the propagation constant γ will be real and the wave will be decayed (evanescent mode) or no propagation in this case. Therefore, the propagation constant must be positive quantity as well as wave decays apart from the source by using the form $e^{-\gamma z}$ [1].

Negative refractive index may be obtained from formula (3.2a) based on the relative constative parameters of a material ε_r and μ_r. However, these relative parameters can occur negatively in nature but not at the same time or simultaneously or not be discovered yet.

To achieve a negative refractive index when relative constitutive parameters are negative [1] as formula (3.6)

$$\varepsilon_r = -|\varepsilon_r| = |\varepsilon_r| e^{\pm j\pi}$$

$$\mu_r = -|\mu_r| = |\mu_r| e^{\pm j\pi}$$

$$\varepsilon_r \mu_r = |\varepsilon_r||\mu_r| = |\varepsilon_r||\mu_r| e^{\pm 2j\pi}$$

$$n = \sqrt{\varepsilon_r \mu_r} = j\sqrt{|\varepsilon_r|}.\,j\sqrt{|\mu_r|} = \pm\sqrt{|\varepsilon_r||\mu_r|} \tag{3.6}$$

3.4 Metamaterials Structures

Several structures of MMs are realized and synthesized over the past twenty years and electromagnetic MMs become an active field among researchers in both the physics and distinct engineering fields. Here in this section, a spot on the commonly used of MM structures or patterns will be covered. As on interdisciplinary research, MMs structures may be classified into distinct categories based on several criteria. From a resonant frequency point of view or operating wavelength, MMs can be categorized as microwave MMs, terahertz MMs, and photonic MMs.

From a spatial order point of view, there are one-dimension (1D) MMs, two-dimensions (2D) MMs, and three-dimensions (3D) MMs. From a material point of view, there are metallic and dielectric MMs [79]. In Figure 3.2 the construction of microwave MM is classified and shown.

3.4.1 Resonant Structures

Pendry and Smith et al. have constructed experimentally the resonant structures which having electrical and magnetic resonance over the past twenty years single or double negative parameters [18, 77-78].

The resonant MM structures work based on the principle of lagging between electric plasmas and magnetic dipole with respect to electric and magnetic fields about 180^0 and once the frequency is somewhat below the resonance [18, 77].

Based on thin metallic wires for negative constitutive parameters (negative permittivity materials and negative permeability materials) the analysis of low frequency for narrow bandwidth plasma wave structures is synthesized and given in [18]. After three years, in 2001, from theoretical analysis, practical Negative Refractive Index (NRI) material which means obtaining both negatives of constative parameters by using thin wires and SRRs with each other was experimented and demonstrated [78].

Most electromagnetic MM elements are considered as resonant structures and then the challenge arises on how to make those resonant structures small (reducing size of application). It is not trivial to satisfy the desired for the elements to be resonant and concurrent to be small relative to the wavelength of the electromagnetic wave inside material [79].

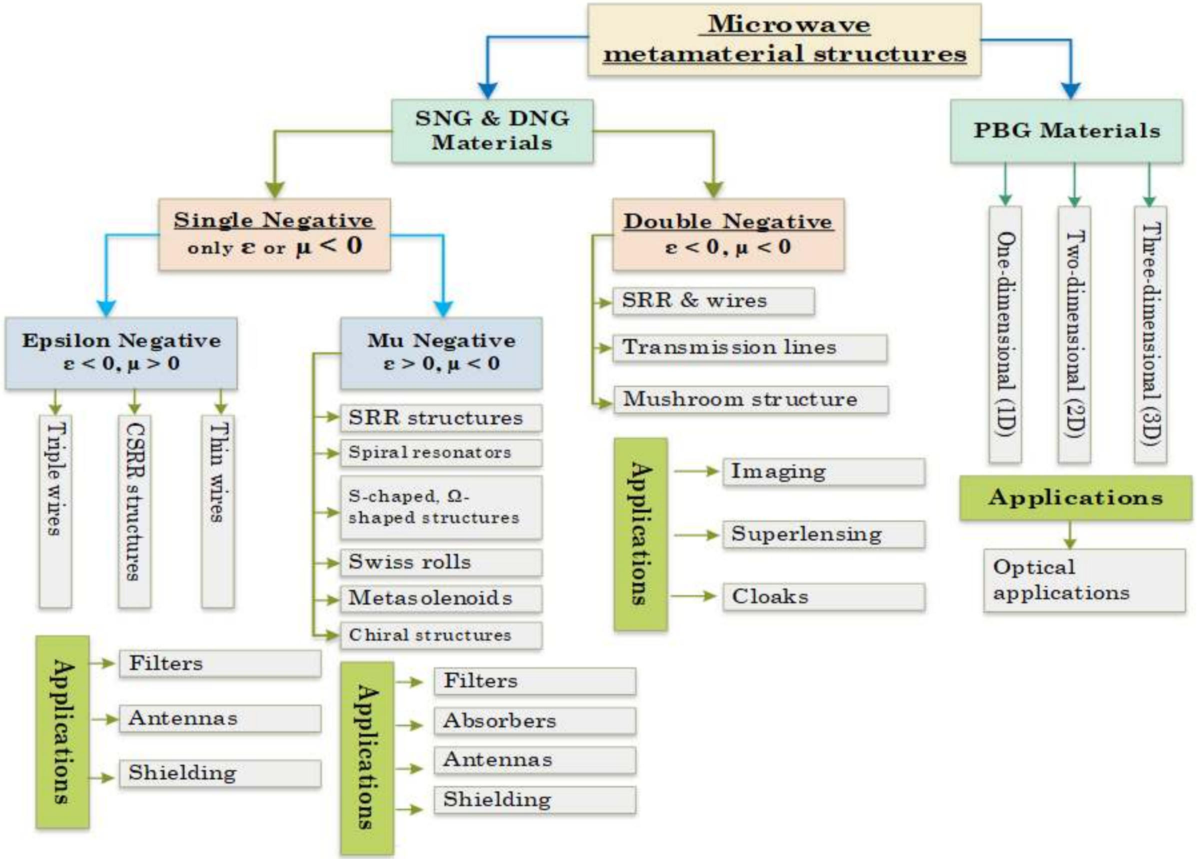

Figure 3.2 Microwave metamaterial classification.

3.4.2 Magnetic or μ-Negative Metamaterials

At high frequencies, due to the materials inherently small magnetic dipole moments, the responses of natural diamagnetism materials are almost negligible as mentioned in [18, 80-81]. Pendry has created and proposed a strong diamagnetism by using an array of artificial substances [18] and known as SRRs as shown in Figure 3.3 and Figure 3.4, SRRs (round or square geometrically) are considered the most widely and the first structure used mu-negative MNG-structure and they are depicted as high conductive resonance model or structure due to the high the inductance balances [21]. The inductance balance is because of the existence capacitance (gap) between two rings or loops [21].

Theoretically, the responses of SRRs are modeled based on the effective medium approach as given in [18]. As shown in Figure 3.3(b), SRRs are constructed and composed by having metallic rings or loops, with a hollow gap between each ring, and the gaps far away 180^0 from each other [18]. The gap between two rings (inner and outer rings) acts as a capacitor, and the rings themselves act like inductors (surface charges), structured LC resonant circuits [18, 72, 82]. Due to the SRR, the magnetic dipole will be lagging the magnetic field by roughly 180^0 and resulting negative permeability as given in [72].

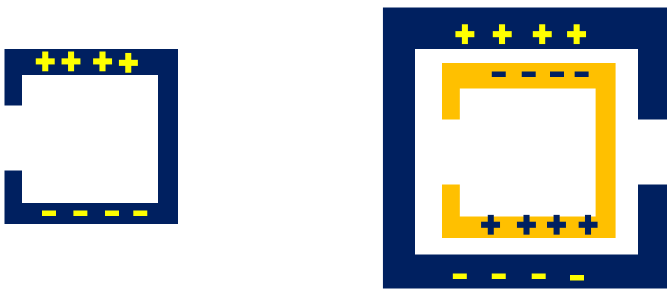

(a) (b)

Figure 3.3 (a) Single SRR square shape, and (b) double DSRR square shape.

$$\mu_{eff} = 1 - \frac{\frac{\pi r^2}{a^2}}{1 - \frac{3lc}{\pi \omega^2 ln\left(\frac{2b}{d}\right) r^3} + \frac{2l\sigma}{\omega r \mu_0} i} \tag{3.6}$$

where r is the inner radius of the inside loop, b is the thickness of the loop, d is the spacing between loops, a is the constant of a grid of an SRR in the plane of the loops, l is the grid constant along the axis of the loops as shown in Figure 3.4. The main disadvantage of SRRs is the narrow-band frequency where $\mu_{eff>0}$ as well as increase electromagnetic loss.

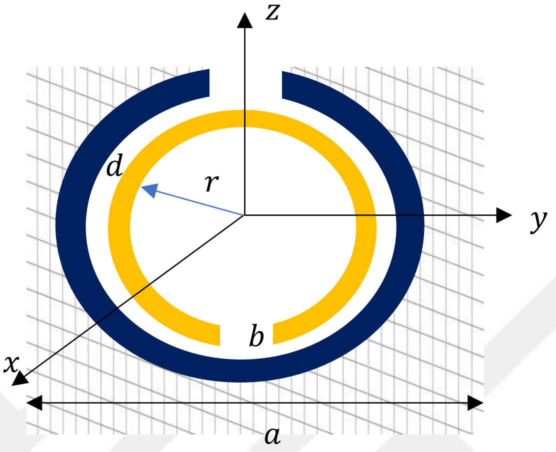

Figure 3.4 double split ring (loop) resonator (circular shape).

3.4.3 Electrical or ε-Negative Metamaterials

Similarly, the Electric SRRs (ESRRs) have the properties of SRR and full analogy with them in general [16]. The design of ESRR MM, as shown in Figure 3.5, has two gaps exhibit capacitive and placed on the opposite sides on the ring/loop. The resonant frequency (operating wavelength) can be excited when the radiation is incoming and has an electric field polarized along the ring or loop itself on x-axis [16].

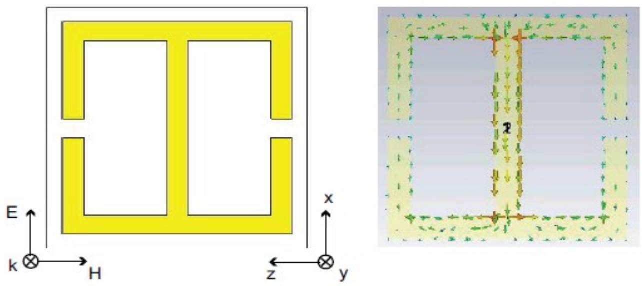

(a) (b)

Figure 3.5 (a) A schematic of an electric split ring resonator (ESRR). (b) Current through the ERR [16].

Applying or exciting electric field $\vec{E}$ to a conductor, and according to Maxwell's equations, electrons will be generated and move along the conductor causing an internal electric filed but on the opposite direction of applied $\vec{E}$ [1]. This case is fully analogy to a simple harmonic oscillator [80]. Pendry in 1996 used thin wire array to achieve high inductance and hence, increased the effective mass of electrons which is the ratio of the exerted force to the acceleration of an electron [80].

Nevertheless, increasing the effective mass of electrons is inversely proportional to the square of plasma frequency ω_p, and then using the thin wire array is likely to bring plasma frequency into the microwave portion [80]. Plasma frequency ω_p and effective electrical permittivity ε_{eff} are given by following formulas [16,80,83]

$$\omega_p = \frac{c}{a}\sqrt{\frac{2\pi}{\ln\left(\frac{a}{r}\right)}} \tag{3.7}$$

$$\varepsilon_{eff} = 1 - \frac{\omega_p{}^2}{\omega\left(\omega - \frac{i\varepsilon_0 a^2 \omega_p{}^2}{\pi r^2 \sigma}\right)} \tag{3.8}$$

where r is conductor (individual thin wire) radius and smaller than a, a is distance or spacing between wires, c is speed light in vacuum, and σ is the conductivity of a material.

Interestingly, if the incident plane wave of a magnetic field $\vec{H}$ or its vector is perpendicular to the SRR structure Figure 3.3 or Figure 3.4, similarly, negative permeability will be observed MNG. Hence, if the vector of the magnetic field is incident parallelly with SRRs, there will not be any influence of charges or induced current, or in other words, negative effective permeability μ_{eff} will not exist in such a case [22]. With a view to beat the disadvantage of SRR anisotropy, a method by placing the same SRR planar in three orthogonal space directions, as a result, a group matrix of unit cells will be achieved [78].

The CSRRs structures are a negative image of the SRRs structures, and CSRRs belong to epsilon negative materials and negative effective permittivity is achieved. In this thesis we will see in next chapter using this type of MM to design the proposed bandpass filter based on CSRR unit cell as shown in Figure 3.6 where w is the metal etched width, d is the width of metal, a is the width of the cell and r is the radius of the circle.

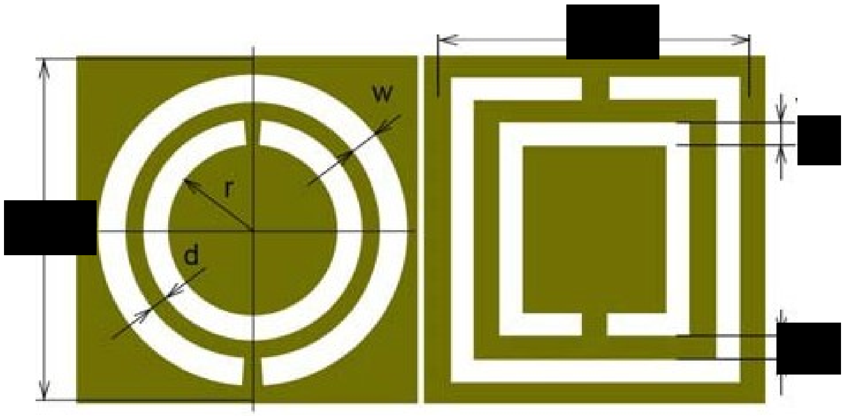

Figure 3.6 Unit cell of CSRR circular and square shapes.

3.4.4 Photonic Crystal PBG Metamaterials

Photonic Bandgap (PBG) materials or photonic crystal materials are engineered structures which could control the Electromagnetic Wave (EM) propagation inside material, and the way of designing the PBG materials is able to inhibit the propagation of electromagnetic wave or permits electromagnetic wave (include light waves) to propagate solely aligned with specific direction and usually is defined[84-86]. This type of MM based on frequency band with optical frequencies and the wavelength period differentiates the photonic crystal MM from PBG materials [86].

The principle of propagation of the electromagnetic wave in PBG materials is like the principle of the electronic band structure in semiconductor; therefore, the ability to control EM radiation proceeding from photonic band structure [84]. The electrical permittivity ε of the PBG materials alters regularly or periodically in space with a period which passes Bragg diffraction of electromagnetic wave [84].

Photonic crystal materials have the advantage of periodicity of electric permittivity alternating so selecting the frequency band range of photonic bandgap material. PBG materials are composed of dielectric or/and metal and could be 1D, 2D, and 3D depending on the number of spatial directions that the changing of the refractive index could be recognized.

The property of PBG weaknesses is extensively used in waveguides and micro-resonators based on photonic crystal material. The widespread applications in microwave technology include photonic integrated circuits as well, microwave filter components with high selectivity, and Global Positioning Satellite (GPS) based antenna [22].

3.4.5 Double Negative DNG Metamaterials

As aforementioned, double negative materials have both permittivity and permeability are negative and accordingly, the refractive index is negative. The most popular tactics to fabricate and design MMs with a negative refractive index are divided into three main approaches: Thin wires & SRRs, Transmission lines, and Mushroom structures. In [78], Smith et al have already mentioned and discussed the combination of thin wires array and SRR with each other. Negative values of constitutive parameters are obtained from a corresponding constructed structure is confirmed experimentally. The essential properties of the composite structure have been tested numerically as well [87].

Another approach to designing DNG MMs is transmission line techniques which are prevalently used in the microwave approach [21, 72, 89]. Unlike the SRR with a thin wires approach, the transmission line technique is mostly planar and non-resonant structure. The transmission line MM approach is typically composed of SRR and its image CSRR which are coupled by microstrip technology or by embedding the structure to a waveguide, and to enhance bandwidth with minimizing losses the lumped element circuit could be added in a unit cell [72, 89].

The third method to design DNG MMs is using Mushroom structure [90] and was given this name because of its shape which simulates a mushroom caps and stems. To design DNG MM unit cells, metal patches are designed by row and columns like matrix over the conductivity layer and the gaps between matrix elements form capacitive and vias from inductive [84, 90] as shown in Figure 3.7.

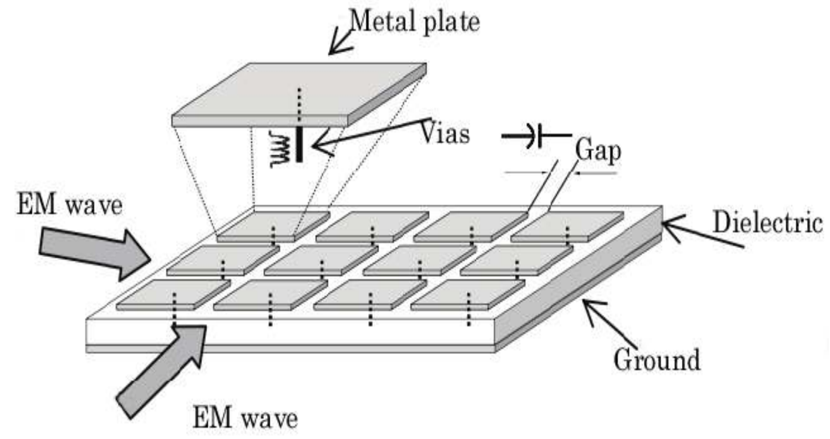

Figure 3.7 DNG metamaterials based mushroom techniques [84].

3.4.6 Bi-isotropic and Bi-anisotropic Metamaterials

Based on the independency of electric filed $\vec{E}$ or magnetic field $\vec{H}$ responses which realized by the constitutive parameters, electric permittivity, and magnetic permeability, MMs are divided into a single negative (SNG) and double negative MMs (DNG). Nevertheless, in electromagnetic MMs examples, the time-varying current generates a varying electric field and then the electric field generates a magnetic field that they are coupled with each other as Maxwell mentioned in his equations and called electromagnetic coupling. Such material stands for as bi-isotropic material or media since this material exhibits electromagnetic coupling (electric-magnetic coupling) and that is anisotropic as well as called sometimes bi-anisotropic [84, 85].

3.4.7 FSS and Metamaterials

Frequency Selective Surface (FSS) or metasurfaces & metafilms represent planar MMs [91]. Planar MMs are the main class of low dimensional engineered or fabricated materials. Generally, FSS materials are formed periodically by metal films on a subwavelength scale and ignoring thickness which those wavelengths mostly thinner than the wavelength of light waves. Planar MMs are two-dimensional 2D materials unlike MM three-dimensional 3D materials [21, 91].

FSS or metasurface materials robustly interact with electromagnetic coupled waves that planar materials can resonantly absorb, reflect or transmit without diffracting electromagnetic radiation [91]. However, planar MMs play a vital role in improving the functionalities and performances of the optical components and devices within narrow frequency bands that could be fabricated and engineered such as polarizers, lenses, filters, splitters, and prisms, etc. [91].

3.5 Application of Metamaterials

Thanks to their abnormal interaction and complementary with the electromagnetic field, MMs offer many different viewpoints as well as unexplored solutions. MMs gave answers to exciting inquiries and questions, which solved many design problems easily and prevailed the substantial limitations and drawbacks of conventional and novel technologies. As of the first MM verification that had been made and tested experimentally that given in [78], it is now familiar in electromagnetics research to think similarly in terms of materials with negative refractive index, negative magnetic permeability, negative electrical permittivity with distinct values whether very low or very high. By this new methodology and technology, the whole classical electrodynamics and the whole applied electromagnetics concepts were possible to revisit with a completely distinct perspective, which led to:

a. New electromagnetic material properties are found,
b. Electromagnetic concepts are generalized and broadened along with different fields,
c. Essential limitations of conventional materials are overcome,
d. The performances of existing applications are improved and developed through several designs implicating the new properties of the negative index materials (MMs),
e. New devices are applied and conceived conceptually.

It is worth mentioning here using MMs has led to enhance the performance of electromagnetic devices as well as it has helped to miniaturize the overall physical size of EM devices that have been designed by MMs. For instance, the usage of MMs has allowed achieving microwave filters, antennas, absorbers, clocking, superlens, Invisible submarines, solar cells, photonics OR optoelectronics, and ultra-high capacity storage device [16, 72, 83-92], so forth and so on.

There are many and various applications areas of MMs. Among these areas, in this thesis we will concentrate on application of MMs to microwave bandpass filter.

3.5.1 Metamaterial Microwave Filters

Filters, in general, are components designed with the purpose of selecting or transmitting signals over the specified band and rejecting signals over the other bands. Despite various forms of microwave filters are available in the literature, they all have the same common viewpoint by which their performance is evaluated using the distributed network concept, assuming that they usually consist of periodic structures exhibiting passband and stopband characteristics in various frequency bands [1].

A variety of waveguide filters with distinct characteristics of low insertion loss, high-quality Q factor, and sharp frequency selectivity have been proposed for various applications [24-25, 93-95]. For example, inductive irises-coupled resonators are implemented into waveguide [95], stepped-impedance resonators are employed in the design of an X-band waveguide filter [96]. Furthermore, a co-planar waveguide filter by using the bent stub and folded structure [30], E-plane waveguide filter with periodically loaded resonators [42], T-shaped resonators [36], Substrate-Integrated Waveguide (SIW) technique [40], microwave filters with quarter-wavelength resonator based on impedance and admittance inverters' method [33], an aperture engraved in the middle common ground of the vertically stacked cavities [39], U-shape slots on substrate integrated Waveguide with low temperature co-fired ceramic (LTCC) [41], and 3D printed inserted into waveguide filter [45] are implemented.

Thus far, and as mentioned above, all microwave filters are designed conventionally and used one or both positive constitutive parameters electrical permittivity and magnetic permeability. In recent studies and based MMs, many microwave filter structures are synthesized and designed. For instance, SRRs played a vital rule in the design of microwave filters because of resonance structures of SRRs and their resonance behavior, they can be used for miniaturizing overall microwave devices and enhancing the filter sharpness.

Waveguides embedded with MM in various forms with diverse electromagnetic properties are designed to reduce the size of the filter [97]; to have a narrow-band filter in a rectangular waveguide using CSRR has been proved [98].

Using different models of CSRRs inside rectangular waveguide to design bandpass filter for single and dual-mode has been demonstrated [99], and a compact dual-band waveguide band-stop filter using double SRR structure is designed [100]. In addition to these studies, gradually, MMs have spread out in many syntheses and designs to improve performance whether cutoff frequency or bandwidth of filter by using coupled SRRs and a negative image of CSRRs [5, 101-103] are proposed and designed.

All previous studies have discussed and focused on limitations of filter specifications, such as dimensions of meta-resonators, insertion loss, quality factor, bandwidth and selectivity of the filter. In the next chapter, we will show and discuss in deep detail of microwave filter based on MM and enhancing bandwidth with shortening physical size. Finally, most of the MMs, such as SNG structures (ε negative or μ negative), DNG structures, or combination of DPS and DNG structures, are strongly implemented in waveguides applications, power dividers, resonators, absorbers, couplers, filters, and antennas.

Metamaterials technology play a vital role in innovative designs of microwave and millimeter-wave devices particularly in microwave engineering field and based on the its unnatural properties, miniaturizing microwave filters, antenna technology as Multi Inputs Multi Outputs (MIMO), microwave hybrid ring, resonators, dual-band filters, and directional couplers based transmission lines are studied and implemented over the conventional technologies [104].

3.6 Summary

In this chapter, we discussed and explained the MM technology and its types based on electromagnetic constitutive parameters and frequency bands. Then we have shown the applications of MMs and how this technology miniaturized the microwave components and how MMs became modern technology for researchers throughout the world particularly in designing filters, antennas and anther applications based on SRRs or CSRRs structures. Finally, a full microwave MM structure is built up and shown in this chapter.

CHAPTER 4

DESIGN OF X-BAND WAVEGUIDE FILTER BASED CSRR

4.1 Introduction

The waveguide filter is a crucial device in a vast variety of microwave systems, containing mobile radio systems, satellite, and radar transceiver communications circuits. This chapter exhibits design and synthesis of bandpass Chebyshev waveguide filter for X-band $[9.15\ \text{GHz} - 10.44\ \text{GHz}]$. Two waveguide filters have been synthesized and designed, the first filter is implemented on the conventional technology by using waveguide H-plane junctions between resonators, and the second is metamaterial waveguide filter based on modern technology of Complementary Split Ring Resonator (CSRR). The implementation of the microwave filter is done by using rectangular waveguide resonators that are fitting for low cost and easy to design and fabrication. In addition, the rectangular waveguide has advantages in microwave frequencies because of their high unloaded quality factors Q_u and their capability of dealing with high power [1].

Theoretically, rectangular waveguide resonators in terms of the design technique of the waveguide cavity components are discussed first. Next, the extraction of the coupling coefficients matrix among resonators (internal and external coupling) and quality factor Q from the physical structure will be explained. Then, various coupling structures involving capacitive and inductive apertures will be illustrated in this chapter as well. Lastly, the design and simulation results of the proposed waveguide filter implemented by Computer Simulation Computer (CST) with the optimization method will be presented throughout this chapter.

4.2 Waveguide and Cavities

Waveguides, such as transmission lines, are structures used to guide electromagnetic radiation from the source to the sink. However, the pattern of waves within waveguides and transmission lines is quite dissimilar Transverse Electromagnetic (TEM) Transverse Electric (TE) and Transverse Magnetic (TM). The distinction in these modes comes from the basic differences in geometry or physical structure for a transmission line and a waveguide [1]. While TEM mode is not supported by waveguides, it is the fundamental type of mode for transmission lines below 1 GHz [1]. Modes of waves within waveguides are TE or TM.

In general, waveguides can be categorized as either hollow rectangular or circular metal waveguides as shown in Figure 4.1 or rectangular or circular dielectric waveguides as shown in Figure 4.2. Metal waveguides regularly take the form of an enclosed conducting metal line or pipe.

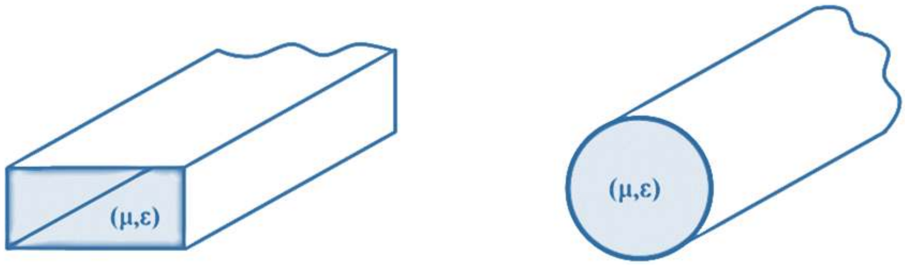

Rectangular waveguide cross section Circular waveguide cross section

Figure 4.1 Metal circular and rectangular waveguides [1].

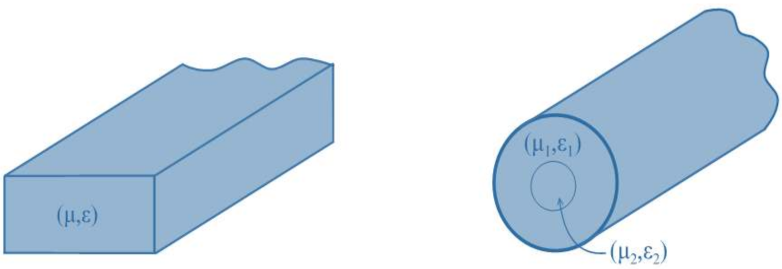

Rectangular dielectric slab waveguide Circular optical fiber waveguide

Figure 4.2 Dielectric circular and rectangular waveguide [1].

The propagating of waves inside the conducting waveguide can be represented by a reflection from the conducting walls of the waveguide. The dielectric waveguides consist of dielectrics and employ reflections from dielectric interfaces usually covered by air to propagate the EM energy along the waveguide [1].

The rectangular waveguide is one of the earliest types of transmission lines and famous among waveguide resonators that are used to transfer microwave signals at high frequency and are still used currently in many applications due to their less power consumption and high-power handling capacity [1]. A wide range of microwave components such as isolators, filters, detectors, couplers, and attenuators are widely available for various standard waveguide sizes and frequency bands from 1 GHz to over 220 GHz [1].

A rectangular waveguide cavity or waveguide resonator which its physical dimensions $a > b$ can be considered as a small part of a waveguide (rectangular cross section) and shorted at both sides with conducting plates. Figure 4.3 shows a section of a rectangular waveguide cavity with dimensions width a, height b, and length d, for $b < a < d$ [1].

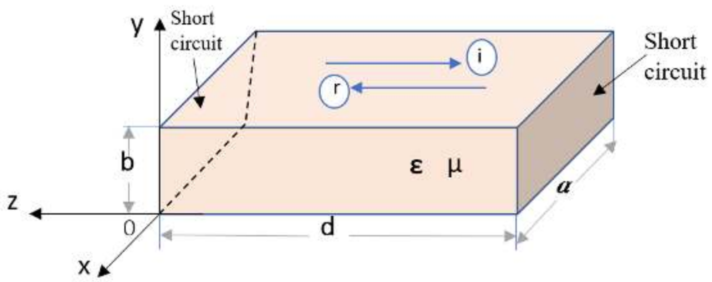

Figure 4.3 Rectangular Waveguide Cavity.

Generally, for a rectangular waveguide, the transverse electric fields (E_x , E_y) of the TE_{mn} or TM_{mn} mode can be written as [1]

$$\bar{E_t}(x, y, z) = \vec{e}(x, y)\left[A^+ e^{-j\beta_{mn}z} + A^- e^{j\beta_{mn}z}\right] \tag{4.1}$$

where $\vec{e}(x, y)$ represents the transverse variations of electric field intensity in $\hat{x}$ and $\hat{y}$ directions, A^{+} and A^{-} are the random magnitudes of the waves which are traveling in the $\mp\hat{z}$ directions. The propagation constant or phase shift β_{mn} is given by

$$\beta_{mn} = \sqrt{k^2 - \left(\frac{m\pi}{a}\right)^2 - \left(\frac{n\pi}{b}\right)^2} \tag{4.2}$$

where $k = 2\pi f_0\sqrt{\mu\varepsilon}$, and μ and ε are the magnetic permeability and electrical permittivity of the material inside the waveguide, and m and n are integer numbers represent the variations of modes in $\hat{x}$ and $\hat{y}$ direction, respectively.

Application of the boundary conditions for the rectangular waveguide cavity at $z = 0, d$ requires that $\overline{E_t}(x, y, z) = 0$. Stipulating the case $E_t = 0$ at $z = 0$ to equation (4.1) yields $A^{+} = -A^{-}$, and by applying the supposed case $E_t = 0$ at $z = d$, will yield $\beta_{mn} d = l\pi$ where $l = 1, 2, 3 \cdots$.

This means that the length of the waveguide cavity section has to be multiple integers of the half-guided $\frac{\lambda_g}{2}$ at the resonant frequency f_0 of waveguide. The cut-off wavenumber of the rectangular waveguide cavity can be defined as [1]

$$k_{mnl} = \sqrt{\left(\frac{m\pi}{a}\right)^2 + \left(\frac{n\pi}{b}\right)^2 + \left(\frac{l\pi}{d}\right)^2} \tag{4.3}$$

where the indices m, n, l represent the number of half wavelength variations in the $\hat{x}$, $\hat{y}$ and $\hat{z}$ directions, respectively. The Transverse Electric TE_{mnl} or the Transverse Magnetic TM_{mnl} modes will have a resonant frequency as

$$f_{mnl} = \frac{c k_{mnl}}{2\pi\sqrt{\mu_r \varepsilon_r}} = \frac{c}{2\pi\sqrt{\mu_r \varepsilon_r}} \sqrt{\left(\frac{m\pi}{a}\right)^2 + \left(\frac{n\pi}{b}\right)^2 + \left(\frac{l\pi}{d}\right)^2} \tag{4.4}$$

where $\boldsymbol{c}$ is the velocity of light $3\times10^8 m/s$, If $b < a < d$, the mode or pattern of the dominant mode which is known the lowest resonant frequency, here is considered TE_{101} mode in this synthesis. The pattern of the TE_{101} is shown in Figure 4.4, where the solid lines with circles denote the electric field intensity and the dashed lines denote the magnetic field intensity variations [106].

4.3 Unloaded Quality Factor

Generally, the unloaded quality factor Q_u is an important parameter for a waveguide cavity and should be taken into consideration for filter design. It illustrates the quality of the waveguide cavity with respect to the loss and energy stored in the electromagnetic field within the resonator at the center frequency.

In addition to that, the quality factor measures the strength of coupling between cavities as well. For instance, a high Q means that the cavity implies low energy loss inside the waveguide resonator and exhibits a good energy storage component, whereas a low Q cavity implies a higher loss inside the waveguide resonator [2]. A general interpretation for Q_u that applies to any kind of cavity is

$$Q_u = \omega \frac{Time-average\ energy\ stored\ in\ the\ resonator}{Average\ power\ lost\ in\ the\ resonator} \tag{4.5}$$

The losses in a waveguide cavity, in general, may be correlated to or linked with the dielectric material, conductor, and radiation within the medium [1]. The total Q_u may be stated by adding the overall losses together

$$\frac{1}{Q_u} = \frac{1}{Q_c} + \frac{1}{Q_d} + \frac{1}{Q_r} \tag{4.6}$$

where Q_c is the quality factor related to the conductor loss, Q_d is the quality factor related to the dielectric loss, and Q_r the quality factor related to the radiation from the cavity. The loaded quality factor Q_l can be realized with respect to the Q_u factor and the Q_e factor as follows [1]

$$\frac{1}{Q_L} = \frac{1}{Q_u} + \frac{1}{Q_e} \tag{4.7}$$

where Q_e is the external quality factor for a cavity related to the effective loss within the external coupling circuit, and it is defined as the ratio of the energy stored in the resonator to the energy coupled to the external coupling circuit. To extract the external Q_e for a circuit from the physical structure will be derived and explained later through this chapter.

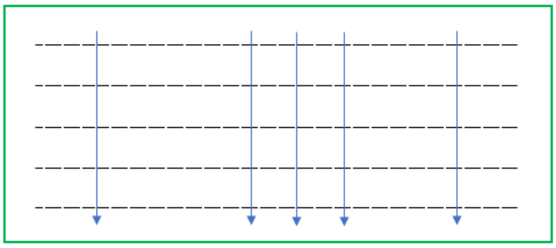

(a)

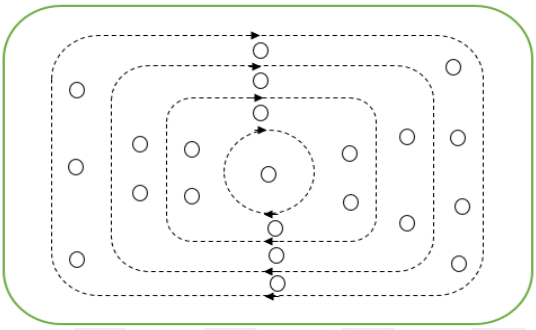

(b)

Figure 4.4 Field configuration of dominant TE_{101} (a) pattern the dashed lines denote to the magnetic field variations, and the solid lines (b) the circles denote to the electric field.

Supposing that an air-filled waveguide resonator $\eta = \eta_0 = 120\pi$, for the TE_{101} mode, the Q_u factor in that the loss within the conducting walls of the waveguide is derived by [1]

$$Q_c = \frac{(k_{101}ad)^3 b\eta}{2\pi^2 R_s(2a^3b+2bd^3+a^3d+ad^3)} \tag{4.8}$$

where $\eta = \sqrt{\mu/\varepsilon}$ is the intrinsic or wave impedance of a medium, and R_s is the surface resistance of the conducting walls with the parameter of conductivity σ, and it is given by [1]

$$R_s = \sqrt{\frac{\omega\mu}{2\sigma}} \tag{4.9}$$

In electric or magnetic coupled-resonators circuits with a filtering response, cavities with finite Q_u factor leads to passband insertion loss. As the Q_u factor value of the resonators decreases, not only the insertion loss of passband of the filtering response increases and enhances, but also the selectivity of filtering response becomes poor. Therefore, it is important and should be taken into account for the designers or engineers to choose a resonator with high Q_u values so that insertion loss is met as desired. Commonly, the insertion loss for filtering response is directly proportional to the number of resonators N of the filter circuit and inversely proportional to the FBW of the filter circuit. The increase in (dB) of insertion loss (ΔIL) at the resonant frequency f_0 of the filtering response is given by [1]

$$\Delta IL = 4.343 \sum_{i=1}^{n} \frac{\Omega_c}{FBW.Q_{ui}} g_i \quad dB \tag{4.10}$$

where Ω_c is the cut-off frequency of the lowpass prototype filter circuit, and g_i denotes the lowpass prototype element value of cavity or resonator i.

4.4 Coupling of Resonators in Physical Terms

After resolving and obtaining the normalized coupling matrix $[k]$ for a coupled resonators topology as shown in chapter 2, the actual coupling matrix $[K]$ of a coupled resonators circuit with a given specification can be obtained by prototype de-normalization of the matrix $[k]$ at the desired bandwidth BW and the center frequency f_0, as follows [2]

$$K_{i,j} = k_{i,j}.FBW \tag{4.11}$$

where FBW, and the actual Q_e is related to the normalized quality factor q_e is given by [2]

$$Q_e = \frac{q_e}{FBW} \tag{4.12}$$

The next step on extracting quality factor is to build up and design a circuit of coupled resonators and apply the required coupling coefficients matrix $[K]$ physically. The extraction of the coupling coefficient K_{ij} of two adjacent coupled cavities and the Q_e factor from the physical structure will be presented.

4.4.1 Coupling Coefficient from the Physical Structure

Generally, every two adjacent coupled resonators may have the same or distinct resonant frequency ω_0, where the coupling coefficient k_{ij} between the resonators is defined as the ratio of coupled energy between resonators to stored energy [107]. Moreover, in the coupled resonators circuit, the coupling between resonators can be magnetic, electric, or electric-magnetic coupling as shown in Figure 4.5. Here, the coupling coefficients for a selected coupled resonators can be realized from the physical structure using electromagnetic (EM) simulation such as Computer Simulation Technology (CST). Hence, to extract the coupling coefficient between asynchronously coupled resonators with non-equal resonant frequencies, a general formula can be applied for any type of coupled resonators [108]

$$K = \pm\frac{1}{2}\left(\frac{\omega_{02}}{\omega_{01}} + \frac{\omega_{01}}{\omega_{02}}\right) \times \sqrt{\left(\frac{\omega_2^2-\omega_1^2}{\omega_2^2+\omega_1^2}\right)^2 - \left(\frac{\omega_{02}^2-\omega_{01}^2}{\omega_{02}^2+\omega_{01}^2}\right)^2} \qquad (4.13)$$

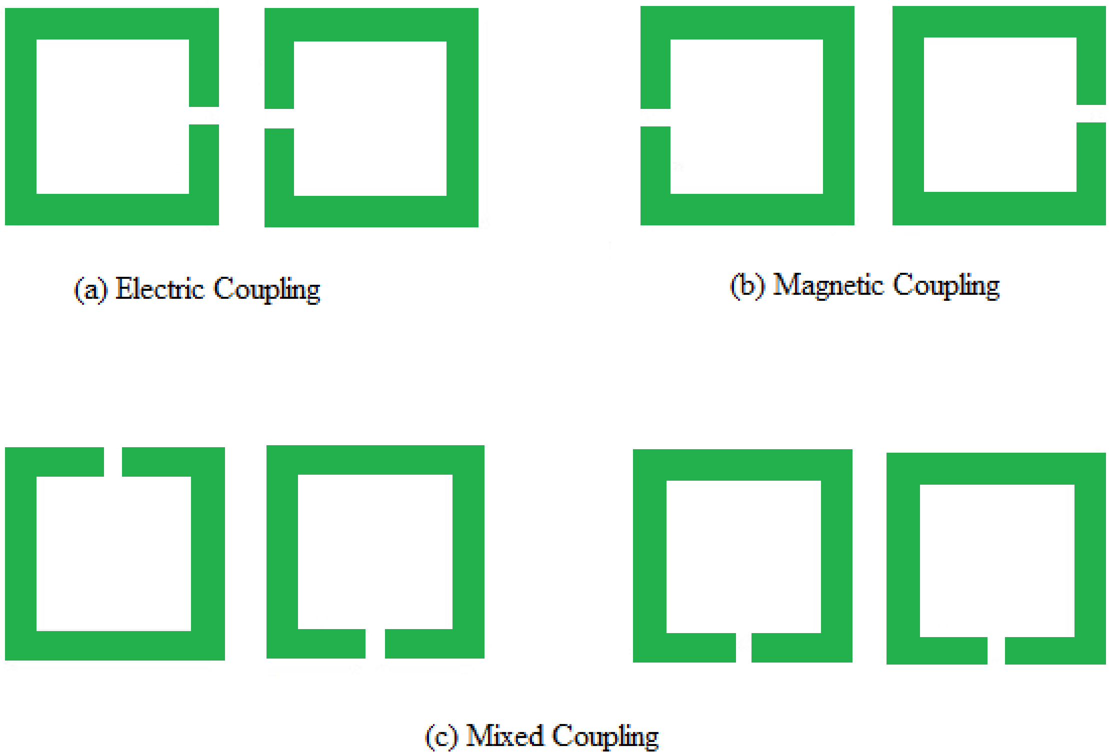

(a) Electric Coupling

(b) Magnetic Coupling

(c) Mixed Coupling

Figure 4.5 Coupling types between microwave resonators [2].

where ω_{01} and ω_{02} are the resonant frequencies of the two adjacent coupled cavities which $\omega_0 = 2\pi f_0$, ω_1 and ω_2 are the lower and higher frequencies in the magnitude of S_{21} response of the two adjacent coupled cavities circuit, with weakly coupled ports to the external resonators as shown in Figure 4.6.

The characteristic parameters of coupled resonators ω_{01} , ω_{02} , ω_1 and ω_2 can be obtained using full-wave EM simulator CST. Figure 4.6 shows an example of a physical structure of two inductively *H-plane* coupled waveguide cavities which are enough weakly coupled to the ports, and Figure 4.7 illustrates the simulated $|S_{21}|$ response of the filter and shows the frequency peaks ω_1 and ω_2 .

As shown in Figure 4.5, the coupling between any two adjacent microwave resonators depends on the separation or distance between resonators, for instance, if the distance between resonators is large then the coupling will be weak and vice versa. The coupling between microwave resonators may be electric as shown in Figure 4.5a, magnetic as shown in Figure 4.5b and mixed electric-magnetic coupling as shown in Figure 4.5c, and coupling is shown in chapter 2 Figure 2.10 as lumped elements.

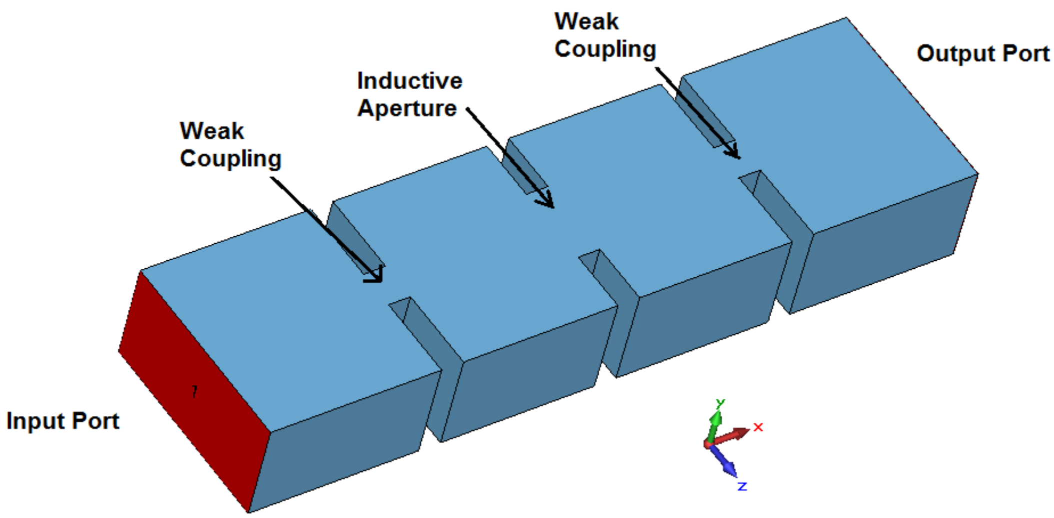

Figure 4.6 Inductively coupled waveguide resonators.

The formula as equation (4.13) is applicable for synchronously coupled adjacent cavities, and in this situation, it is simplified to [107,109]

$$K = \pm\frac{\omega_2^2-\omega_1^2}{\omega_2^2+\omega_1^2} = \pm\frac{f_2^2-f_1^2}{f_2^2+f_1^2} \tag{4.14}$$

The coupling coefficient normally corresponds to an electric coupling or magnetic coupling. The two types of coupling between microwave resonators manifest an opposite sign of the coupling coefficient [107].

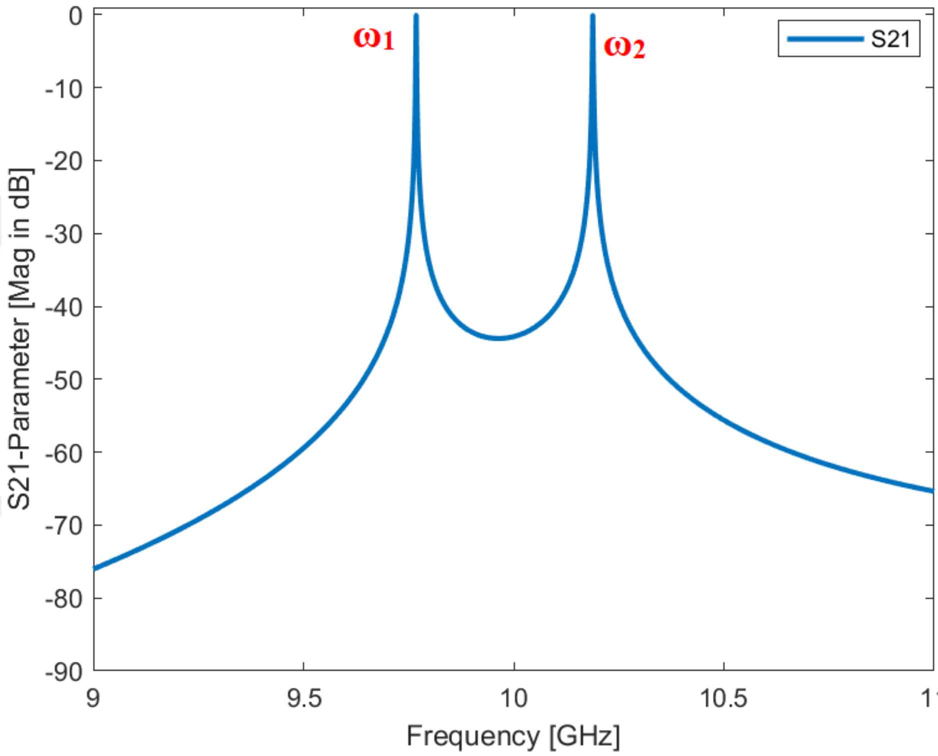

Figure 4.7 $|S_{21}|$ for two coupled waveguide resonators with two frequency peaks

4.4.2 Extraction of Q_e from Physical Structure

The external quality factor Q_e of a cavity with port could be found by simulating passband $|S_{21}|$ response with one weakly coupled port and strongly coupled port. For instance, Figure 4.8 shows a waveguide cavity that is externally coupled to the input port via inductive *H-plane* aperture and weakly coupled to the output port. The Q_e factor can be obtained from the simulated passband $|S_{21}|$ response using the 4.15 formula [108]

$$Q_e = \frac{\omega_0}{\Delta\omega_{\pm 3dB}} \tag{4.15}$$

where ω_0 is the cutoff frequency of the loaded cavity and $\Delta\omega_{\pm 3dB}$ is the $-3dB$ bandwidth, as shown in Figure 4.9.

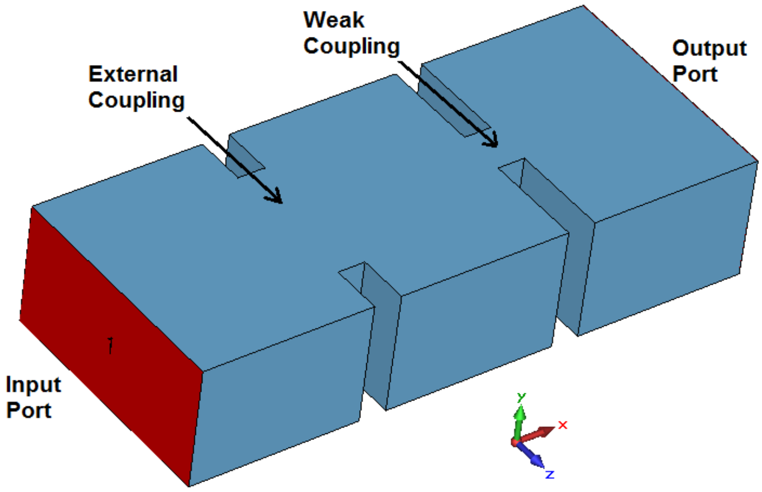

Figure 4.8 Externally coupled waveguide cavity.

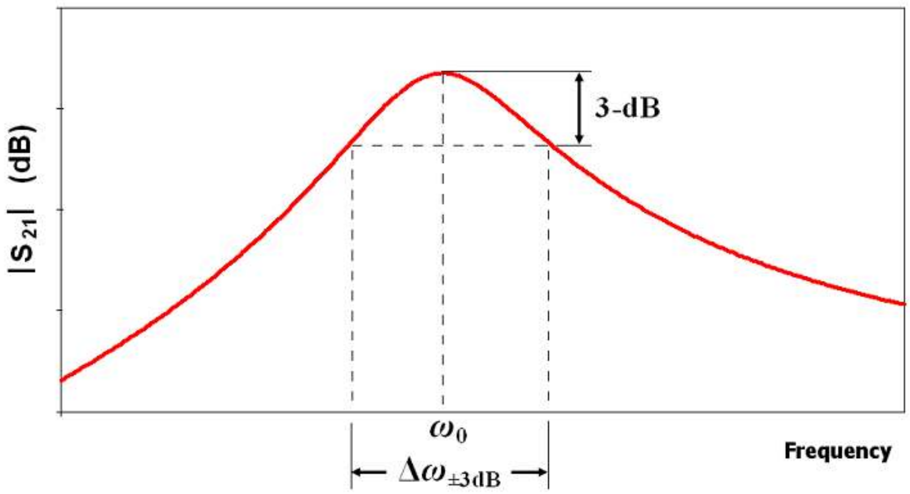

Figure 4.9 Response of $|S_{21}|$ for loaded resonator.

4.4.3 Inductive and Capacitive Apertures

Coupled resonators of filter circuit have been implemented using rectangular waveguide cavities $a > b$ with initial length $d = \frac{\lambda_g}{2}$. The initial dimensions of the coupled apertures can be obtained for the required coupling matrix by the procedure discussed in section 2.3 in a systematic manner.

Figure 4.10 depicts the distinct coupling structures between two adjacent rectangular waveguide resonators which are coupled together using capacitive E-plane or inductive H-plane apertures. Half guided wavelength that resonates at the fundamental TE_{101} mode is generally used in rectangular waveguide filtering circuits design [108].

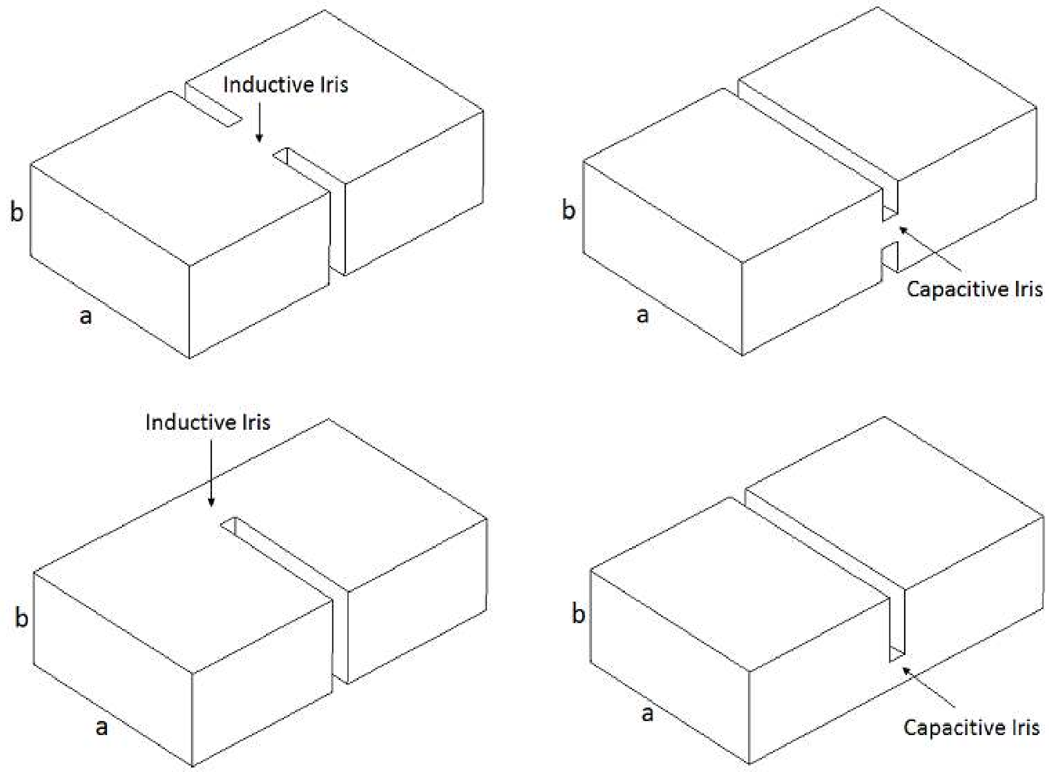

Figure 4.10 Coupling structures for capacitive and inductive apertures [109].

4.5 Design of Conventional X-Band Waveguide Filter

Firstly, X-band waveguide Chebyshev filter response at 10 GHz center frequency with a different number of resonators for $N = 1,2,3,4,$ and 5 have been synthesized and designed. The waveguide bandpass filter for X-band applications is designed according to the H-plane inductive iris (aperture) with symmetric electromagnetic coupling between adjacent waveguide resonators as shown and discussed in section 2.11. The waveguide filter is designed at X- band frequency for many applications such as RADAR transceiver circuits and aligned Low Noise Amplifier (LNA) along with antenna in the telecommunication system [110]. The input and output external quality factors for X-bandpass waveguide filter circuit and the magnetic coupling coefficients are computed for fractional bandwidth $\text{FBW} = 20\%$ as discussed and shown in section 2.3.

According to the lowpass prototype filter circuit as discussed in section 2.5, the $g's$ parameters for lowpass filter which has order $N = 5$ are symmetric as shown in Table 2.1 as follows

$$g_0 = 1$$
$$g_1 = 0.9714$$
$$g_2 = 1.3721$$
$$g_3 = 1.8014$$
$$g_4 = 1.3721$$
$$g_5 = 0.9714$$
$$g_6 = 1$$

The calculated values of symmetrical internal and external coupling coefficients of the lowpass filter circuit are obtained as discussed in section 2.11 as follows

$$k_{12} = k_{45} = 0.1624$$
$$k_{23} = k_{34} = 0.1192$$
$$q_e = 0.205$$

The transformation of elements from the lowpass prototype filter circuit to the practical BPF circuit is shown in Figure 4.11, which its values as follows [1]

$$L_s = \left(\frac{\Omega_c}{FBW\omega_0}\right) Z_0 g \tag{4.16}$$

$$C_s = \frac{1}{{\omega_0}^2 L_s} \tag{4.17}$$

$$C_p = \left(\frac{\Omega_c}{FBW\omega_0}\right) \frac{g}{Z_0} \tag{4.18}$$

$$L_p = \frac{1}{{\omega_0}^2 C_p} \tag{4.19}$$

From equations (4.16) to (4.19), subscript s means series component and p means parallel component in the lumped-elements circuit. Series inductor g component in lowpass prototype circuit is transformed to L_s inductor and C_s capacitor in series, while the shunt capacitor g component in lowpass prototype circuit is transformed to L_p inductor and C_p capacitor in parallel. Then, using these equations of the transformation of elements from LPF prototype filter to BPF filter circuit we obtained as follows

$$R_1 = R_2 = 498\ \Omega$$
$$C_1 = C_5 = 0.002644\ Pf$$
$$C_2 = C_4 = 0.693244\ Pf$$
$$C_3 = 0.00113\ Pf$$
$$L_1 = L_5 = 122.7\ nH$$
$$L_2 = L_4 = 0.3653\ nH$$
$$L_3 = 227.54\ nH$$

By using the electromagnetic simulator CST, particularly the Microwave Studio (MWS) module [111] which based on the Finite Integral Technique (FIT) calculation methodology [108,111], the initial physical dimensions of the waveguide cavities and the coupled inductive irises of the filter are obtained for distinct N as shown in Figures 4.12 to 4.15.

Every pair of coupled cavities have been simulated separately (cascaded) to extract the dimensions of the waveguide resonators such as length, and width of the coupled *H-plane* irises (junctions) which corresponds to the required coupling coefficients $[k]$ for each N. essentially, the first waveguide resonator is synthesized and designed at X-band frequency and 10 GHz center frequency. The purpose of this step is to obtain the length of resonator and external quality factor as shown in Figures 4.9 and 4.12.

The physical dimensions of the coupled irises or apertures between adjacent waveguide resonators are corresponding to the external quality factors Q which have been found by CST simulator previously. The design of the waveguide bandpass filter is initially structured with obtaining the initial values of the overall physical dimensions for a diverse number of resonators $N = 1,2,3,4$ as shown in Figures 4.12 to 4.15. CST simulation response of the initial overall structure of the final waveguide 5th order filter is obtained as shown in Figures 4.16. After that, from the initial response of the overall waveguide filter designed with the 5th order, the waveguide bandpass filter is optimized by CST frequency-domain solver.

The physical lengths of the cavities and the widths of the coupled apertures have been optimized to obtain the final response given in Figure 4.17. The coupling matrix for waveguide bandpass filter 5th order as follows

$$k = \begin{bmatrix} 0 & 0.1624 & 0 & 0 & 0 \\ 0.1624 & 0 & 0.1192 & 0 & 0 \\ 0 & 0.1192 & 0 & 0.1192 & 0 \\ 0 & 0 & 0.1192 & 0 & 0.1624 \\ 0 & 0 & 0 & 0.1624 & 0 \end{bmatrix}$$

$$K_e = \frac{1}{4.857} = 0.205$$

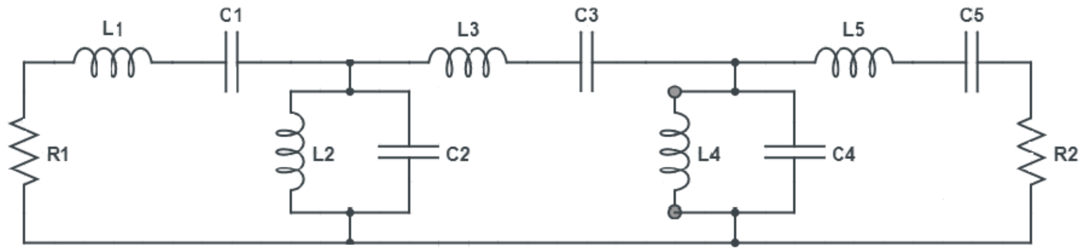

Figure 4.11 Lumped circuit model of a symmetrical waveguide BPF for the Chebyshev filter response after transformation method from lowpass prototype filter R1= R2 = 498 Ω, C1= C5 = 0.002644 pF, and C4 = C2 = 0.693244pF, C3 = 0.001133pF, L1= L5 =122.7nH, L2 = L4 = 0.3653 nH, L3 = 227.54 nH.

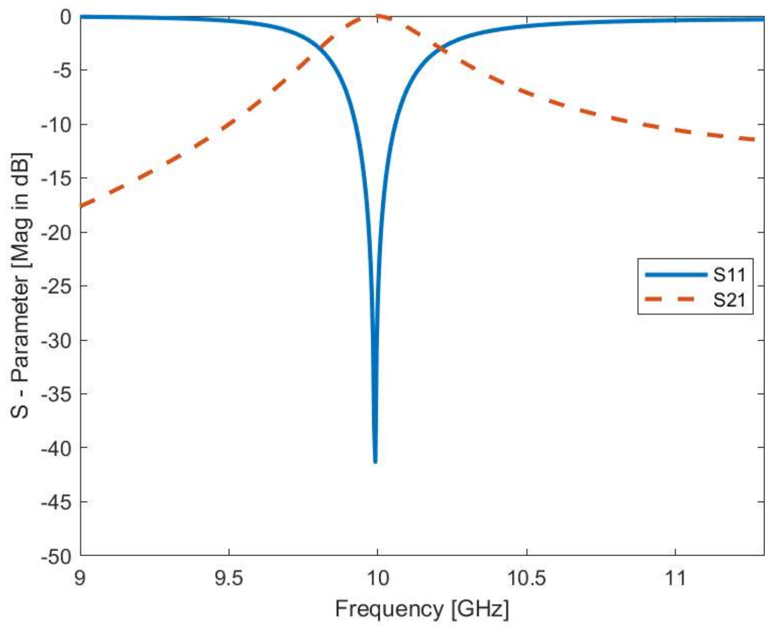

Figure 4.12 Waveguide filter response with loaded first resonator $N = 1$.

Similarly, to reach the overall physical dimensions of waveguide filter with five resonators as shown in Figures 4.18 - 4.19, we insert resonator by resonator to obtain a new physical length for added one and previous one of resonators simultaneously as well as determine the width of waveguide inductive irises between resonators. Furthermore, change the physical length of resonators affect directly on the resonant frequency, shifts to left if the physical length increases or to the right if the physical length decreases. Change in ports external H-plane junctions will directly influence on the overall bandwidth of waveguide filter.

As shown in Figure 4.16, the initial filter response is not good enough as desired particularly in its return loss S_{11} and insertion loss S_{21} as well, and the response is not centralized at 10 GHz center frequency as required, so in such case, the optimizing of the overall dimensions of the physical structure should be taken into consideration, by using the Interpolated Quasi-Newton optimizer which built-in CST simulator [111] to reach to Figure 4.17 with better performance.

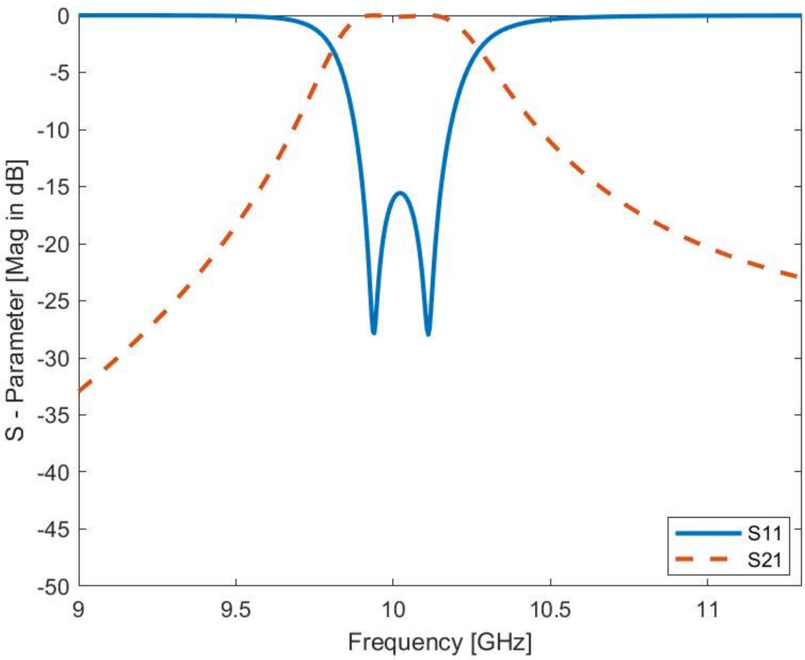

Figure 4.13 Waveguide filter response with loaded second resonator $N = 2$.

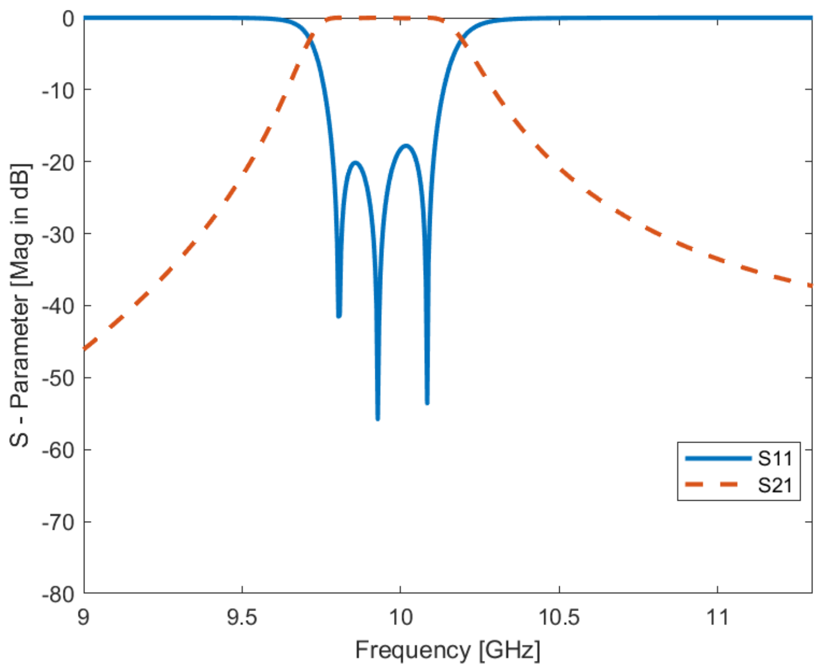

Figure 4.14 Waveguide filter response with loaded third resonator $N = 3$.

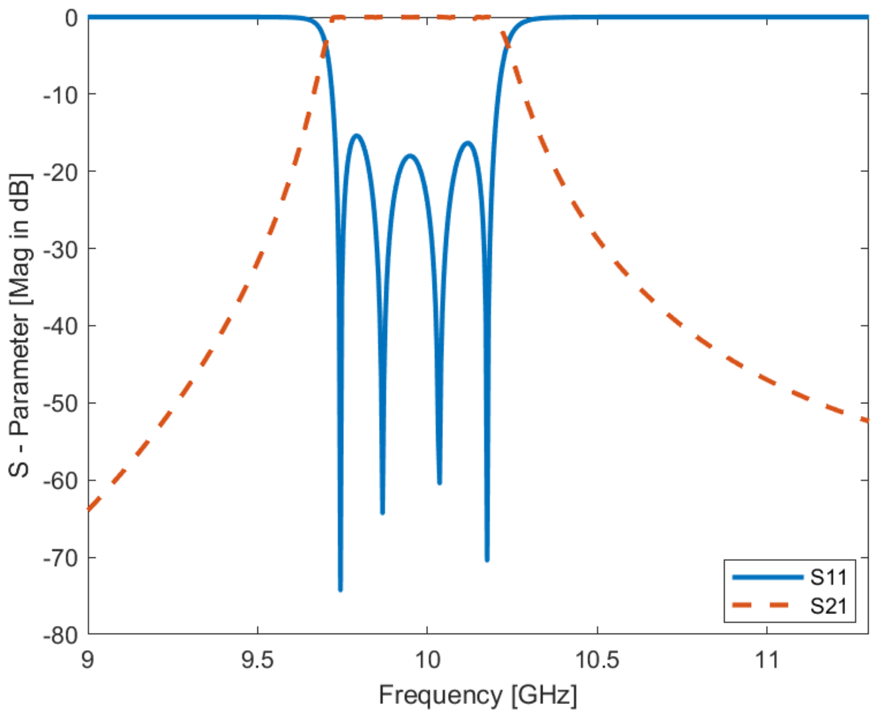

Figure 4.15 Waveguide filter response with loaded fourth resonator $N = 4$.

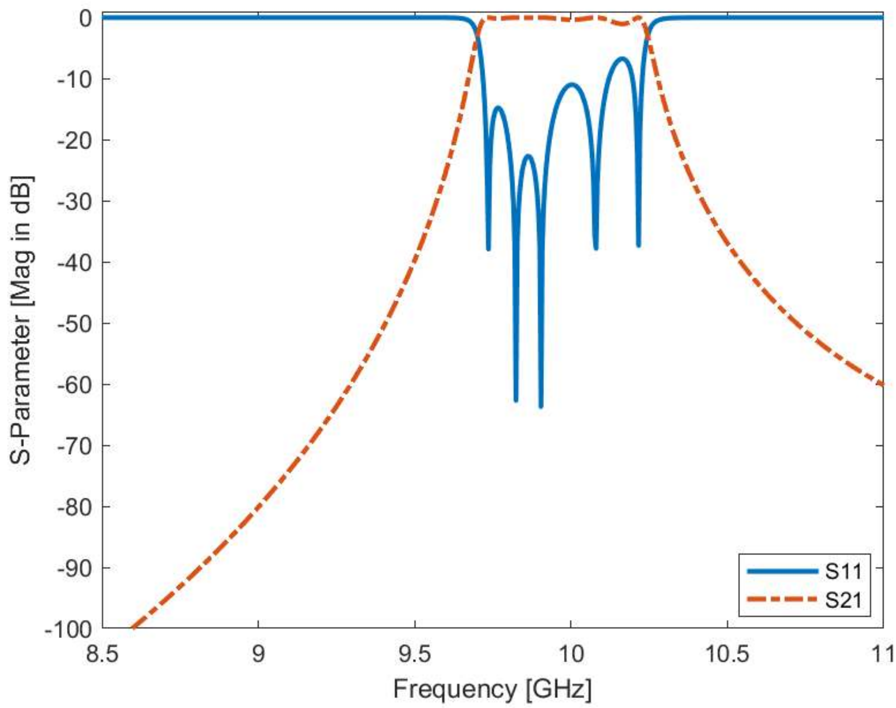

Figure 4.16 Initial response of X-band bandpass waveguide filter.

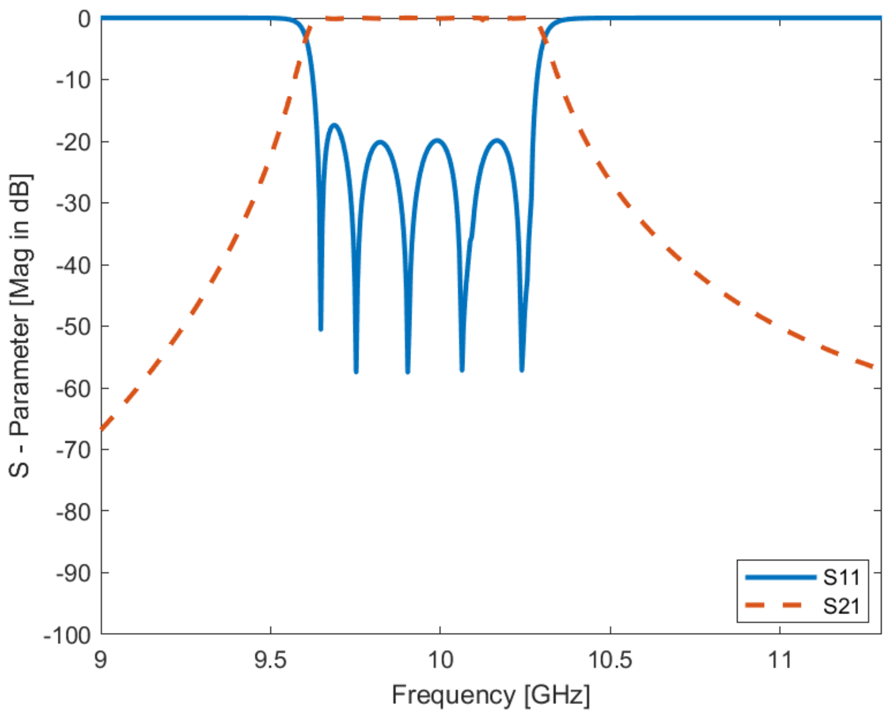

Figure 4.17 Final optimized Waveguide filter response with loaded all waveguide resonators $N = 5$.

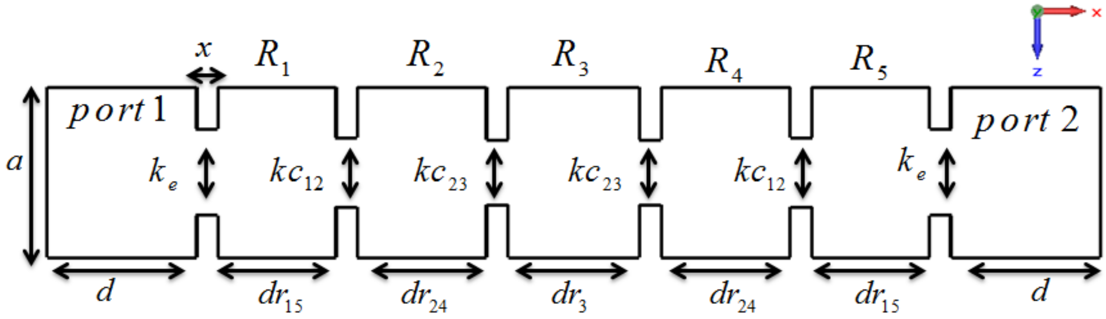

Figure 4.18 Layout of a conventional waveguide bandpass filter with inductive irises [112].

As shown in Figure 4.18 the overall layout of the desired conventional waveguide filter for X-band and after optimization method to enhance the overall filter performance, the return loss S_{11} of the filter is enhanced and is below $-20dB$, the insertion loss S_{21} of passband filter response is better and near to $0.043\ dB$ as well, as well as the bandwidth of the filter is $550\ MHz$, yet is still under the narrow band.

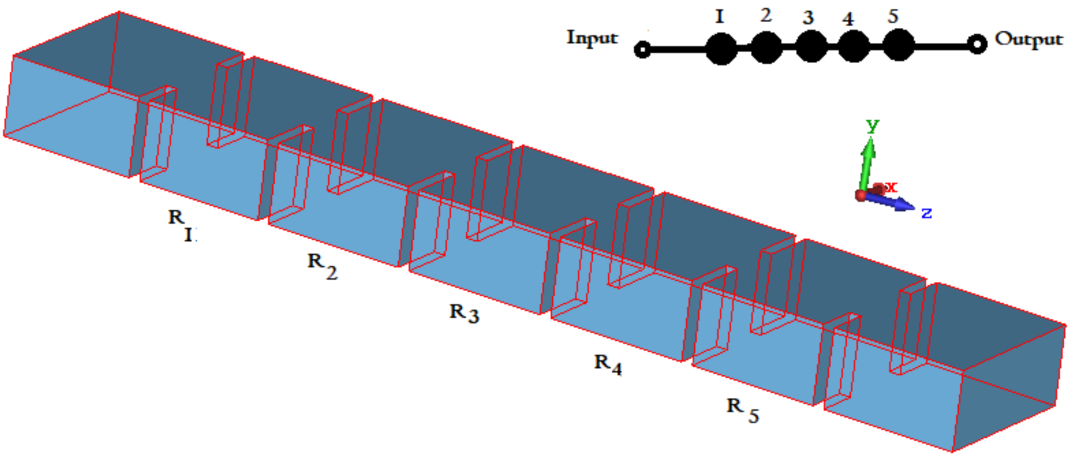

Figure 4.19 Overall designed conventional waveguide bandpass filter for X-band with inductive irises N=5.

In this work, to improve the miniaturization of Chebyshev bandpass waveguide filter based CSRR metamaterials over a conventional filter as shown in Figures 4.11 to 4.19 at 10 GHz center frequency with five resonators, Besides, to improve its selectivity and insertion loss alongside bandwidth as well, metamaterial property is used.

Simple double symmetric unit cells with electric coupling between CSRRs which are engraved from the center to facilitate and tune the resonating frequency at 10 GHz are used. The CSRRs have been designed with shifting between the upper and lower sections [112].

The shifting between two CSRRs—right or left from each other—means the changing of electromagnetic coupling between cavities (resonators), and, due to this change in EM coupling, the resonant frequency will be affected with respect to this shifting between CSRR. In addition, with the proper change in CSRR's physical dimensions besides the shift between two loops (rings), the optimal waveguide filter-based MMs is obtained in a systematic manner as it will be shown in the next section. Cutoff frequency, quality factor Q, and S-parameters are studied and calculated by using computer simulation technology (CST). Moreover, a circuit simulator Advanced Design System 2016.01 (ADS) is used to implement and simulate a lumped element bandpass filter as well. After that, a comparison will be done between conventional and proposed metamaterial bandpass Chebyshev filter [112].

Unlike the conventional filters and their designs methodology, the proposed filter is designed based on the metamaterial resonators' technology that are coupled directly without *H-plane* waveguide junctions between cavities that give the design important factors, especially for telecommunication applications such as compactness, simplicity, and wide bandwidth. So, according to the filter features, the proposed filter can be employed aligned with Low Noise Amplifier (LNA) for X-band receiver circuits which works at 10 GHz center frequency (9.15 GHz–10.44 GHz) to suppress the unwanted signal bands, and waveguide size is critical in such circuits as well [110, 112]. Furthermore, the proposed waveguide bandpass filter can be employed in line with X-band power amplifier at 10 GHz center frequency to achieve the maximum power and extend the desired bandwidth [10].

An X-band Radar transceiver circiuts/modules that work at the same frequency band (9.15 GHz–10.44 GHz) can be inserted with high selectivity and a high-quality factor [5].

4.5.1 Design of Proposed Waveguide Filter Based CSRRs

Veselago in the late 1960s who has paved the way and guided researchers to use artificial materials or engineered medium (unnatural material) which not exist naturally with negative constitutive parameters, negative magnetic permeability μ and/or negative electric permittivity ε [17]. At Veselago time there were not materials that have simultaneous negative constitutive parameters. Considerably later and after thirty years from Veselago's idea of artificial materials, the evidence of medium with simultaneous negative magnetic permeability and negative electric permittivity was demonstrated experimentally by Pendry [18] and Smith et al [87].

As discussed, and shown in [98], one can use the CSRR section (negative image of SRR) to design a compact waveguide filter by an engraving or etching the metallic sheet. Here, in this thesis, a double rings CSRR meta-resonators (unit cell) which engraved from the center of the ring as shown in Figure 4.20. As discussed in chapter 3, CSRRs generate negative electric permittivity and slightly used more than SRRs due to the wide bandwidth. Using this methodology reduces the overall physical size of the bandpass waveguide filter coupled with inductive or/and capacitive cavities (resonators).

The etching rings on the copper plane are not mutually aligned to each other, however, the upper etched ring and the lower etched ring are not on the same vertical line (shifted). Nevertheless, the shifting of etched rings as shown in Figure 4.20 plays another role besides selecting proper CSRR physical dimensions to move the center frequency as desired and in a systemic manner [112]. Furthermore, based on the coupling phenomena, shifting changes the coupling between two coupled etched rings as shown in Figure 4.20 and Figure 4.21, so that selecting a good shift with a proper physical dimension of CSRR gives a quick response at desired resonant frequency 10 GHz as shown in Figure 4.22.

The equivalent LC circuit of the CSRR has been analyzed and simulated using circuit simulator ADS. The resonance frequency can be expressed as [1]

$$f_0 = \frac{1}{2\pi\sqrt{L_0 C_0}} \tag{4.20}$$

where L_0 is the total inductance of resonator and C_0 is the total capacitance of the resonator at 10 GHz center frequency. The ABCD parameters of two ports network of the RLC circuit or lumped element resonator circuit is shown in Figure 4.21 and be calculated using [1]

$$\begin{bmatrix} A & B \\ C & D \end{bmatrix} = \begin{bmatrix} cos\beta l & jz_0 sin\beta l \\ jY_0 sin\beta l & cos\beta l \end{bmatrix} \begin{bmatrix} 1 & 0 \\ Y & 1 \end{bmatrix} \begin{bmatrix} cos\beta l & jz_0 sin\beta l \\ jY_0 sin\beta l & cos\beta l \end{bmatrix} \tag{4.21}$$

where $Y = j\frac{\omega^2 L_0 C_0 - 1}{\omega L_0}$

when the ABCD parameter of the lumped element resonator circuit as shown in Figure 4.20 and Figure 4.21 has been analyzed and found as shown in Figure 4.22, the corresponding scattering S-parameters can be obtained using the method provided in [1].

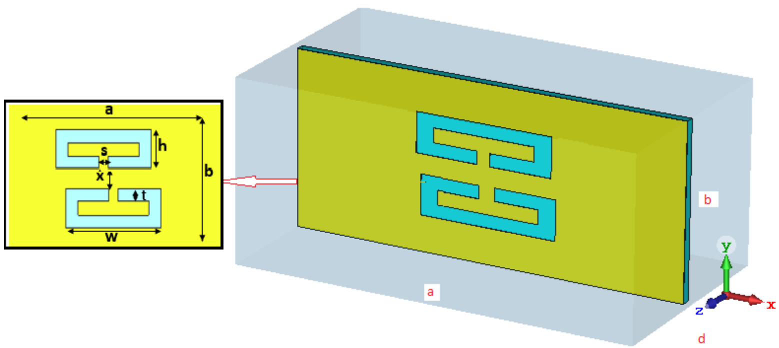

Figure 4.20 Rectangular meta-resonator CSRR unit cell with $a > b$ [112].

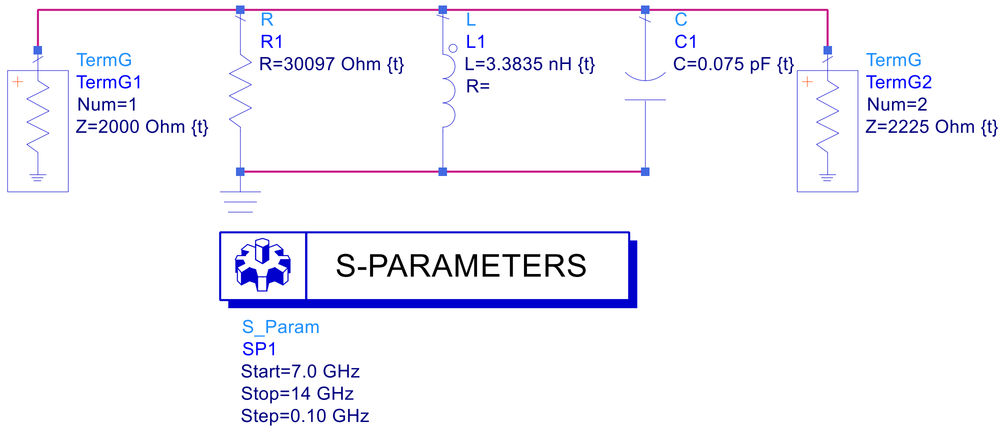

Figure 4.21 Equivalent lumped circuit model of the CSRR.

As shown in Figure 4.17, the electromagnetic simulator, Computer Simulation Technology (CST) is used to mimic a rectangular waveguide resonator based metamaterial CSRR which its initial length $d = \lambda_g/2$ at 10 GHz resonant frequency for X-band applications with a lower cutoff frequency $f_l = 9.15\ GHz$, the higher cutoff frequency $f_h = 10.44\ GHz$, and 0.043 dB passband ripple [112].

Furthermore, using substrate material (RT/Duroid) with a thickness of 0.5 mm, electric permittivity constant $\varepsilon_r = 2.2$, and appropriate mesh density selection 10 $steps\ per\ wavelength$ with 20 min number of steps were selected. Annealed copper (lossy material) with conductivity $s = 5.8 \times 10^7$ [S/m], thickness 30 μm is chosen for metallic layer and impedance at the resonant frequency $Z_0 = 499\Omega$ [112].

The first step to obtain the overall Chebyshev bandpass waveguide filter based CSRR was designing the unit cell as shown in Figure 4.20 at center frequency 10 GHz as shown in Figure 4.18. The design is based on filter specifications such as return loss, insertion loss, wider bandwidth, and good selectivity [112].

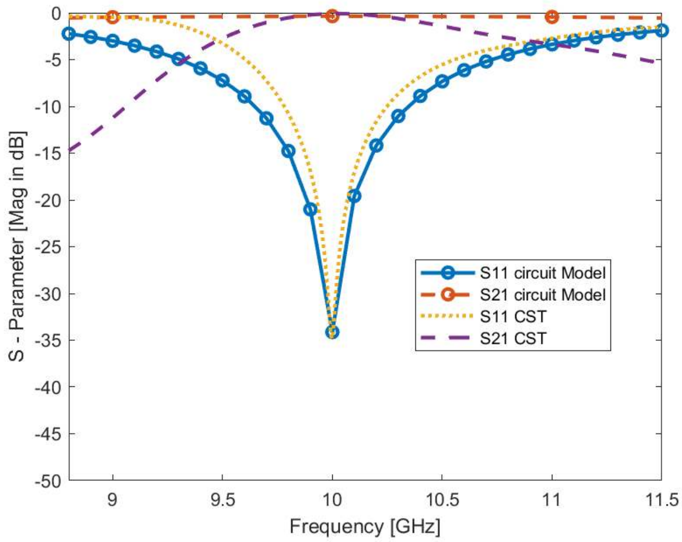

Figure 4.22 S-parameter frequency response of waveguide meta-resonator S_{11} and S_{21} which is compared by using (CST) and a circuit simulator (ADS) [112].

The microwave resonant circuits in high frequency behave as *RLC lumped* elements series or parallel in low frequency circuits (including ohmic losses) that can be excited by external magnetic source. In other words, to attain the lumped elements model *RLC* from the distributed model, values of *RLC* components that are calculated using equations (4.22) – (4.24) as proposed in [99]. The equivalent lumped elements model for the proposed meta-resonator (microstrip unit cell) is shown in Figures 4.21 and 4.23.

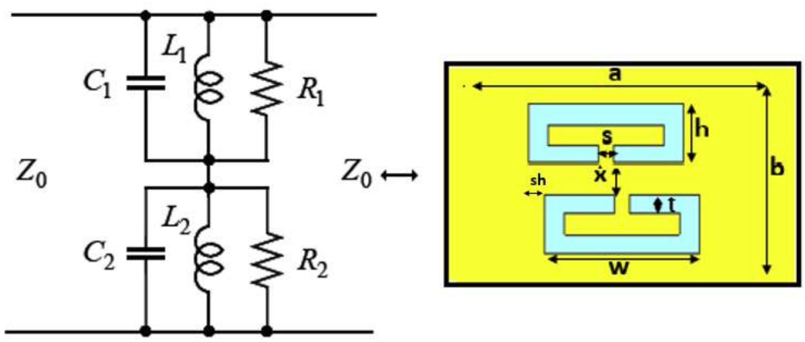

Figure 4.23 Rectangular meta-resonator and its simple lumped model circuit [112].

However, here in this design, the upper and lower etched CSRRs will be symmetric, this means that the design will have the same values for both CSRR rings parameters.

$$R_i = Z_0 \frac{|S_{21}(j\omega_0)|}{2(1-|S_{21}(j\omega_0)|} \tag{4.22}$$

$$L_i = B_{3dB} Z_0 \frac{S_{21}(j\omega_0)}{2\omega_0^2} \tag{4.23}$$

$$C_i = \frac{2}{B_{3dB} Z_0 |S_{21}(j\omega_0)|} \tag{4.24}$$

where ω_0 is the angular frequency (rad/sec), B_{3dB} is the bandwidth at a specific frequency at $3dB$, Z_0 is the port impedance and S_{21} is the insertion loss parameter at the considered center frequency. Based on what has been proposed in [99] and the definition of RLC circuit parameters, shown in Figure 4.23, and, because of symmetry between two CSRRs rings, the values are obtained at $10\ GHz$ resonant frequency by using Equations (4.22) – (4.24) as follows [112]

$$Z_0 = 499\ \Omega$$
$$B_{3dB} = 0.07\ GHz$$
$$R_{1,2} = 5989.65\ \Omega$$
$$C_{\ 1,2} = 0.0508\ pF$$
$$L_{1,2} = 4.9807\ nH$$

4.5.2 Bandpass Waveguide Filter Based Symmetric CSRRs

Previously, a single waveguide meta-resonator based on CSRR and according to the simulation results of meta-resonator as shown in Figure 4.22 has been designed and analyzed. It is noticed that the change of the CSRR physical parameters such as shift (sh), width (w), etched (s) and length (h) introduce a shift of the resonant frequency and effect directly on the filter bandwidth according to the main values of the same Figure 4.20 at the center frequency $f_0 = 10\ GHz$ and bandwidth $B_{3dB} = 0.07\ GHz$ [112].

As listed in Table 4.1 and already has been shown in Figures 4.24–4.29. Changing the shift between upper and lower CSRRs will affect the bandwidth and resonant frequency as shown in Figure 4.24. The changing of CSRR etching width ($\boldsymbol{s}$) which engraved symmetrically from the center of two loops leads to change the resonant frequency according to the variation coupling capacitance as shown in Figure 4.25.

Once etching width (s) increases, the resonant frequency increases as well, meaning that the resonant frequency is shifted to the right. Figure 4.26 shows the effect of variations of vertical separation (x) between two CSRR loops and its effect on the change electrical coupling between both loops as well, and as a result of increasing the separation (x), the resonant frequency will be decreased and will then move to the left. Figure 4.27 shows an increase in the height (h) of the CSRR loop, which will decrease the resonant frequency and move to the left. In Figure 4.28, variations in the line width of loops has a direct effect on the resonant frequency, meaning that decreases (t) parameter will increase the resonant frequency due to the variation of currents which move along a path of the CSRR loops [112].

Changing the width of the loops (upper and lower rings), the bandwidth and the resonant frequency are changed accordingly, and any an increase in CSRR width ($\boldsymbol{w}$) parameter will decrease the resonant frequency as shown in Figure 4.29. For the waveguide bandpass filter design, $WR - 90$ standard, $a > b,\ a = 22.86\,mm, b = 10.16\,mm$, and Chebyshev response are used here.

The Chebyshev response that exhibits the equal-ripple passband and maximally flat stopband [1-2,106]. The change of the Chebyshev response as well as change the bandwidth and sharpness (selectivity) of a filter can be affected based on the number of its resonators, order N. This means that an increase in filter order N, will give more sharpness (selectivity of filter will be better) and enhance the bandwidth, in the meanwhile, filter design will be more complicated due to increasing number of resonators as discussed in section 2.5.2.

Table 4.1 The influence of change physical parameters of the CSRRs and its effect on cutoff frequency and bandwidth.

Physical parameter	Resonant Frequency	Bandwidth
w ↑	←	decreases
s ↑	→	increases
h ↑	←	decreases
t ↑	No change	increases
x ↑	←	decreases
sh ↑	←	increases

Note that, (←) the response is shifted to the left, (→) the response is shifted to the right [112].

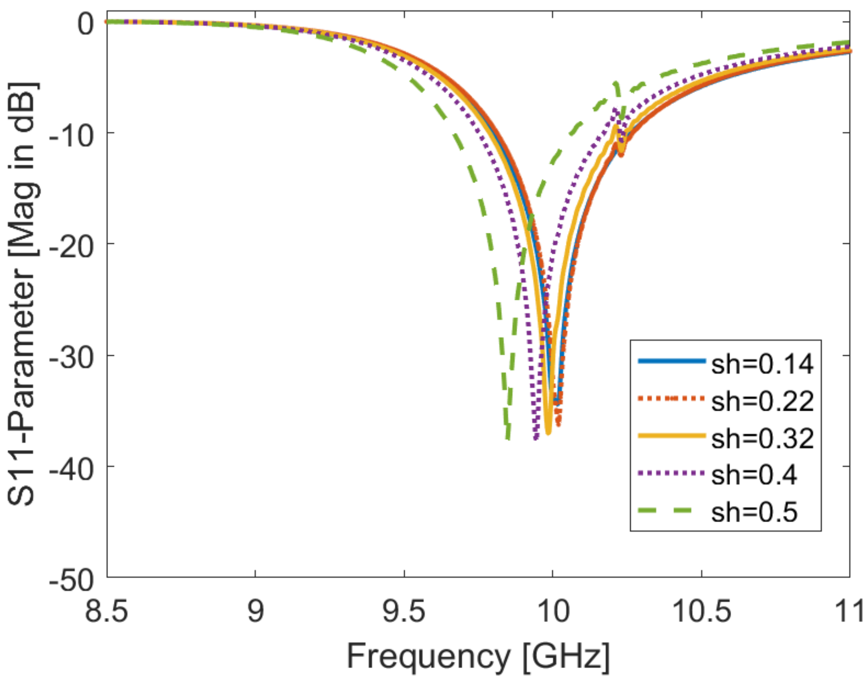

Figure 4.24 Change of horizontal shift between both CSRR rings (upper and lower) sh-parameter (shift), for $sh = 0.14, 0.22, 0.32, 0.4, 0.5\ mm$; resonant frequency is shifted to the left once the sh-parameter is increased [112].

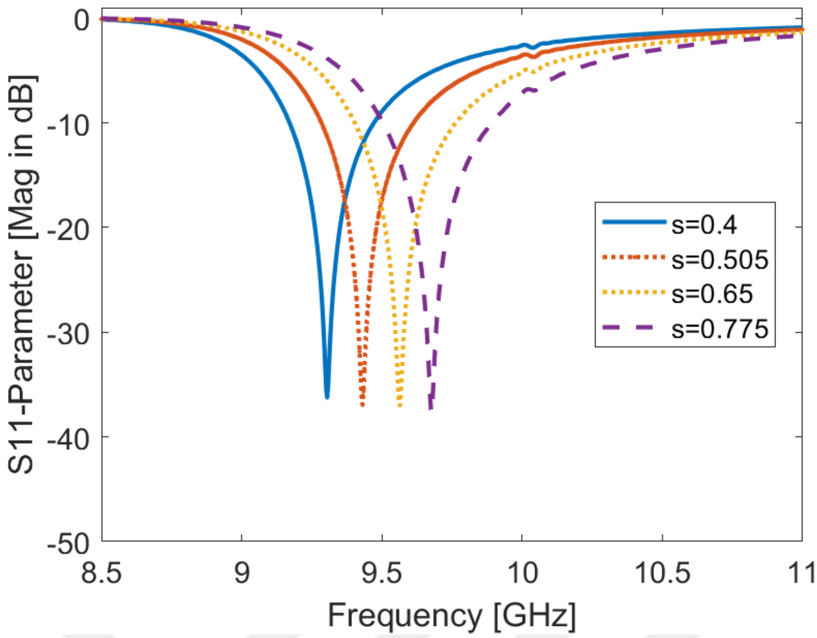

Figure 4.25 Engrave the center of CSRR width, the s value for both loops and its changing $s = 0.4{,}0.505{,}0.65{,}0.775\ mm$; the resonant frequency is shifted to the right because of changing capacitance [112].

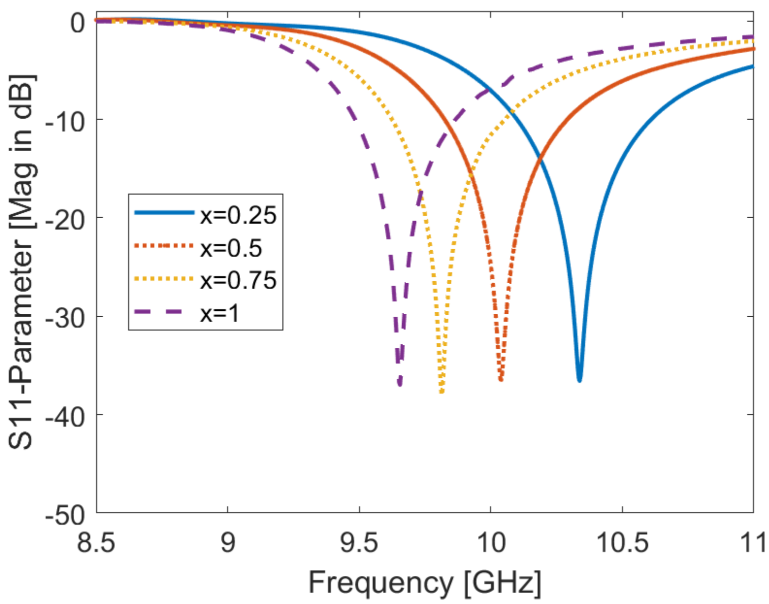

Figure 4.26 Variation of both CSRR rings (upper and lower loops) vertical separation, x −value for $x = 0.25, 0.5, 0.75, 1\ mm$, and the resonant frequency is shifted to the left according to the coupling effect [112].

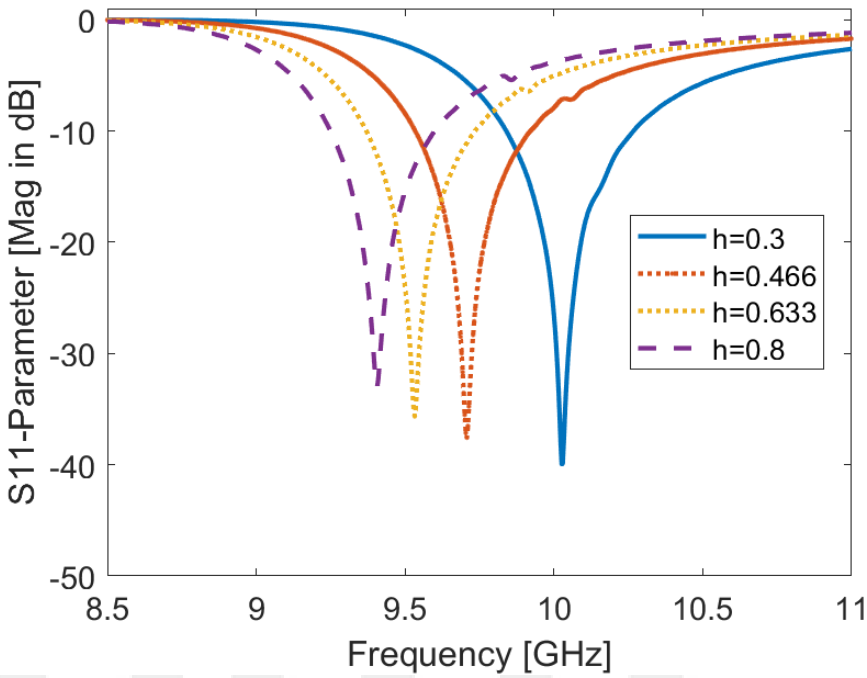

Figure 4.27 Variation of CSRR height, h-value for $h = 0.3, 0.466, 0.633, 0.8\ mm$, and the resonant frequency is shifted to the left [112].

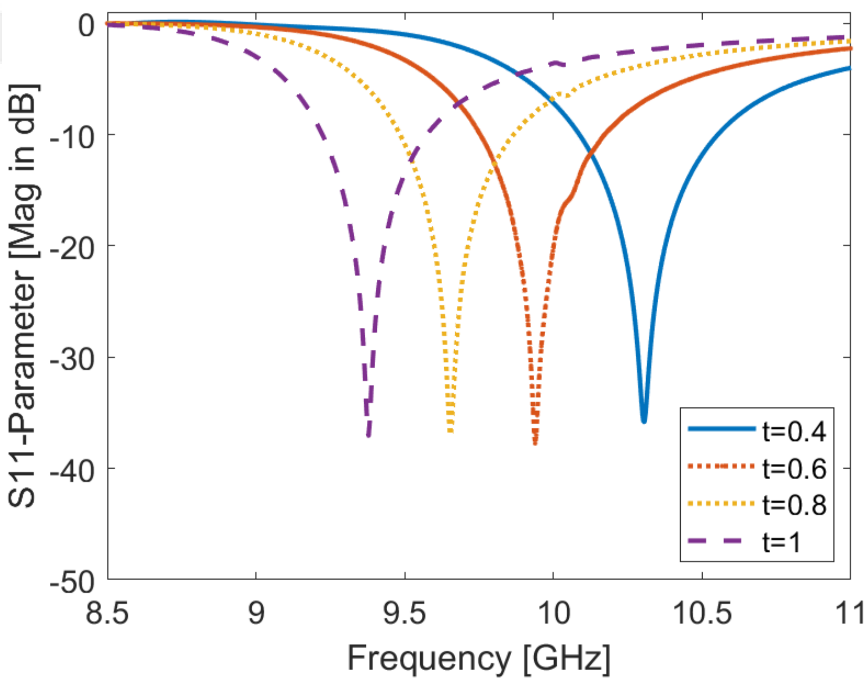

Figure 4.28 Changing the line width t −parameter of both CSRR rings, for $t = 0.4, 0.6, 0.8, 1\ mm$, the resonant frequency is shifted to the left and the changing is high in frequency according to this parameter [112].

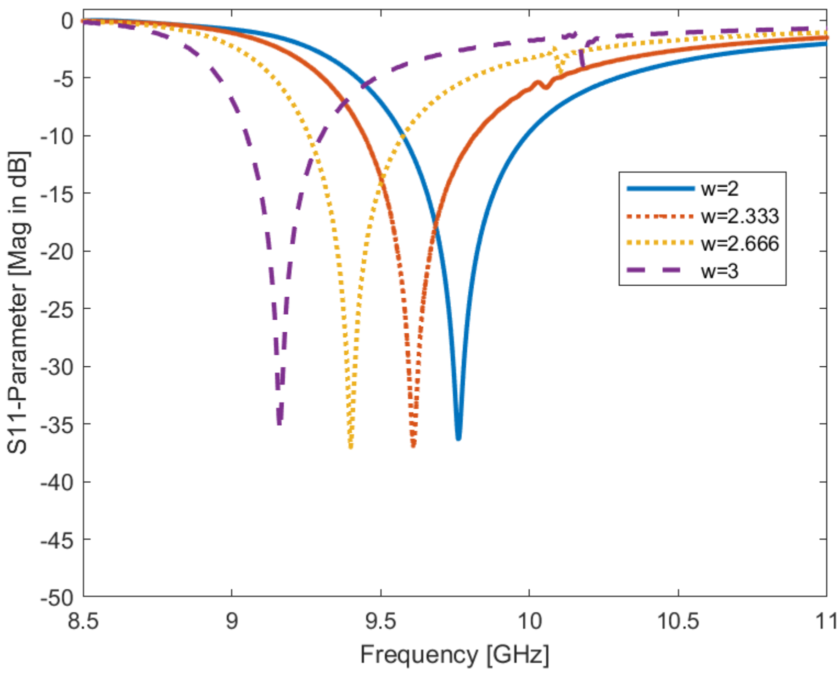

Figure 4.29 Change of CSRR rings width $w -$ parameter and its effect on resonant frequency $w = 2, 2.333, 2.666, 3\ mm$; resonant frequency is shifted to the left as well as the bandwidth is being decreased [112].

4.5.3 Design of *X*-Bandpass Waveguide Filter

Modes or microwave patterns in waveguides take different shapes in terms of dimension and cross section. The increasing value of propagation patterns (modes) in the waveguide, attenuation already increases as well (evanescent mode); notably, the waveguide acts as a high-pass filter and supports all possible modes higher than cutoff frequency $f > f_0$, however, the attenuation losses are minimum in the lower order mode. Thus, if the dominant pattern of propagation is TE_{101} for the cavity (resonator), meaning that the transverse electric TE or there are no components of electric field in the direction of propagation $E_z = 0$, and magnetic components exist in the same direction of propagation $H_z \neq 0$.

The proposed Chebyshev bandpass waveguide filter has the symmetry modeling of resonators based on the CSRRs, so this feature of using symmetry reduces the number of variables of design (physical dimensions). The structure of the bandpass waveguide filter initially used quarter wavelength $\lambda_g/4$ distance between adjacent CSRR resonators inside the waveguide [112]. The gap between the inserted metamaterial CSRRs and the metallic walls of waveguide is less than $30\ \mu m$ [112].

The procedure used here to design the bandpass waveguide filter is proposed in [38], which depends on the coupling effect between cascaded meta-resonators. The first waveguide resonator is run and optimized at $10\ GHz$ center frequency as shown in Figure 4.20 and Figure 4.22, the initial length of the waveguide resonator without inserting metamaterial is $40\ mm$ and with inserting metamaterial is $17\ mm$. After that, another resonator has been inserted within the waveguide or in cascade with the previous one, and so on, as shown in Figure 4.31 to Figure 4.35.

Once the overall waveguide filter is designed, the initial response is optimized by using a CST optimization to reach the desired filter specifications at $10\ GHz$ as shown in Figure 4.35, and final filter response after optimization in Figure 4.37.

The flowchart of the filter design procedure is shown in Figure 4.30. It is noticed that, at $10\ GHz$, the return loss s_{11} is below $-20dB$ with insertion loss s_{21} being close to $0.05\ dB$, cutoff at $-70\ dB$, and Q factor is 7,563.

4.5.4 Discussion

After designing and finalizing the proposed Chebyshev metamaterial bandpass waveguide filter at $10\ GHz$ center frequency, and based on the initial design specifications of filter, the resonant frequency f_0, number of resonators (cavities) N or filter order, relative bandwidth BW, low pass prototype with element values g_i, and the insertion loss s_{21} of the bandpass filter is being assumed, then the conventional waveguide resonators are designed to obtain the desired bandpass filter.

To attain the bandpass filter from a low pass prototype filter with g parameters which $g_0 = g_6 = 1,\ g_1 = 0.9714,\ g_2 = 1.372,\ g_3 = 1.8014,\ g_4 = 1.3721,\ g_5 = 0.974$ the frequency transformation method is used here as mentioned in [1, 5] and shown in Figure 4.11.

If the conventional bandpass waveguide filter for X-band application as shown in Figure 4.19 with its design method (insertion loss method) as has been proposed in [1,5] that consists of five waveguide resonators with inductive apertures (*H-plane* discontinuities), and the proposed metamaterial bandpass waveguide filter (cascaded meta-resonators without junctions) as shown in Figure 4.36 are compared with each other, the use of metamaterial technology reduces the overall physical length of the waveguide filter by 31% and enhancing the bandwidth up to $1.22\ GHz$ with an increase of 37.5% at $10\ GHz$ improves [112].

In Table 4.2, a quick comparison between two waveguide fifth order filters has been summarized. In Figure 4.38, both responses s_{21} of the conventional and the proposed bandpass waveguide filters are shown [112].

Table 4.2 Comparison between conventional waveguide bandpass filter and the metamaterial waveguide filter for the X-band at $10\ GHz$.

Filter Type	$f_0(GHz)$	$L\ (mm)$	$s_{11}\ (dB)$	$z_w(\Omega)$	$BW\ (GHz)$
Proposed filter	10	51	-20	499	1.22
Conventional filter	10	97.1	-19	497	0.550

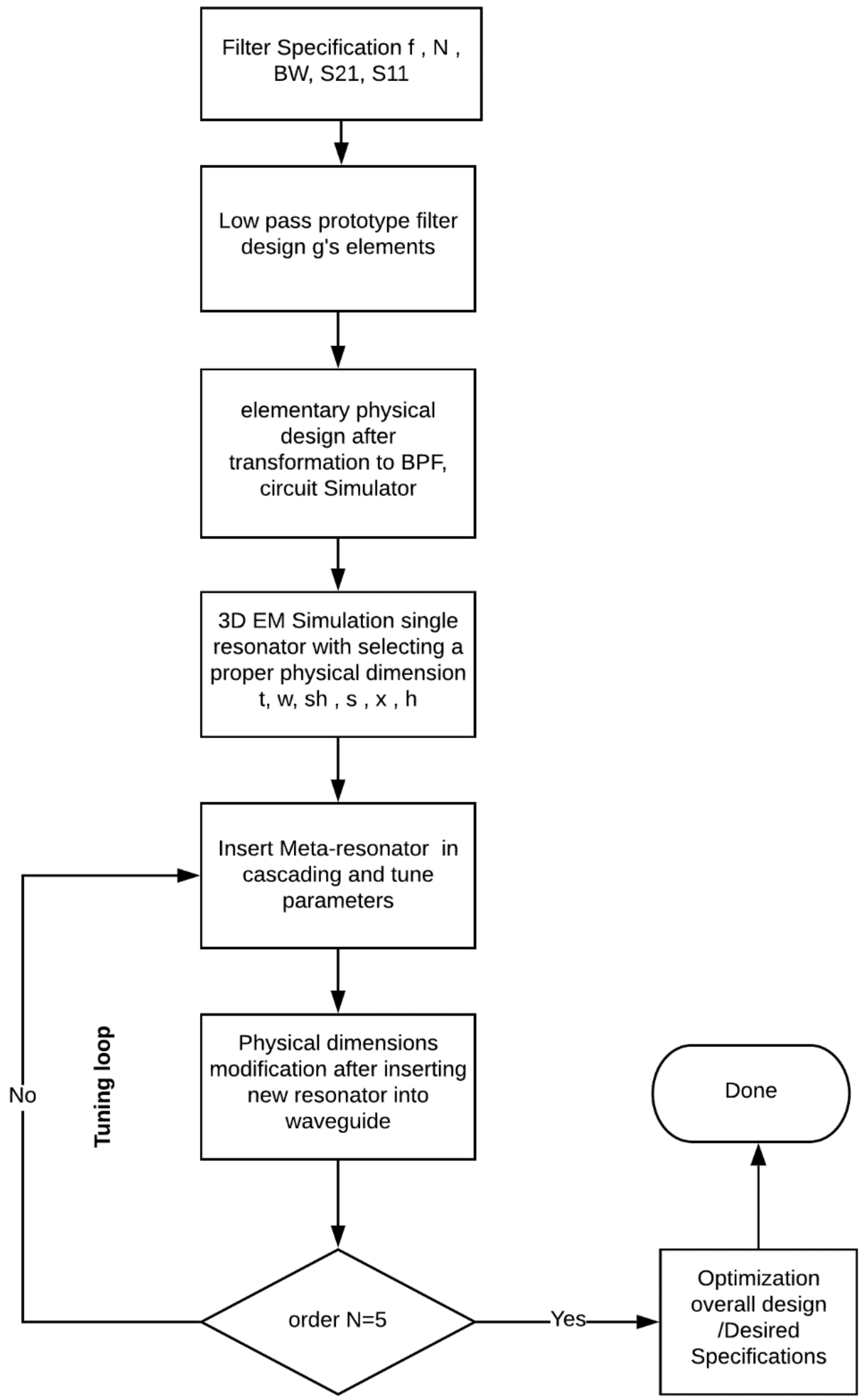

Figure 4.30 Flowchart of the waveguide filter design methodology [112].

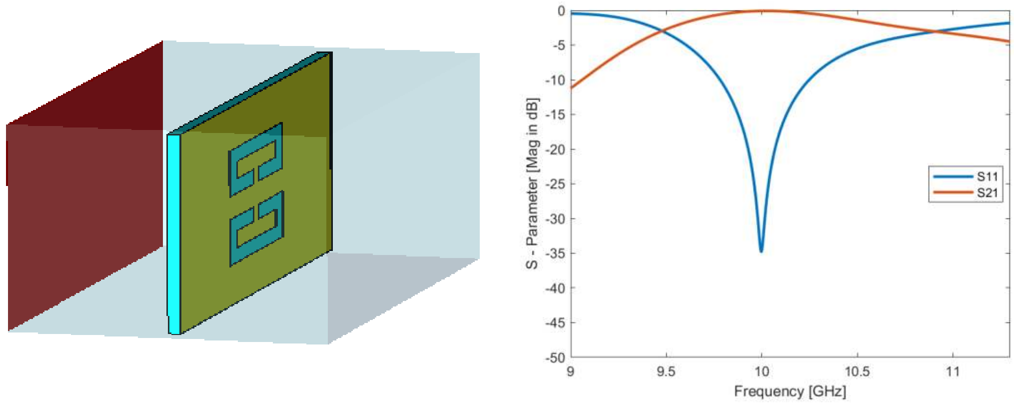

Figure 4.31 Design of bandpass waveguide filter based on rectangular meta-resonator CSRR and its S-parameters for the first resonator and its S-parameter [112].

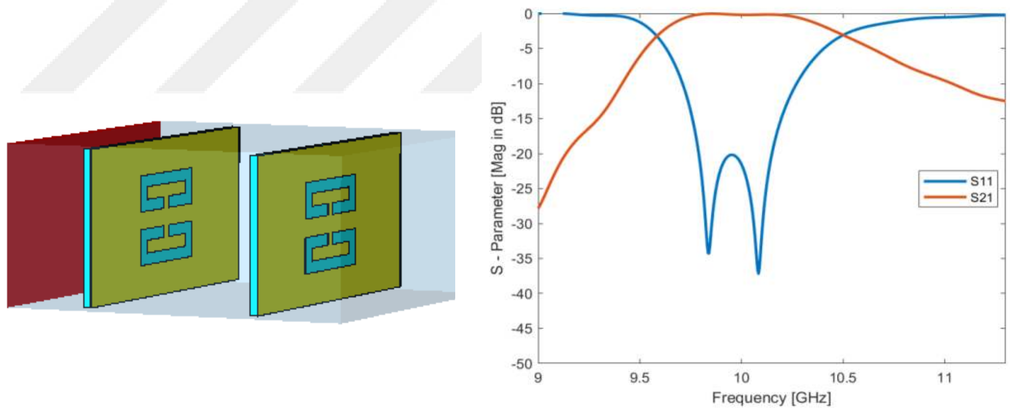

Figure 4.32 Design of bandpass waveguide filter based on rectangular meta-resonator CSRR and its S-parameters for the second resonator is added to the first one and its S-parameter [112].

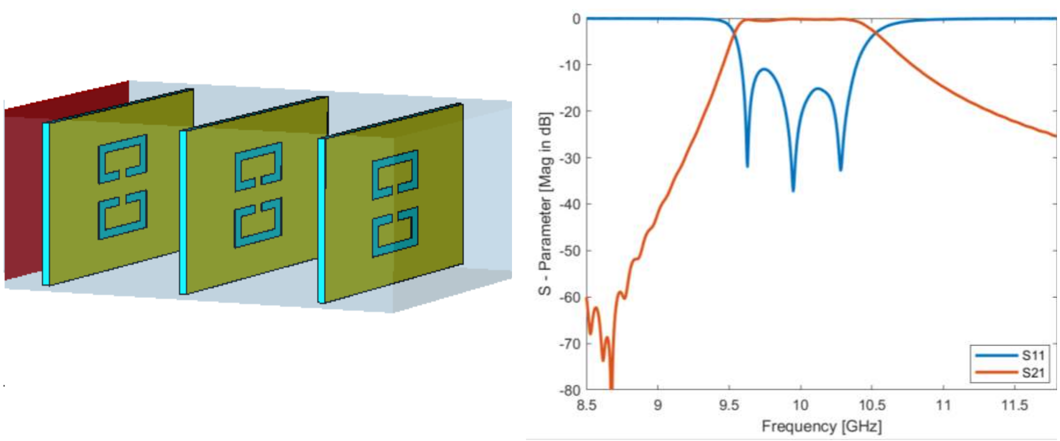

Figure 4.33 Design of bandpass waveguide filter based on rectangular meta-resonator CSRR and its S-parameters for the third resonator is added to both resonators and its S-parameter [112].

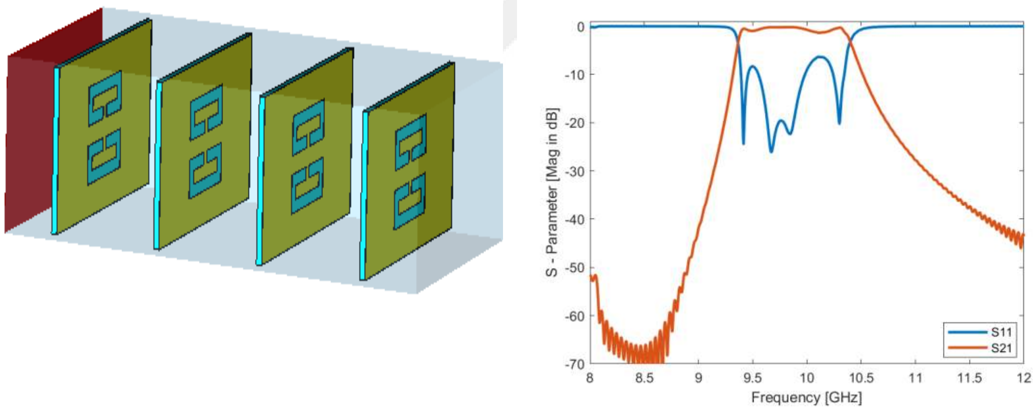

Figure 4.34 Design of bandpass waveguide filter based on rectangular meta-resonator CSRR and its S-parameters for the fourth resonator is added in cascaded to three resonators and its S-parameter [112].

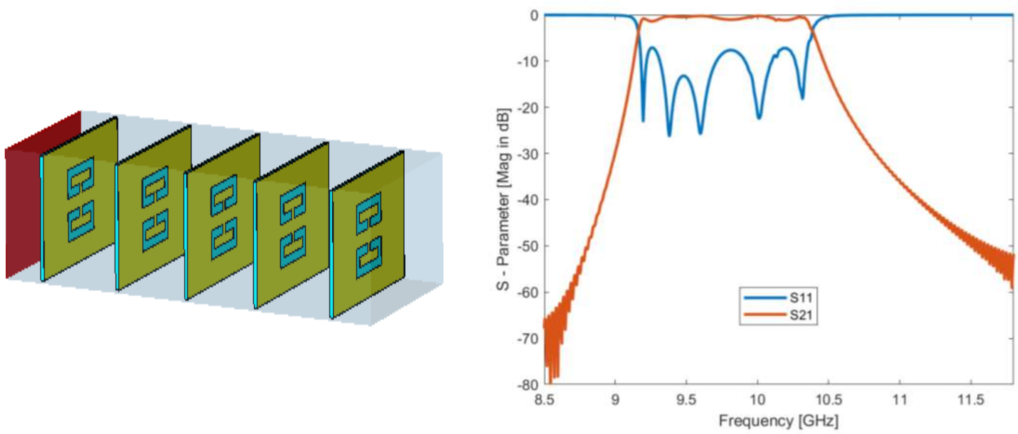

Figure 4.35 Design of overall bandpass waveguide filter based on rectangular meta-resonator CSRR and its S-parameters for the fifth resonator is added in cascaded to four resonators and its S-parameter [112].

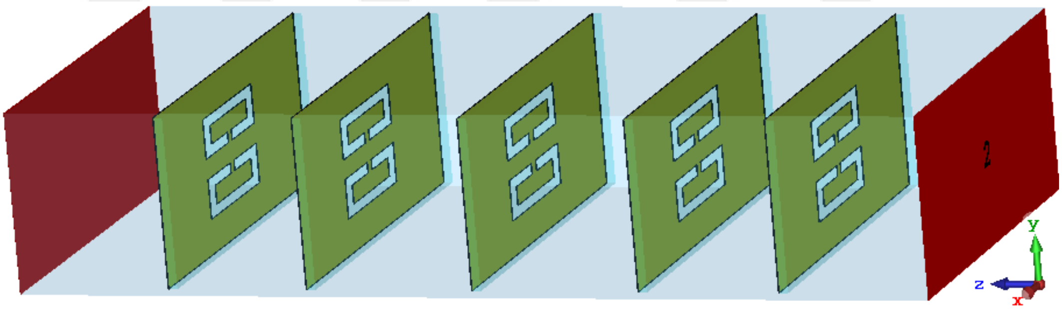

Figure 4.36 Final design of the proposed waveguide meta-resonator filter $N = 5$ for X-band at resonant frequency 10 GHz [112].

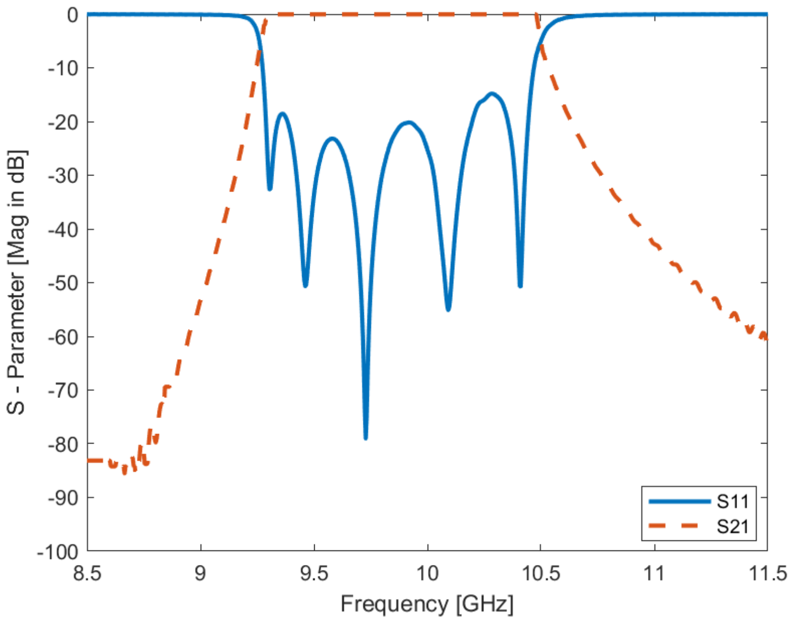

Figure 4.37 Optimized final response of the proposed waveguide meta-resonator filter and its S-parameters s_{11} below $-20\ dB$ and insertion loss s_{21} around $0.045\ dB$ at center frequency $10\ GHz, N = 5$ [112].

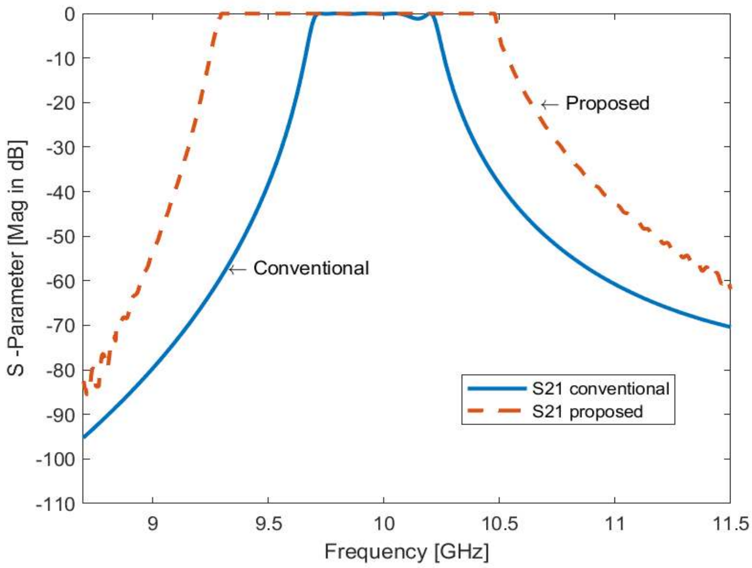

Figure 4.38 $\boldsymbol{S_{21}}$ comparison between conventional rectangular waveguide filter with direct waveguide junctions and meta-resonator waveguide filter without H-plan junctions for X-band, $N = 5$ [112].

As shown in Figure 4.38, two waveguide filters are designed at the same center frequency 10 GHz. The conventional bandpass filter gives good selectivity but narrow bandwidth at the resonant frequency, whereas the proposed filter enhanced and developed the selectivity of bandpass filter as well as the 1.22 GHz bandwidth obtained. The selectivity of the proposed waveguide filter is $-75\ dB$.

Finally, as shown in Figures 4.31 - 4.37, the CSRR waveguide filter is achieved and attained the desired specifications as planned. We noticed that metamaterials technology could control bandwidth and enhance the selectivity of the desired filter as well as reduced the overall physical size of the waveguide bandpass filter [112].

4.6 Summary

In this chapter, a simple methodology to control bandwidth and cutoff frequency of waveguide filter is proposed and simulated. Inserting CSRRs in the same plane of transverse in the waveguide filter for X-band applications at [9.15 GHz -10.44 GHz] frequency band such as RADAR transceiver circuits in satellite communication system and LNA harmonized with the antenna system. A CSRR-loaded bandpass waveguide filter with a Chebyshev response using symmetry structure with a shifted upper or lower ring of CSRR is designed and discussed in this chapter. Adding a meta-resonator to another at the same time in the structure within a rectangular waveguide, with an initial distance $\frac{\lambda_g}{4}$ between resonators is simulated. A fifth order CSRR-loaded bandpass waveguide filter is designed and simulated by CST along with a circuit simulator (ADS). The filter's physical dimensions are obtained, optimized and tuned toward the desired center frequency at $10\ GHz$, as well as the shifting of upper and/or lower rings from each other. The bandwidth of the proposed bandpass filter increases up to $1.22\ GHz$, meaning that the bandwidth of the filter is increased by 37.5% over the conventional waveguide filters, and the filter's size reduced by 31% as well if it is compared with the conventional X-band bandpass filter, which is designed by using the insertion loss method at the same center frequency $10\ GHz$.

CHAPTER 5

CONCLUSIONS AND FUTURE WORK

5.1 Conclusion

In this thesis, two waveguide bandpass filters are synthesized and designed to meet an X-band system, specifically for [9.15 GHz – 10.44 GHz] frequency band which has permitted worldwide for high capacity link point-to-point wireless communications system for high bitrates connectivity.

- The microwave filters' design is based on two technologies, first technology is designing the waveguide filter by symmetric H-plane waveguide junction or irises between adjacent waveguide resonators. The second technology used metamaterials particularly CSRRs (resonators within a waveguide without junctions).

- At first, each waveguide bandpass filter is designed individually, to have fractional bandwidth (FBW) 20% at $10\ GHz$ center frequency and $-20\ dB$ return loss. 5th pole Chebyshev filter with a passband ripple of $0.0432\ dB$ is chosen for design X-band filter. The waveguide filter consists of five coupled rectangular waveguide resonators that are coupled together using inductive apertures for the conventional filter. Rectangular complementary split ring resonators (CSRRs) are used without junctions for the proposed microwave bandpass filter.

- CST and ADS software are used for simulation and design the microwave filters for both technologies and using parameter sweep and optimization methods to obtain the desired specification.

- The evaluation of the attained results shows that a common H-plane junction gives satisfactory results for return loss of $-19\,dB$ and insertion loss of 0.045dB but it has given a narrow bandwidth near to $550\,MHz$. while the waveguide filter designed based on CSRRs has given better results according to the return loss and wide bandwidth near to $1.22\,GHz$.

- conventional *H-plane* waveguide junctions and CSRRs within a waveguide are used to form an overall microwave bandpass filter for communication systems such as antenna, Radar, or LNA. The symmetric resonators methodology has been used in the design to mitigate physical size parameters as much as possible of waveguide filters through simulation. Using the new metamaterial technology such as CSRRs in microwave filter designs has improved the return loss below $-20\,dB$, selectivity $-70\,dB$, compactness size by $31\,\%$, and bandwidth of filter up to $37.5\,\%$.

5.2 Future Work

The work on waveguide filters is considered vital research in communication systems particularly for high frequencies, and it can be further developed rapidly due to researchers' interests in this field. Using metamaterial technology in filter design played a vital role in communication system development, so that, this technology will be employed to design microwave diplexers for more compactness and improve isolation between uplink and downlink communication channels. Using this methodology, the microwave diplexer will be miniaturized, isolation will be better, and the response will be sharper. It is intended to get the microwave diplexers fabricated and tested to validate the design method. The fabrication will be done in a place where fabrication and measurement equipments are available.

REFERENCES

[1] Pozar, D. M. (2012). Microwave engineering. *Wiley*.

[2] Hong, J. S. G., Lancaster, M. J. (2004). *Microstrip filters for RF/microwave applications* **(167)**. John Wiley & Sons.

[3] Bagad, V. S. (2009). *Microwave engineering*. Technical Publications.

[4] Neill, S. P., Hashemi, M. R. (2018). *Fundamentals of ocean renewable energy: Generating electricity from the sea*. Academic Press.

[5] Fathnan, A. A., Amrullah, Y. S., Wijayanto, Y. N., Mahmudin, D., Daud, P. (2015). A compact X-Band Bandpass Filter Using Rectangular Split Ring Resonators for Radar Applications. In *2015 International Conference on Radar, Antenna, Microwave, Electronics and Telecommunications (ICRAMET)* (pp. 60-63). IEEE.

[6] Palla, R., Naik, K. K. (2019). Design of CPW fed E-shaped Patch Antenna with Meandered Slots for X-band Applications. *International Journal of Microwave and Optical Technology,* **14(2)**.

[7] Chongder, P., Biswas, A. (2016). Novel HMSIW Cavity Based Bandpass Filter for X-band Application. In *2016 Asia-Pacific Microwave Conference (APMC)* (pp. 1-3). IEEE.

[8] Hanna, S. M. (1999). Applications of X-band Technology in Medical Accelerators. In *Proceedings of the 1999 Particle Accelerator Conference (Cat. No. 99CH36366)* **(4)**, pp. 2516-2518), IEEE.

[9] Damou, M., Nouri, K., Feham, M., Chetioui, M. (2017). Design and Optimization of Rectangular Waveguide Filter Based on Direct Coupled Resonators. *International Journal of Electronics and Telecommunications,* **63(4)**, 375-380.

[10] Chen, R., Li, R., Zhou, S., Chen, S., Huang, J., Wang, Z. (2019). An X-Band 40 W Power Amplifier GaN MMIC Design by Using Equivalent Output Impedance Model. *Electronics*, **8(1)**, 99.

[11] Guglielmi, M., Jarry, P., Kerherve, E., Roquebrun, O., Schmitt, D. (2001). A new Family of All-inductive Dual-mode Filters. *IEEE Transactions on Microwave Theory and Techniques*, **49(10)**, 1764-1769.

[12] ETSI, T. (2006). 102 524, Fixed Radio Systems. *Point-to-Point Equipment; Radio Equipment and Antennas for Use in Point-to-Point Millimetre Wave Applications in the Fixed Services (mmwFS) Frequency Bands 71 GHz to 76 GHz and 81 GHz to 86 GHz*.

[13] Balanis, C. A. (1999). *Advanced engineering electromagnetics*. John Wiley & Sons.

[14] Jin, J. Y., Lin, X. Q., Deng, X. L., Fan, Y. (2013). A novel Miniaturized Waveguide Bandpass Filter Using Metamaterial. In *2013 Cross Strait Quad-Regional Radio Science and Wireless Technology Conference* (pp. 12-14). IEEE.

[15] Shehan, J. W., Adams, R. S. (2015). X-band Horn Antenna with an Integrated Tunable Notch Filter. In *2015 IEEE International Symposium on Antennas and Propagation and USNC/URSI National Radio Science Meeting* (pp. 2213-2214). IEEE.

[16] Chen, W. (2014). *Metamaterials, Surface Waves, and Their Applications* (Doctoral dissertation, Boston College. Graduate School of Arts and Sciences).

[17] Veselago, V. G. (1968). Electrodynamics of Substances with Simultaneously Negative Electrical and Magnetic Permeabilities. *Physics-Uspekhi*, **10(4)**, 504-509.

[18] Pendry, J. B., Holden, A. J., Robbins, D. J., Stewart, W. J. (1999). Magnetism From Conductors and Enhanced Nonlinear Phenomena. *IEEE Transactions on Microwave Theory and Techniques*, **47(11)**, 2075-2084.

[19] Pendry, J. B., Holden, A. J., Robbins, D. J., Stewart, W. J. (1998). Low Frequency Plasmons in Thin-Wire Structures. *Journal of Physics: Condensed Matter*, **10(22)**, 4785.

[20] Ekmekci, E., Turhan-Sayan, G. (2013). Multi-Functional Metamaterial Sensor Based on A broad-Side Coupled SRR Topology with A multi-Layer Substrate. *Applied Physics A*, **110(1)**, 189-197.

[21] Eleftheriades, G. V., Balmain, K. G. (2005). *Negative-refraction metamaterials: Fundamental principles and applications*. John Wiley & Sons.

[22] Engheta, N., Ziolkowski, R. W. (Eds.). (2006). *Metamaterials: Physics and engineering explorations*. John Wiley & Sons.

[23] Christensen, S., Zhurbenko, V., Johansen, T. K. (2014). Compact Microstrip Bandpass Filter with Tunable Notch. *20th International Conference on Microwaves, Radar and Wireless Communications (MIKON)* (pp. 1-4). IEEE.

[24] Levy, R., Cohn, S. B. (1984). A history of Microwave Filter Research, Design, and Development. *IEEE Transactions on Microwave Theory and Techniques*, **32(9)**, 1055-1067.

[25] Levy, R., Snyder, R. V., Matthaei, G. (2002). Design of Microwave Filters. *IEEE Transactions on Microwave Theory and Techniques*, **50(3)**, 783-793.

[26] Abuhussain, M. M. (2013). An E-band Diplexer for Gigabit Wireless Communications Systems (Master Thesis) .

[27] Cohn, S. B. (1957). Direct Coupled Resonator Filters. *Proceedings of the IRE*, **45(2)**, 187-196.

[28] Morelli, M., Hunter, I., Parry, R., Postoyalko, V. (2002). Stopband Performance Improvement of Rectangular Waveguide Filters Using Stepped-Impedance Resonators. *IEEE Transactions on Microwave Theory and Techniques*, **50(7)**, 1657-1664.

[29] Goussetis, G., Budimir, D. (2003). Novel Periodically Loaded E-Plane Filters. *IEEE Microwave and Wireless Components Letters*, **13(6)**, 193-195.

[30] Liao, S. S., Sun, P. T., Chen, H. K., Liao, X. Y. (2003). Compact-Size Coplanar Waveguide Bandpass Filter. *IEEE Microwave and Wireless Components Letters*, **13(6)**, 241-243.

[31] Bell, H. C. (2007). The Coupling Matrix in Low-Pass Prototype Filters. *IEEE Microwave Magazine*, **8(2)**, 70-76.

[32] Dong, B., Feng, Q., Yang, S. (2009). Research and Design of X-Band SIR Microstrip Filters. In *2009 International Conference on E-Business and Information System Security* (pp. 1-4). IEEE.

[33] Zhou, S., Wang, Z., Xu, R., Shen, D., Zhan, M. (2009). A novel X-Band Half Mode Substrate Integrated Waveguide (HMSIW) Bandpass Filter. *Asia Pacific Microwave Conference* (pp. 1387-1389). IEEE.

[34] Zhou, J. (2010). Microwave filters. In *Microwave and Millimeter Wave Technologies from Photonic Bandgap Devices to Antenna and Applications*. IntechOpen.

[35] Shang, X., Wang, Y., Nicholson, G. L., Lancaster, M. J. (2012). Design of Multiple-Passband Filters Using Coupling Matrix Optimisation. *IET Microwaves, Antennas and Propagation*, **6(1)**, 24-30.

[36] Budimir, D., Glubokov, O., Potrebić, M. (2011). Waveguide Filters Using T-Shaped Resonators. *Electronics Letters*, **47(1)**, 38-40.

[37] Mohottige, N., Glubokov, O., Budimir, D. (2013). Ultra Compact Inline E-Plane Waveguide Extracted Pole Bandpass Filters. *IEEE Microwave and Wireless Components Letters*, **23(8)**, 409-411.

[38] Shang, X., Xia, W., Lancaster, M. J. (2014). The Design of Waveguide Filters Based on Cross-Coupled Resonators. *Microwave and Optical Technology Letters*, **56(1)**, 3-8.

[39] Jin, C., Chen, J. X., Chu, H., Bao, Z. H. (2014). X-Band Differential Bandpass Filter with High Common-Mode Suppression Using Substrate Integrated Waveguide Cavity. *Electronics Letters*, **50(2)**, 88-89.

[40] Chen, X. P., Wu, K. (2014). Substrate Integrated Waveguide Filters: Design Techniques and Structure Innovations. *IEEE Microwave Magazine*, **15(6)**, 121-133.

[41] Wong, S. W., Chen, R. S., Wang, K., Chen, Z. N., Chu, Q. X. (2014). U-Shape Slots Structure on Substrate Integrated Waveguide for 40-GHz Bandpass Filter Using LTCC Technology. *IEEE Transactions on Components, Packaging and Manufacturing Technology*, **5(1)**, 128-134.

[42] Mohottige, N., Glubokov, O., Jankovic, U., Budimir, D. (2016). Ultra Compact Inline E-Plane Waveguide Bandpass Filters Using Cross Coupling. *IEEE Transactions on Microwave Theory and Techniques*, **64(8)**, 2561-2571.

[43] Ertay, A. O., Şimşek, S. (2016). A compact Bandstop Filter Design for X-Band Applications. *International Symposium on Fundamentals of Electrical Engineering (ISFEE)* (pp. 1-6). IEEE.

[44] Belayev, B. A., Lemberg, K. V., Serzhantov, A. M. (2016). An X-Band Magnetically Tunable Bandpass Filter Based on Novel Waveguide Cavity Resonator. *Asia-Pacific Microwave Conference (APMC)* (pp. 1-4). IEEE.

[45] Dahle, R., Laforge, P., Kuhling, J. (2017). 3-D Printed Customizable Inserts for Waveguide Filter Design at X-Band. *IEEE Microwave and Wireless Components Letters*, **27(12)**, 1080-1082.

[46] Tubail, D., Skaik, T. (2017). A Direct Approach for Coupling Matrix Synthesis for Coupled Resonator Diplexers. *Journal of Microwaves, Optoelectronics and Electromagnetic Applications*, **16(4)**, 942-953.

[47] Delmonte, N., Bozzi, M., Perregrini, L., Tomassoni, C. (2018). Miniaturization and Quality-Factor in Substrate Integrated Waveguide

Cavities. *IEEE MTT-S International Conference on Numerical Electromagnetic and Multiphysics Modeling and Optimization (NEMO)* (pp. 1-4). IEEE.

[48] Masood, M. H., Suseela, S. B. (2018). Compact Bandpass Filter with Reconfigurable X-Band Using Stepped Impedance Resonator and Folded Structure. *The Journal of Engineering*, **2018(3)**, 162-165.

[49] Smadi, L., Sharif, H., Faouri, Y. S. (2019). Dual-Band Tunable Microwave Bandpass Filter Using Stepped Impedance Technique. *IEEE Jordan International Joint Conference on Electrical Engineering and Information Technology (JEEIT)* (pp. 827-830). IEEE.

[50] Vallerotonda, P., Pelliccia, L., Tomassoni, C., Cacciamani, F., Sorrentino, R., Galdeano, J., Ernst, C. (2019). Compact Waveguide Bandpass Filters for Broadband Space Applications in C and Ku-Bands. *European Microwave Conference in Central Europe (EuMCE)* (pp. 116-119). IEEE.

[51] Hong, J. S. G., Lancaster, M. J. (2004). *Microstrip filters for RF/microwave applications* **(167)**. John Wiley & Sons.

[52] *Doumanis, E., Bulja, S., Kozlov, D. (2017). Compact Coaxial Filters for BTS Applications. IEEE Microwave and Wireless Components Letters,* **27(12)***, 1077-1079.*

[53] *Wu, Y., Gajaweera, R., Everard, J. (2016). Dual-band Bandpass Filter Using Coaxial Stepped Impedance Resonators. International Conference for Students on Applied Engineering (ICSAE) (pp. 181-185). IEEE.*

[54] Sun, D., Xu, J. (2016). A novel Iris Waveguide Bandpass Filter Using Air Gapped Waveguide Technology. *IEEE Microwave and Wireless Components Letters*, **26(7)**, 475-477.

[55] Gao, Y., Shang, X., Guo, C., Powell, J., Wang, Y., Lancaster, M. J. (2019). Integrated Waveguide Filter Amplifier Using the Coupling Matrix

Technique. *IEEE Microwave and Wireless Components Letters*, **29(4)**, 267-269.

[56] Zhu, Y. Y., Li, Y. L., Chen, J. X. (2018). A novel Dielectric Strip Resonator Filter. *IEEE Microwave and Wireless Components Letters*, **28(7)**, 591-593.

[57] Le Coq, M., Rius, E., Favennec, J. F., Quendo, C., Potelon, B., Estagerie, L., El Mostrah, A. (2015). Miniaturized C-Band SIW Filters Using High-Permittivity Ceramic Substrates. *IEEE Transactions on Components, Packaging and Manufacturing Technology*, **5(5)**, 620-626.

[58] Marín, S., Martínez, J. D., Valero, C. I., Boria, V. E. (2016). Microstrip Filters with Enhanced Stopband Based on Lumped Bisected Pi-Sections with Parasitics. *IEEE Microwave and Wireless Components Letters*, **27(1)**, 19-21.

[59] Chen, S., Shi, L. F., Liu, G. X., Xun, J. H. (2017). An alternate Circuit for Narrow-Bandpass Elliptic Microstrip Filter Design. *IEEE Microwave and Wireless Components Letters*, **27(7)**, 624-626.

[60] Dong, J., Shi, J., Xu, K. (2019). Compact Wideband Differential Bandpass Filter Using Coupled Microstrip Lines and Capacitors. *IEEE Microwave and Wireless Components Letters*, **29(7)**, 444-446.

[61] Xu, J., Xiao, F., Cao, Y., Zhang, Y., Tang, X. (2018). Compact Microstrip Filter with Third-Order Quasi-Elliptic Bandpass Response. *IEEE Access*, **(6)**, 63375-63381.

[62] Jia, H., Mansour, R. R. (2019). Millimeter-Wave Ultra-Wideband Multilayer Superconducting Filter. *IEEE Transactions on Applied Superconductivity*, **29(5)**, 1-5.

[63] Wang, Y., Yang, B., Tian, Y., Donnan, R. S., Lancaster, M. J. (2014). Micromachined Thick Mesh Filters for Millimeter-Wave and Terahertz Applications. *IEEE Transactions on Terahertz Science and Technology*, **4(2)**, 247-253.

[64] Narayan, S., Gulati, G., Sangeetha, B., Nair, R. U. (2018). Novel Metamaterial Element Based FSS for Airborne Radome Applications. *IEEE Transactions on Antennas and Propagation*, **66(9)**, 4695-4707.

[65] Pradhan, B., Gupta, B. (2015). Ka-Band Tunable Filter Using Metamaterials and RF MEMS Varactors. *Journal of Microelectromechanical Systems*, **24(5)**, 1453-1461.

[66] Vishnu, M., Choudhury, B., Nair, R. U. (2016). Metamaterial Based K-Band Substrate Integrated Waveguide Filter for Advanced Communication Systems. *International Conference on Emerging Trends in Communication Technologies (ETCT)* (pp. 1-4). IEEE.

[67] Tan, C., Wang, Y., Yan, Z., Nie, X., He, Y., Chen, W. (2019). Superconducting Filter Based on Split-Ring Resonator Structures. *IEEE Transactions on Applied Superconductivity*, **29(4)**, 1-4.

[68] Gil, A., Segura, J., Temme, N. M. (2007). *Numerical methods for special functions* **(99)**. Siam.

[69] Vendelin, G. D., Pavio, A. M., Rohde, U. L. (2005). *Microwave circuit design using linear and nonlinear techniques*. John Wiley & Sons.

[70] IEEE Standard for Microwave Filter Definitions (2011). *IEEE Std 1549-2011, pp.1-22, doi: 10.1109/IEEESTD.2011.5771512.*

[71] Gangwar, K., Gangwar, R. P. S. (2014). Metamaterials: Characteristics, Process, and Applications. *Advance in Electronic and Electric Engineering,* **4(1)***, 2231-1297.*

[72] Baena, J. D., Bonache, J., Martin, F., Sillero, R. M., Falcone, F., Lopetegi, T., Sorolla, M. (2005). Equivalent-Circuit Models for Split-Ring Resonators and Complementary Split-ring Resonators Coupled to Planar Transmission Lines. *IEEE Transactions on Microwave Theory and Techniques,* **53(4)***, 1451-1461.*

[73] Seo, B. J., Ueda, T., Itoh, T., Fetterman, H. (2006). Isotropic Left-Handed Material at The Optical Frequency with Dielectric Spheres Embedded in a Negative Permittivity Medium. *Applied Physics Letters,* **88(16)***, 161122.*

[74] Lim, S., Caloz, C., Itoh, T. (2004). Metamaterial-Based Electronically Controlled Transmission-Line Structure as A novel Leaky-Wave Antenna with Tunable Radiation Angle and Beamwidth. *IEEE Transactions on Microwave Theory and Techniques,* **52(12)***, 2678-2690.*

[75] Holloway, C. L., Kuester, E. F., Baker-Jarvis, J., Kabos, P. (2003). A double Negative (DNG) Composite Medium Composed of Magnetodielectric Spherical Particles Embedded in A matrix. *IEEE Transactions on Antennas and Propagation,* **51(10)***, 2596-2603.*

[76] Caloz, C., Itoh, T. (2002). Application of The Transmission Line Theory of Left-Handed (LH) Materials to The Realization of A microstrip" LH Line". *IEEE Antennas and Propagation Society International Symposium (IEEE Cat. No. 02CH37313)* **(2)***, pp. (412-415). IEEE.*

[77] Pendry, J. B., Martin-Moreno, L., Garcia-Vidal, F. J. (2004). Mimicking Surface Plasmons with Structured Surfaces. *Science,* **305(5685)***, 847-848.*

[78] Shelby, R. A., Smith, D. R., Schultz, S. (2001). Experimental Verification of A Negative Index of Refraction. *Science,* **292(5514)***, 77-79.*

[79] Solymar, L., Shamonina, E. (2009). *Waves in metamaterials*. *Oxford University Press.*

[80] Pendry, J. B., Holden, A. J., Stewart, W. J., Youngs, I. (1996). Extremely Low Frequency Plasmons in Metallic Mesostructures. *Physical review letters*, **76(25)**, 4773.

[81] Serdiukov, A., Semchenko, I., Tertyakov, S., Sihvola, A. (2001). Electromagnetics of Bi-Anisotropic Materials-Theory and Application **(11)**. *Gordon and Breach science publishers*.

[82] Hasar, U. C., Barroso, J. J. (2015). Scattering Parameter Analysis of Cascaded Bi-Anisotropic Metamaterials. *Optics Communications*, **(348)**, 13-18.

[83] Hudlicka, M., Machac, J., Nefedov, I. S. (2006). A triple Wire Medium as An Isotropic Negative Permittivity Metamaterial. *Progress In Electromagnetics Research*, **(65)**, 233-246.

[84] Buriak, I. A., Zhurba, V. O., Vorobjov, G. S., Kulizhko, V. R., Kononov, O. K., Rybalko, O. (2016). Metamaterials: Theory, Classification and Application Strategies. *8,* **4 (2**)*, 04088-1.*

[85] Singh, G., Marwaha, A. (2015). A Review of Metamaterials and Its Applications.

[86] Priyanka, A. (2014). A Review Paper on Metamaterial. *International Journal of Engineering Sciences and Research Technology*, **3(12)**, 612-618.

[87] Smith, D. R., Schultz, S., Markoš, P., Soukoulis, C. M. (2002). Determination of Effective Permittivity and Permeability of Metamaterials from Reflection and Transmission Coefficients. *Physical Review B*, **65(19)**, 195104.

[88] Liu, L., Caloz, C., Chang, C. C., Itoh, T. (2002). Forward Coupling Phenomena Between Artificial Left-Handed Transmission Lines. *Journal of Applied Physics*, **92(9)**, 5560-5565.

[89] Eleftheriades, G. V., Iyer, A. K., Kremer, P. C. (2002). Planar Negative Refractive Index Media Using Periodically LC-Loaded Transmission Lines. *IEEE Transactions on Microwave Theory and Techniques*, **50(12)**, 2702-2712.

[90] Liu, W., Chen, Z. N., Qing, X. (2013). Metamaterial-Based Low-Profile Broadband Mushroom Antenna. *IEEE Transactions on Antennas and Propagation*, **62(3)**, 1165-1172.

[91] Kasap, S., Capper, P. (Eds.). (2017). *Springer handbook of electronic and photonic materials*. Springer.

[92] Bilotti, F., Sevgi, L. (2012). Metamaterials: Definitions, Properties, Applications, and FDTD-Based Modeling and Simulation. *International Journal of RF and Microwave Computer-Aided Engineering*, **22(4)**, 422-438.

[93] Hunter, I. C., Billonet, L., Jarry, B., Guillon, P. (2002). Microwave Filters-Applications and Technology. *IEEE Transactions on Microwave Theory and Techniques*, **50(3)**, 794-805.

[94] Zou, X., Tong, C. M., Yu, D. W. (2011). Design of An X-Band Symmetrical Window Bandpass Filter Based on Substrate Integrated Waveguide. In *Proceedings of 2011 Cross Strait Quad-Regional Radio Science and Wireless Technology Conference* **(1)**, (pp. 571-574). *IEEE.*

[95] Skaik, T., AbuHussain, M. (2013). Design of Diplexers for E-Band Communication Systems. *13th Mediterranean Microwave Symposium (MMS)* (pp. 1-4*). IEEE.*

[96] Valencia, J., Guglielmi, M., Cogollos, S., Vague, J., Boria, V. E. (2017). Enhancing The Performance of Stepped Impedance Resonator Filters in A Rectangular Waveguide. *47th European Microwave Conference (EuMC)* (pp. 989-992). *IEEE.*

[97] Hrabar, S., Bartolic, J., Sipus, Z. (2005). Waveguide Miniaturization Using Uniaxial Negative Permeability Metamaterial. *IEEE Transactions on Antennas and Propagation*, **53(1)**, 110-119.

[98] Ortiz, N., Baena, J. D., Beruete, M., Falcone, F., Laso, M. A. G., Lopetegi, T., Sorolla, M. (2005). Complementary Split-Ring Resonator for Compact Waveguide Filter Design. *Microwave and Optical Technology Letters*, **46(1)**, 88-92.

[99] Stefanovski, S. L., Potrebić, M. M., Tošić, D. V. (2013). Design and Analysis of Bandpass Waveguide Filters Using Novel Complementary Split Ring Resonators. *11th International Conference on Telecommunications in Modern Satellite, Cable and Broadcasting Services (TELSIKS)* **(1)**, pp. 257-260). IEEE.

[100] Fallahzadeh, S., Bahrami, H., Tayarani, M. (2009). A Novel Dual-Band Bandstop Waveguide Filter Using Split Ring Resonators. *Progress in Electromagnetics Research*, **(12)**, 133-139.

[101] Odabasi, H., Teixeira, F. L. (2013). Electric Field Coupled Resonators as Metamaterial Loadings for Waveguide Miniaturization. *Journal of Applied Physics*, **114(21)**, 214901.

[102] Bage, A., Das, S. (2017). Stopband Performance Improvement of CSRR-Loaded Waveguide Bandpass Filters Using Asymmetric Slot Structures. *IEEE Microwave and Wireless Components Letters*, **27(8)**, 697-699.

[103] Torabi, Y., Dadashzadeh, G., Oraizi, H. (2016). Miniaturized Sharp Band-Pass Filter Based on The Complementary Electric-LC Resonator. *Applied Physics A*, **122(4)**, 273.

[104] Dong, Y., Itoh, T. (2011). Miniaturized Dual-Band Substrate Integrated Waveguide Filters Using Complementary Split-Ring Resonators. *IEEE MTT-S International Microwave Symposium* (pp. 1-4). IEEE.

[105] Vendik, I. B., Vendik, O. G. (2013). Metamaterials and Their Application in Microwaves: A Review. *Technical Physics*, **58(1)**, 1-24.

[106] Bahl, I. J., Bhartia, P. (2003). Microwave solid state circuit design. John Wiley & Sons.

[107] Hong, J. S. (2000). Couplings of Asynchronously Tuned Coupled Microwave Resonators. *IEE Proceedings-Microwaves, Antennas and Propagation,* **147(5)***, 354-358.*

[108] Hong, J., (2011). Microstrip filters for RF/microwave applications, *Second Edition. Hoboken, N.J.: Wiley.*

[109] Skaik, T. F. (2011). Synthesis of Coupled Resonator Circuits with Multiple Outputs Using Coupling Matrix Optimization (Doctoral Dissertation).

[110] Yoon, K. C., Kim, S. C., Lee, J. C. (2016). Compact Low Noise Amplifier with High Stable Gain Using Distributed CRLH Metamaterial. *Microwave and Optical Technology Letters,* **58(7)**, 1715-1720.

[111] CST Microwave Studio. Darmstadt, Germany, (2017) CST Intl.: http://www.cst.com/, 16.06.2020.

[112] AbuHussain, M., Hasar, U. C. (2020). Design of X-Bandpass Waveguide Chebyshev Filter Based on CSRR Metamaterial for Telecommunication Systems. *Electronics*, **9(1)**, 101.

CURRICULUM VITAE (CV)

Mahmoud ABUHUSSAIN

Personal Profile

Place of Birth : Gaza / Gaza strip / Palestine

Date of Birth : 26th Nov 1984

Gender : Male

Nationality : Palestinian

Marital Status : Married, 3 children

Address : Turkey, Gaziantep

Education

10th Oct – 20th June 2015 – 2020	Electrical and Electronics Engineering Gaziantep University - GAUN Gaziantep, Turkey Degree attained Ph.D. Electrical and Electronics Engineering Electromagnetic Engineering and Microwave Techniques, GPA (97.9%). Website: https://www.gantep.edu.tr/
21st Sep – 4th June 2010 -2013	Electrical Engineering Islamic University of Gaza - IUG Gaza, Gaza Strip, Palestine Degree attained M.Sc. Electrical Engineering Telecommunication Systems, GPA (90.5%) Website: http://www.iugaza.edu.ps/

20th Sep – 9th Jan 2002 -2007

Electrical and Control Engineering
Islamic University of Gaza - IUG
Gaza, Gaza Strip, Palestine
Degree attained B.Sc. Electrical Engineering
Electrical and Control Engineering, GPA (84.68%)
Website: http://www.iugaza.edu.ps/

20th Sep– 10th Aug 2001 -2002

Khalil Al-Wazeer high School – Science
Gaza, Gaza Strip, Palestine
Certificate attained High School Certificate score (95.1%)

Experiences

- 2017-2020 Teaching Assistant, Gaziantep University, Arabic Department
  Electrical and Electronics Engineering, courses:
  - Electric Circuits I, II
  - Fundementals of Electronics Circuits
  - Electromagnetics I, II
  - Antenna and Propagation
  - Fiber Optics Enginnering
  - Microwave Engineering
  - Advanced topics in Microwave Engineering
  - Calculus A, B
  - Differential Equations
  - Graduation Projects
- 2015 – present Humanitarian actor with many UN/INGO, Gaziantep
  - Data Management Expert
  - Processing and Case Management Officer
  - MEAL Officer
  - ER, Shelter and Livelihood Senior Assistant
  - ToT CCCM Cluster
  - XB Project Officer

Publications

- Design of X-Bandpass Waveguide Chebyshev Filter Based on CSRR Metamaterial for Telecommunication Systems.
  https://doi.org/10.3390/electronics9010101
- New topology of X-Band Waveguide Filter Based on Rectangular Resonators
  https://www.researchgate.net/profile/Mahmoud_Abuhussain2/publications
- Design of Diplexers for E-Band Communication Systems
  DOI: 10.1109/MMS.2013.6663087